STUDY ON NOVEL SOLAR PHOTOVOLTAIC INTEGRATED VACUUM GLAZING FOR LOW-ENERGY BUILDINGS

HUANG JUNCHAO

PhD

The Hong Kong Polytechnic University

2021

The Hong Kong Polytechnic University

Department of Building Services Engineering

Study on Novel Solar Photovoltaic Integrated Vacuum Glazing for Low-energy Buildings

Huang Junchao

A thesis submitted in partial fulfilment of the requirements for

the degree of Doctor of Philosophy

June 2021

CERTIFICATE OF ORIGINALITY

I hereby declare that this thesis is my own work and that, to the best of my knowledge and belief, it reproduces no material previously published or written, nor material that has been accepted for the award of any other degree or diploma, except where due acknowledgement has been made in the text.

_____(Signed)

HUANG Junchao (Name of student)

ABSTRACT

Abstract of thesis entitled: Study on novel solar photovoltaic integrated vacuum glazing for low-energy buildings

Submitted by: Huang Junchao

For the degree of: Doctor of Philosophy

at The Hong Kong Polytechnic University in June 2021

Building-integrated photovoltaic (BIPV) panels can replace the traditional building envelope materials for simultaneous thermal regulation and on-site power supplies, which becomes an effective approach to energy efficient buildings. Numerous studies have investigated PV integrated windows including single-glazed PV windows, PV insulating glass units, and PV double-skin façades. These types of PV windows are proved with great energy saving potential owing to the generated solar power and enhanced thermal performance, compared with the conventional clear glass or double-pane windows. Attributed to the air gap, hollow PV glazing (PV insulating glass units), and PV double-skin façades have better thermal performances than the single-glazed PV windows, leading to lower air conditioning load. To further improve the thermal performance of PV glazing, vacuum glazing has become an

emerging research focus given its remarkable performance in both thermal and sound insulation.

The first attempt to laminate glazed PV and vacuum glazing together was made in 2017, followed by very limited studies. Though it is found that the photovoltaic vacuum glazing can offer several benefits, such as generating electricity, thermal insulation, and reducing solar heat gain and noise level. The applicability of such PV envelope systems in diverse meteorological conditions has not been thoroughly discussed and its integration with other architectural design parameters has not been sufficiently addressed. Existing numerical models to predict the thermal behavior of composite photovoltaic vacuum glazing was built based on quasi-steady state and one dimension. There is a lack of a 3D dynamic thermal model to appropriately describe the whole heat transfer processes. Moreover, no research has studied the integration of additional air cavity with photovoltaic vacuum glazing. And the impact from design factors like thermal properties, vacuum pillar dimension and separation, Low-E coating and air cavity width have not been investigated. The overall energy performance of composite photovoltaic vacuum glazing with or without intermediate air cavity also needs further studies. Currently, indoor tests are the main approach to find out the thermal and electrical properties of photovoltaic vacuum glazing, and only limited work has been done for horizontally placed

samples. Field tests have not been conducted to measure the real time data for practical performance analysis.

To fulfil the research gaps, the first part of this thesis presents a comprehensive investigation of the thermal and power performance of the PV vacuum glazing as well as an integrated design optimization of photovoltaic envelope systems. A prototype office building model with a curtain wall design is first constructed in EnergyPlus to compare the heat gain, heat loss, thermal load, lighting energy and PV generation for different curtain walls. The comparative analysis proves the excellent thermal insulating performance of the PV vacuum glazing, which can reduce up to 81.63% and 75.03% of the heat gain as well as 31.94% and 32.03% of the heat loss in Hong Kong and Harbin, respectively. With the application of PV vacuum glazing in all available facades of the prototype building, net energy savings of 37.79% and 39.82% can be achieved in diverse climatic conditions. Furthermore, screening and variance-based sensitivity analyses are conducted to prioritize building integrated photovoltaic design parameters with respect to specific weather conditions. Selected important design parameters are then optimized with the non-dominated sorting genetic algorithm-II, by which the optimum building design can achieve a net energy consumption reduction of 48.72% and 60.80% compared to benchmarking designs in Hong Kong and Harbin.

Secondly, this thesis proposes an integrated photovoltaic vacuum glazing unit with an intermediate air cavity and a calibrated modelling approach to quantify its thermal properties and evaluate the heat transfer performance. Three-dimensional heat transfer models are established and cross-validated against previous publications. The detailed validation demonstrates the reliability of the developed complex models under different circumstances. Furthermore, four PV vacuum glazing configurations are compared in terms of the temperature distribution and overall heat transfer coefficient (i.e., U-value). Simulation results show that the photovoltaic vacuum double glazing can achieve the optimum performance among the four configurations based on simultaneous consideration of the PV module temperature and U-value. Sensitivity analyses of main glazing design factors are also conducted for the U-value, which is greatly reduced by decreasing the density and diameter of vacuum pillars as well as the glass thermal conductivity. The lowest U-value of 0.23 W/(m2·K) is achieved for the hollow PV vacuum glazing and can be further improved with future design optimizations.

Thirdly, a comprehensive heat transfer analysis has been carried out to determine the surface heat transfer coefficient and reveal the heat transfer process in the air and vacuum gap. A mathematical heat transfer model is established with MATLAB based on measured physical parameters by indoor tests. A test rig for dynamic experiments is also built to collect surface temperature, ambient temperature, surface heat flux, wind speed, electricity output, and solar

irradiance. Under outdoor conditions, the maximum temperature difference between the interior and exterior surface can reach 20.4 ℃ for hollow PV vacuum glazing, which proves its excellent thermal performance. The heat transfer model is validated against both experimental data and published references. Simulated results are in good agreement with collected data from references and experiments. Based on the calculated U-value and solar heat gain coefficient, the window heat gain and power generation are predicted with the model considering the detailed impact of the Low-E coating. Analysis results show that the integration of the vacuum layer can reduce the U-value and solar heat gain coefficient of hollow photovoltaic glazing by 28% and 15%, respectively. In the hollow photovoltaic vacuum glazing, the Low-E coating is more effective in reducing the window heat gain if applied to the vacuum gap rather than the air gap, contributing to a lower U-value (0.45 W/(m2·K)) and solar heat gain coefficient (0.157) than those of photovoltaic vacuum glazing. The composite glazing is more suitable for a hot climate if the Low-E coating faces outside regardless of the coating's position in the vacuum gap or in the air gap. Compared with the double glazing, the Hollow photovoltaic vacuum glazing can help reduce averagely 75.3% energy consumption for heating and cooling in all the studied orientations and climatic zones.

With the energy saving potential proved, a guideline is provided in the thesis for the initial design of the composite PV vacuum glazing to enhance the thermal performance of low-energy

buildings for future carbon neutral building development. The validated heat transfer model proposed in this study can be applied to the heat transfer modelling of PV glazing with diverse structures. References are also provided for selecting PV photovoltaic glazing as the building envelope for energy conservation in different climate regions. This comprehensive study on solar PV vacuum glazing provides good reference for future research and industrial development of this new technology.

Keywords: building integrated photovoltaic; photovoltaic vacuum glazing; overall heat transfer coefficient; solar heat gain coefficient; EnergyPlus; building energy efficiency; envelope system; heat transfer analysis; sensitivity analysis; design optimization; thermal performance; Low-E coating; temperature distribution

PUBLICATIONS DURING PHD STUDY

Journal Papers:

Huang, J., Chen, X., Yang, H., Zhang, W. Numerical investigation of a novel vacuum photovoltaic curtain wall and integrated optimization of photovoltaic envelope systems. Applied Energy, Volume 229, 2018, Pages 1048-1060.

Huang, J., Chen, X., Peng, J., Yang, H. Modelling analyses of the thermal property and heat transfer performance of a novel compositive PV vacuum glazing. Renewable Energy, Volume 163, 2021, Pages 1238-1252.

Huang, J., Wang, Q., Chen, X., Xu, S., & Yang, H. (2021). Experimental investigation and annual overall performance comparison of different photovoltaic vacuum glazings. Sustainable Cities and Society, 103282. https://doi.org/10.1016/J.SCS.2021.103282

Huang, J., Chen, X., Wang, Q., Yang, H. Thermal performance analysis of novel composite photovoltaic vacuum glazing. (Ready for submission)

Huang, J., Yu, J., Yang, H. Effects of key factors on the heat insulation performance of a hollow block ventilated wall. Applied Energy, Volume 232, 2018, Pages 409-423.

Chen, X., **Huang, J.**, Yang, H., Peng, J. Approaching low-energy high-rise building by integrating passive architectural design with photovoltaic application. Journal of Cleaner

Production, Volume 220, 2019, Pages 313-330.

Chen, X., **Huang, J.**, Yang, H. Multi-criterion optimization of integrated photovoltaic facade with inter-building effects in diverse neighborhood densities. (2020) Journal of Cleaner Production, Volume 248, 2020, 119269.

Wang, Q., Shen, B., **Huang, J.**, Yang, H., Pei, G., Yang, H. A spectral self-regulating parabolic trough solar receiver integrated with vanadium dioxide-based thermochromic coating. Applied Energy, Volume 285, 2021, 116453.

Conference papers

Chen, X., **Huang, J.**, Zhang, W., Yang, H. Exploring the optimization potential of thermal and power performance for a low-energy high-rise building. Energy Procedia, Volume 158, 2019, Pages 2469-2474.

Huang, J., Chen, X., Yang, H. A Multi-criterion Optimization for Passive Building Integrated with Vacuum Photovoltaic Insulated Glass Unit. Environmental Science and Engineering, 2020, Pages 857-863.

ACKNOWLEDGEMENTS

No one can walk on the path of scientific research entirely on his own, but it must be the help and support of many people to reach the end of the doctoral thesis. It is a great honor for me to express my gratitude to all those who have helped, supported, and encouraged me.

First and foremost, I would like to express my sincere gratitude to my chief supervisor, Prof. Hongxing Yang, who offered me with the valuable opportunity for doctoral study. If it were not for his wise counsel, patient guidance, generous support, and spurring, this thesis would not have existed. He himself is very diligent in research work and has set an excellent example for PhD students to follow.

My sincere gratitude also goes to my co-supervisor, Prof. Lin Lu, for her constructive advice and attentive teachings during my study. Like my chief supervisor, her rigorous and meticulous academic spirit has benefited me a lot.

Moreover, I appreciate the kind assistance, encouragement, and companionship from the members in Renewable Energy Research Group (RERG). I am grateful to Prof. Jinqing Peng for providing the opportunity to visit and learn from his lab. And many thanks to Dr. Xi Chen and Dr. Qiliang Wang for their help and guidance.

Last but not least, I would like to thank my beloved parents and my blood brother and sister for their unconditional support and being the solid companions on my PhD journey.

TABLE OF CONTENTS

LIST OF FIGURES

LIST OF TABLES

NOMENCLATURE

Abbreviation

ANOVA	analysis of variance
BAPV	building attached photovoltaics
BIPV	building-integrated photovoltaic
BO	building orientation
CdTe	cadmium telluride
COPT	comprehensive optimization
CSWD	Chinese Standard Weather Data
EVA	ethylene-vinyl acetate
FAST	Fourier Amplitude Sensitivity Test
HB	Harbin
HK	Hong Kong
HPVG	hollow photovoltaic glazing
HPVVG	hollow photovoltaic vacuum glazing
HVPVG	hollow vacuum photovoltaic glazing
IACH	infiltration air changes per hour

IWEC	International Weather for Energy Calculations
LSG	light-to-solar gain ratio
NSGA-II	non-dominated sorting genetic algorithm-II
OPF	overhang projection fraction
PV	photovoltaic
PVA	PV module area
PVB	polyvinyl butyral
PVDF	photovoltaic double-skin façade
PVDG	photovoltaic double glazing: glass-PV layer-glass-air cavity-glass
PVLG	photovoltaic laminated glazing: glass-PV layer-glass
PVVDG	photovoltaic vacuum double glazing: outdoor/glass-PV layer-glass-air cavity-vacuum glazing/indoor
PVVG	collective name for different types of photovoltaic vacuum glazing
PVVG	photovoltaic vacuum glazing: outdoor/glass-PV layer-vacuum glazing/indoor
PVVG	collective name for different types of photovoltaic vacuum glazing
PV-VG	umbrella name for all kinds of photovoltaic-vacuum glazing

PVVG-A	photovoltaic vacuum glazing with Low-E coating after vacuum gap
PVVG-B	photovoltaic vacuum glazing with Low-E coating before vacuum gap
SA	sensitivity analyses
SHGC	solar heat gain coefficient
SOPT	simplified optimization
STC	standard test conditions
STPV	semi-transparent photovoltaic
TVG	triple vacuum glazing: glass-vacuum pillars-glass-vacuum pillars-glass
U-value	overall heat transfer coefficient
VG	vacuum glazing: glass-vacuum pillars-glass
VPV IGU	vacuum photovoltaic insulated glass unit
VPVDG	vacuum photovoltaic double glazing: outdoor/vacuum glazing-air cavity-glass-PV layer-glass/indoor
VPVG	vacuum photovoltaic glazing: outdoor/vacuum glazing-PV layer-glass/indoor

VT	visible light transmittance
VT	visible light transmittance
WSH	wall specific heat
WTR	wall thermal resistance
WU	window U-value
WWR	window to wall ratio

Symbols

A	Area (m^2)
AL	air leakage ($m^3/(s \cdot m^2)$)
C_{air}	thermal conductance of the residual gas ($W/(m^2 \cdot K)$)
C_p	specific heat (kJ/kg·K)
C_{pillar}	thermal conductance of the vacuum pillar array ($W/(m^2 \cdot K)$)
d	thickness (m)
g	the acceleration due to gravity (m/s^2)
G	incident solar irradiance (W/m^2)
G_τ	transmitted solar irradiance (W/m^2)
h	heat transfer coefficient ($W/(m^2 \cdot K)$)

H	height of a vacuum pillar (m)
k	thermal conductivity (W/(m·K))
L	height of the air gap (m)
Nu	Nusselt number
P	pressure (Pa)
q	heat flow rate (W/m^2)
Q_{int}	heat flow (W)
r	radius of a vacuum pillar (m)
R	thermal resistance (K/W)
Ra	Rayleigh number
S	vacuum pillar separation (m)
$SHGC$	solar heat gain coefficient
T	temperature (°C or converted to K)
U	overall heat transfer coefficient (W/m^2·K)
α	absorptance
β	thermal expansion coefficient
β_c	temperature coefficient
ε_{eff}	effective emissivity

η	PV module efficiency
μ	dynamic viscosity ($N \cdot s/m^2$)
v	wind speed (m/s)
ρ	density (kg/m^3)
ρ_r	reflectance
σ	Stefan–Boltzmann Constant ($W/(m^2 \cdot K^4)$)
τ	transmittance
ΔT	temperature drop (℃ or converted to K))

Subscripts

c	solar cell
cond	conduction
conv	convection
ext	exterior surface
flu	fluid
g	glass
glazing	glazing layers
in	indoor

int	interior surface
out	outdoor
p	vacuum pillar
rad	radiation
std	standard test condition
sur	surface

CHAPTER 1 INTRODUCTION

1.1 Global Energy and Environment

Energy use is the core of modern industrial society. Every individual living on the planet uses energy in various forms every day. The global demand for energy continues to grow rapidly. While much of this growth is occurring in developing countries and countries with economies in transition to meet the many needs of their populations for lighting, cooking, heating, cooling, mechanics, transportation, communications, and other energy services designed to drive development the energy demand is also increasing in industrialized countries. The growth of global energy consumption in 2018 was reported as the strongest since 2010 and almost doubled the 10-year average (BP, 2019). Led by China, the United States is the second consumer of primary energy in 2018, followed by India, Russian Federation and so on (Statista, 2019). As shown in Figure 1.1, in the U.S., the industrial sector (33%) uses nearly one third of the total energy, transportation sector (26%) follows, and residential (22%) and commercial sector (18%) occupy the remaining part ("Use of energy in explained - U.S. Energy Information Administration (EIA)," n.d.). The Hong Kong Special Administrative Region, by way of comparison, is a different story: commercial sector taking up 44% while industrial sector merely holding 4% of the total energy consumption (EMSD, 2020).

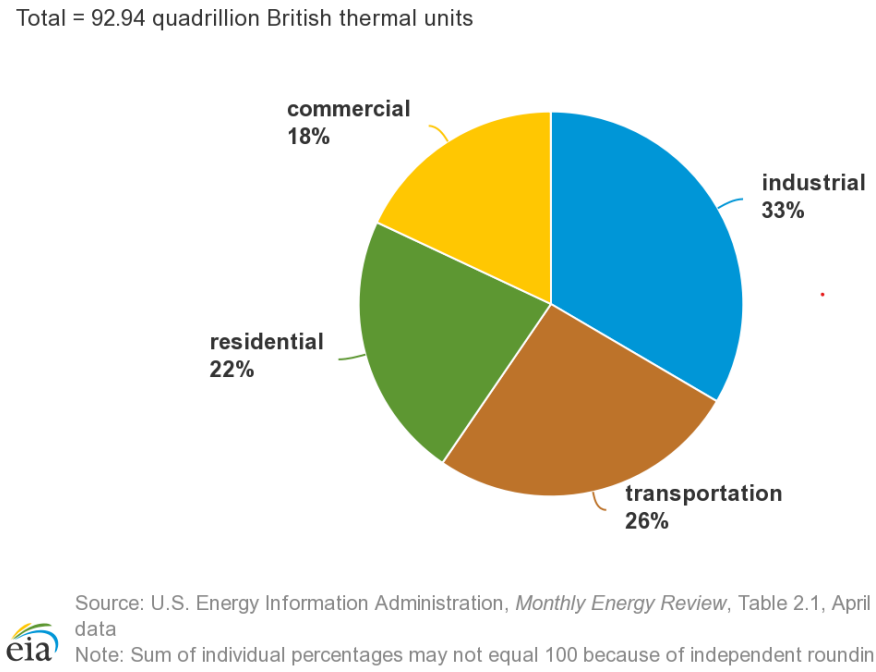

Figure 1.1 Share of total U.S. energy consumption by end-use sectors, 2020

What should be concerned is that with the growing energy demand, the world is still experiencing energy shortage, environment damage, pollution and climate change. Despite significant and remarkable advances in technology, the increasing consumption of energy has often resulted in the erosion of environmental benefits. The use of energy, especially fossil fuels, puts enormous pressure on our natural environment and has a negative impact on human health. World energy consumption results in pollution, environmental degradation and global greenhouse gas emissions (Dincer, 1998). As opposed to clean energy, so-called 'dirty energy' – coal, oil, and natural gas – produces a large amount of polluting smoke and greenhouse gas, threatening the global ecology. However, 'dirty energy' still generates most of electricity and fuel ("Energy and Pollution: Where Do We Pollute the Most? - Nature's Path," n.d.), as clean

energy has not been pushed into a major role yet. About two-thirds of global greenhouse gas emissions are associated with the burning of fossil fuels for heating, power generation, transportation, and industry. Greenhouse gas emissions from the global energy system continue to rise (World Energy Council, 2019), putting the global energy system in front of the dual challenge: the need for 'more energy and less carbon' (BP, 2019).

Renewable energy is the key to replace the consumption of traditional fossil energy and ease the emissions of greenhouse gas. A massive difference can be made by turning to more types of renewable energy, including solar, wind, hydroelectricity and geothermal ("Energy and Pollution: Where Do We Pollute the Most? - Nature's Path," n.d.). China is currently one of the world's leaders in renewable energy, consuming 106.7 Mtoe from sustainable sources in 2017 (Statista, 2019). China is already the global leader in a wide array of low-carbon technologies and maintains this position: it accounts for 30-40% of the global market to 2040 for solar PV, wind, hydro and nuclear power (IEA, 2019b). The "Clean Energy for All Europeans" package sets a renewable energy target of 32% of gross final consumption by 2030. Japan is also targeting expansion of renewable energy to 22-24% in 2030, led by hydro and solar PV.

However, the development and promotion of renewables are still in urgent need for the global wide. Coal and oil still accounted for a large proportion in world energy consumption,

nearly two thirds, while renewable energy merely took up a small percentage (4%) in 2018 (BP, 2019). Figure 1.2 shows the fact that renewables only accounts for about 5% in total energy consumption although efforts have been paid to use cleaner energy (EIA, 2020).The use of renewables needs to expand much more quickly to be on track to meet long-term climate goals, cleaner air objectives, and aims to provide access to modern energy sources (IEA, 2019a). To reduce the consumption of fossil fuels and prevent environmental damage, renewable energy is the promise of the longevity of the human destiny.

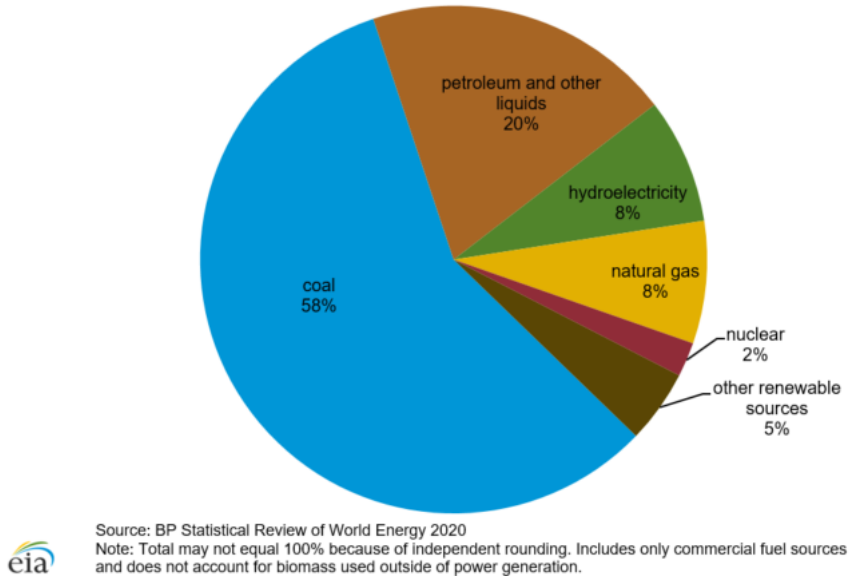

Figure 1.2 China's total primary energy consumption by fuel type, 2019

1.2 Low-Energy Buildings

The building energy plays a critical role in the total energy consumption of human communities, including energy used in residential, commercial and institutional buildings, and non-specified other (IEA, 2019b). Building energy use currently accounts for over 40% of total

primary energy consumption in the U.S. and E.U (Cao, Dai, & Liu, 2016). Moreover, the buildings result in approximately 40% of total direct and indirect CO_2 emissions ("Buildings – A source of enormous untapped efficiency potential," n.d.). According to the literature, building energy consumption accounted for about 30% of the total energy consumption in China between 2005 and 2015 (Huo et al., 2018). Furthermore, this energy consumption is consistently predicted by different organizations to continue to grow by 30% or even more before 2050 (Xu & Wang, 2020). As reported in the statistical year book of 2019 (Figure 1.3), energy consumption of commercial and residential sectors accounted for 65% of total energy use in Hong Kong, with 44% for the commercial and 21% for the residential use (EMSD, 2019). In more detail, the commercial sector includes restaurant (17%), retail (14%), office (11%), accommodation (13%), human health (5%), education (3%), data center (3%) and other commercial (34%), among which air conditioning, lighting and hot water and refrigeration take up 26%, 12%, and 12%, respectively.

It is thus clear that whether the use of energy in buildings is reasonable and efficient will have a significant impact on conservation in both energy and environment. Accompanied by the aggravation of the energy crisis, energy conservation in buildings has received more attention from researchers, with the emerge of concepts of low-energy buildings, nearly zero-

energy buildings, and zero-energy buildings. In fact, the latter two are more complete representations of low-energy buildings.

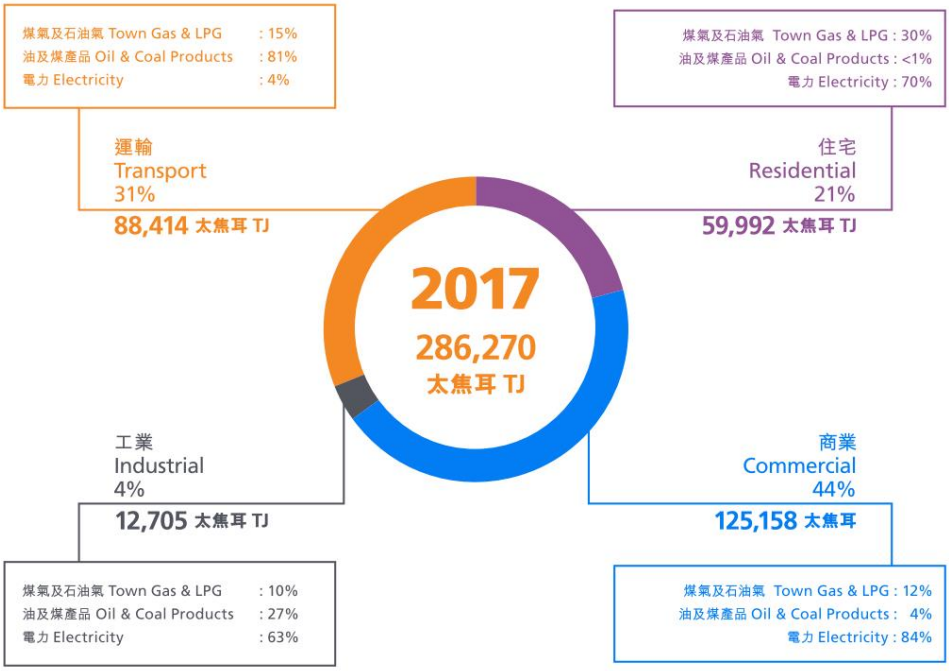

Figure 1.3 Energy consumption by sector and by fuel (EMSD, 2019)

The analysis of the energy use in buildings can help find the access to low-energy buildings. Most of the energy used in buildings is used to maintain a comfortable indoor environment in terms of thermal comfort (heating or cooling) and air quality (ventilation). Other energy uses are electric light, domestic hot water and household appliances or other electrical equipment (refrigerators, computers, TVs etc.) (“Energy use in buildings,” n.d.). Possible approaches to achieve building energy conservation include the utilization of energy-saving building materials, the improvement of insulation and sealing performance, and the efficiency gains in the equipment adopted in the buildings (P. S. Liu & Chen, 2014). A more integrated classification of potential means for low-energy buildings would be passive energy-

saving technologies, energy-efficient building service systems and renewable energy production technologies, proposed by a review article (Cao et al., 2016). To be more specific, the first type includes passive heating and cooling, advanced building envelopes, and thermal energy storage. The second is consist of and not limited to equipment used for heating, ventilation, air conditioning, domestic hot water, and lighting. As for the last one, solar energy, wind energy, bioenergy and geothermal energy are the major sources. Another work summarizes the recommended solutions as adding insulation thickness, using energy-saving windows, improving the efficiency of HVAC systems, and installing photovoltaic (PV) panels (Chastas, Theodosiou, & Bikas, 2016). Some scholars have also suggested efficient thermal insulation system, high-performance window system, good airtightness, fresh air heat recovery system, solar photovoltaic/thermal system, air source heat pump system, ground source heat pump system, and wind power (Z. Liu et al., 2019).

It is obvious that insulation, energy-efficient windows, and photovoltaics are the high-frequency keywords for achieving low-energy buildings, which will be one of the prominent contributors to reducing energy consumption and greenhouse gas emissions. Building integrated photovoltaics (BIPV) is a renewable energy technology that combines mentioned high-frequency terms and can be the ideal solution for low-energy buildings.

1.3 Building-Integrated Photovoltaics

Renewable Energy is derived from natural processes that are replenished constantly. In its various forms, it derives directly or indirectly from the sun, or from heat generated deep within the earth (Akan, Selam, & Firat, 2016). Among the different types of renewable energy, solar energy is the one of the most abundant and freely available energy resources ("Renewable Energy | Types, Forms & Sources | EDF," n.d.). Moreover, solar energy is tremendous, and its exploitation is not limited by topography like other types of renewable energy sources. Although solar energy is recognized as a promising alternative energy source, it merely takes up 1.8% of utilized renewable energy in Hong Kong (EMSD, 2019). On the other hand, the good news is that the residential solar prices continues to decline, down 27% compared to 2014 as shown in Figure 1.4 ("Residential solar prices hit record low in 2020, says EnergySage | Renewable Energy World," n.d.). And local government policies have also driven new installations of PV, like the Feed-in Tariff Scheme released in Hong Kong ("GovHK: Feed-in Tariff," n.d.). As a result, there is still a great potential for developing BIPV, which can help cut down energy bills of the building sector without additional land use (J. Peng, Lu, Yang, & Han, 2013).

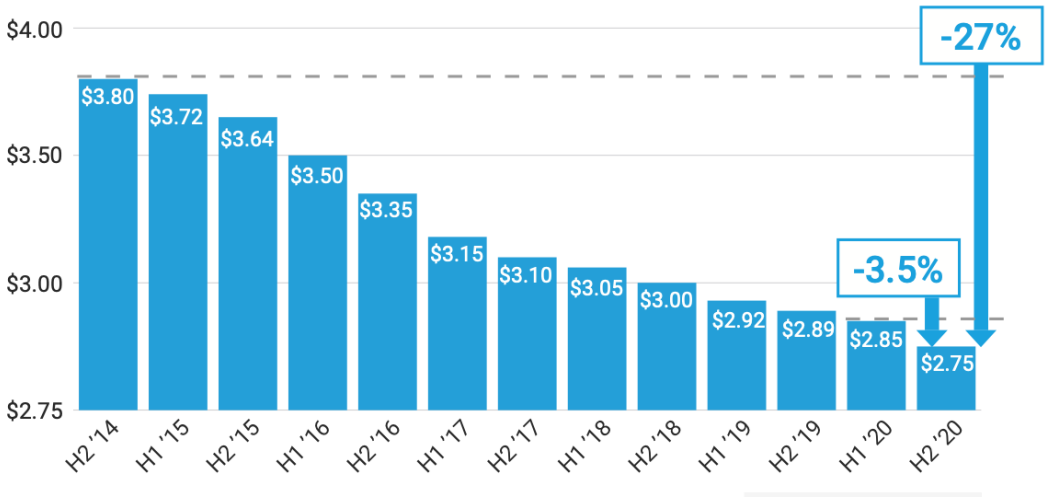

Figure 1.4 The median cost per watt for a residential solar system from 2014-2020, by half year

BIPV generally refers to the integration of solar photovoltaic cells or modules into the building envelopes to form part of the buildings (Kylili & Fokaides, 2014), replacing original roofs, façades, skylights, shadings, windows, or other elements. While opaque PV modules can be used for roofs, facades and shading systems, semi-transparent PV modules offer more possibilities for building facades, including satisfying aesthetic needs. Distinguished by the integration method, another similar expression, building attached photovoltaics (BAPV) means that PV systems are attached to buildings but not become part of the building envelopes (C. Peng, Huang, & Wu, 2011). Hence, the application of BAPV seems to be limited to existing buildings while BIPV has a wider range of options. Figure 1.5 shows the examples of one kind of BAPV and different BIPV.

(a) BAPV

(b) BIPV roof

(c) BIPV tiles

(d) BIPV façade

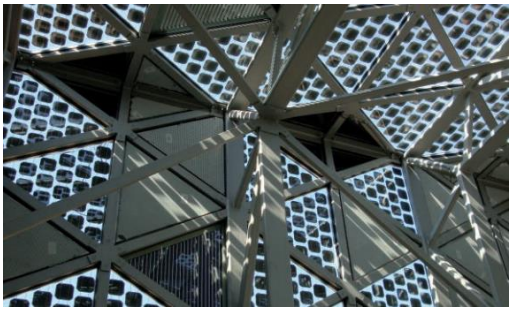

(e) BIPV skylight

(f) BIPV shading

Figure 1.5 Application examples of BAPV and BIPV (Heinstein, Ballif, & Perret-Aebi, 2013; Jelle, 2016; Kalogirou, 2015; C. Peng et al., 2011)

In an attempt to explore the potential of BIPV, a conceptual study investigated a hypothetical vertical square building with five exposed surfaces covered with thin-film silicon solar cells (Kylili & Fokaides, 2014). The electricity production by the most promising building orientations could attain the Passivhaus threshold of 120kWh/m^2 per year under the weather

condition of typical meteorological years, indicating the goal of zero energy building is achievable utilizing BIPV. In addition to the energy yield, BIPV can be multi-functional with many advantages (Kalogirou, 2015):

1) The exterior surfaces of the buildings can be effectively used without taking up additional land resources.

2) Grid-connected power generation can alleviate the need for peak electricity consumption during the day while on-site use can reduce power consumption and save the electricity transmission and losses.

3) The traditional building envelopes can be replaced with more diverse building designs using BIPV.

4) Temperature rise due to conventional building envelopes can be avoided by installing BIPV with enhanced thermal performance, thus reducing cooling load.

5) Photovoltaic power generation is a green process that produces no pollutants, consumes no fuel, and makes no noise.

6) Property owners installing green BIPV would benefit from local supply of electricity without transmission losses, government-backed subsidies, or additional income by selling the generated electricity.

1.4 Advanced Glazing in Buildings

Allowing light into the indoor and providing a vision for the occupants, window is one of the essential elements in buildings but also responsible for nearly 30% of energy used to heat and cool buildings (J. Peng, 2019). In addition to heating and cooling, glazing systems also affect on the daylighting performance (Thomas & Thomas, 2003). Windows are not only used in small scale in residential buildings. It is not surprising to note that most high-rise commercial buildings are covered by large areas of windows or glass curtain wall nowadays. Therefore, the improvement of window performance is of great significance to reduce indoor load and increase indoor comfort. Hence, advanced glazing products emerge from the need for energy efficiency in buildings.

Before understanding the wide variety of advanced glazing in buildings, it is necessary to get familiar with their performance assessment criteria. The main criteria for evaluating window performance include overall heat transfer coefficient (U-value), solar heat gain coefficient (SHGC) and visible light transmittance (VT) (ASHRAE, 2017). U-value represents the heat flow passing through the window and SHGC indicates the ability to control solar heat gain, thus the smaller of U-value and SHGC, the lower the rate of heat flow and solar heat gain. VT is the solar radiation transmitted through windows weighted with respect to the photopic response of the human eye. It physically represents the perceived clearness of the windows and

is likely different from the solar transmittance of the same windows. Moreover, colder regions require high SHGC as their climate makes heating a primary need, while hot regions require low SHGC. An ideal window should block all outdoor infrared and UV radiation and allow all outdoor visible light to enter in hot regions, while allow outside radiation except UV to enter but prevent indoor radiation loss in cold areas (Rezaei, Shannigrahi, & Ramakrishna, 2017). As for the U-value, it is required to be equal to zero in both climates.

Traditional glazing consists of clear glass, tinted glass, and glazing with Low-E coatings or (and) multi-layer structure. Clear glass generally has a visible transmittance around 0.8-0.9, which can be manufactured as the tinted glass if adding some metal elements in the floating process (Rezaei et al., 2017). Tinted glass reduces the transmittance and blocks and (or) reflects various amounts and kinds of light ("Custom Tinted Glass, Cut Tempered Glass | One Day Glass," n.d.), which can also be energy efficient if appropriate color tints are selected. Uncoated glass surface often has a emissivity of 0.837 while the value can be as lower as 0.013 according to the glass library for Berkeley Lab WINDOW if Low-E coating is applied ("WINDOW | Windows and Daylighting," n.d.). Multi-pane windows are able to achieve excellent thermal insulation as they are filled with gases between the glass layers, whose thermal conductivity is much lower than that of the glass itself.

Advanced glazing can be the glazing using functional coatings, aerogel, vacuum technologies, or integrated with photovoltaics, and the smart glazing utilizing thermochromic or electrochromic materials (Rezaei et al., 2017). In addition to the coatings with a low emissivity, coatings can also be made as anti-reflective or self-clean. Besides, aerogel is a porous material, usually composed of air and silica, which is known for excellent thermal insulation as well as light transmittance. Aerogel glazing can help reduce 21% total energy consumption when compared with double glazing (Gao, Ihara, Grynning, Jelle, & Lien, 2016). Vacuum glazing uses an array of vacuum pillars to separate the two layers of glass, and the narrow vacuum gap between which could eliminates most heat conduction and convection. The U-value of a double glazing filled with air is around 2.7 W/m^2K while the vacuum glazing with two layers of glass can lower the U-value to about 1.5 W/m^2K (Cuce & Cuce, 2016). This enhancement is remarkable and indicates the great potential for energy efficiency. Thermochromic and electrochromic glazing rely on the mechanism that color, and optical properties change with the temperature or input DC voltage to achieve energy saving (Rezaei et al., 2017). Among these types of advanced glazing, the integration between glazing and photovoltaics possesses a distinct advantage - harvesting sunlight for electricity generation.

1.5 Organization of the Thesis

This thesis consists of eight chapters. The current chapter illustrates the research

background, by revealing the significant role of low-energy buildings in the global energy and environment and further indicating two important technologies – building integrated photovoltaics and advanced glazing.

The following Chapter 2 is a literature review covering photovoltaics integrated with windows and vacuum insulated windows and emphasizes in detail the combination of the previous two, i.e., photovoltaic vacuum glazing. The research gaps are then identified, followed by the research objectives, and the corresponding methods are proposed in the end.

Chapter 3 focuses on the energy saving potential of using photovoltaic vacuum glazing as the window of a building model in EnergyPlus. The detailed analysis is given in terms of heat gain and loss through the glazing, electricity use of lighting, equipment, heating and cooling, and the photovoltaic power generation. The overall energy performance is as well analyzed at the end of the chapter.

Based on the preliminary exploration in Chapter 3, Chapter 4 presents an optimization study on integrating photovoltaic vacuum glazing with passive building design. Sensitivity analyses are conducted to reveal the intercorrelations between chosen design factors, which are further investigated from both qualitative and quantitative perspectives. The design optimization is then disclosed by clarifying the determined design parameters.

Chapter 5 simulates the heat flow through the photovoltaic vacuum glazing using a three-

dimensional finite element model. The hollow photovoltaic vacuum glazing is proposed and compared with existing photovoltaic vacuum glazing without air layer. This chapter mainly investigate the possible impact from critical design factors on the temperature distribution and U-value of different photovoltaic vacuum glazing.

A mathematical heat transfer is established in Chapter 6 based on a comprehensive heat transfer analysis and reasonable assumptions. The validation against previous studies proves that the heat transfer model can accurately simulate both U-value and SHGC for diverse photovoltaic glazing with the air layer and/or vacuum layer. Temperature distributions through the PV glazing structures are also analyzed, which can be used to predict the power generation by different PV glazing.

Chapter 7 introduces a test rig for monitoring the thermal and electrical performance of different photovoltaic glazing, in addition to necessary measurements of physical properties. The experiments are conducted indoor and outdoor, which means the involved glazing receives no sunlight and real-time solar irradiance. A good agreement is achieved between experimental data and the heat transfer model proposed in Chapter 6.

Validated by published articles in Chapter 6 and experimental data in Chapter 7, the mathematical heat transfer model is utilized to compare the performance between different PV glazing in Chapter 8, with double glazing and vacuum glazing as the reference groups. The

annual overall performance of different glazing is analyzed in terms of heating load, cooling load, and power generation, and from the perspectives of orientation and climate regions.

Finally, Chapter 9 concludes the key findings and contributions of the thesis. The limitations and recommendations for future work are also presented at the end.

CHAPTER 2 LITERATURE REVIEW AND RESEARCH METHODOLOGY

2.1 Introduction

Building energy consumption takes up 40% of the total energy use in the U.S. and E.U. (Cao et al., 2016), and about 60% of the total CO_2 emissions each year in Hong Kong (German Industry and Commerce Ltd., n.d.). Thus, energy efficiency in buildings is of profound significance, as low-energy buildings will become an important contributor to achieve sustainable development and low carbon (Kylili & Fokaides, 2015). Among the total building energy use, building envelopes are responsible for 30% of the cooling loads (Ghabra, Rodrigues, & Oldfield, 2017). Compare with traditional wall, windows or curtain wall is much easier to gain heat in summer and lose heat in winter, which subsequently turns into indoor cooling and heating loads, and ultimately leads to more energy consumption of buildings. On the other hand, solar energy is an abundant source of energy that has the potential to cover most of a building's energy usage, for hot water, space heating and electricity (Zhou et al., 2020). In this context, the promotion of BIPV becomes particularly important. As not only can BIPV replace the conventional building envelopes but also it generates electricity from solar power for field use or grid supply (Barman, Chowdhury, Mathur, & Mathur, 2018). Moreover, if the thermal performance of BIPV was enhanced, the air-conditioning load could as well be cut

down. PV glazing can as well contribute to reduction of artificial lighting energy consumption (Skandalos & Karamanis, 2015). Thus, BIPV becomes a key role in reducing energy use for energy-efficiency buildings, especially PV glazing.

The following content describes the research on PV integrated windows (Section 2.2) and vacuum insulated windows (Section 2.3), then highlights the research work that combines these two techniques (Section 2.4), while later pointing out the research gaps of the existing work and indicating the purpose of the thesis and its realization method. Figure 2.1 reveals the relationships among the following Section 2.2, 2.3 and 2.4.

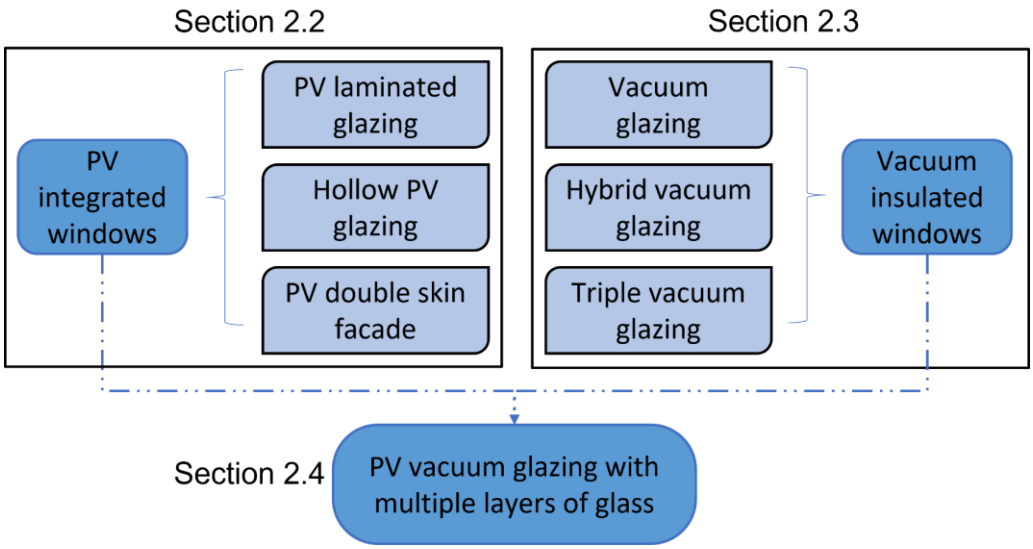

Figure 2.1 The relationships among Section 2.2, 2.3 and 2.4

2.2 Photovoltaics Integrated Windows

BIPV can simultaneously serve as the building component and power generator, and its integration with building facades usually causes no negative impact on their appearance

(Skandalos & Karamanis, 2015). Semi-transparent photovoltaic (STPV) windows, as one prospective BIPV applications, can generate electricity while allowing partial daylight penetration. Given its increased popularity in building envelope designs, many researchers conducted experimental and simulation studies on this new application. Fung and Yang developed a one-dimensional transient heat transfer model to evaluate the heat gain of semi-transparent photovoltaic modules for the building-integrated application (Fung & Yang, 2008). Lu and Law investigated the overall energy performance of a single-pane semi-transparent PV window for office buildings in Hong Kong (L. Lu & Law, 2013). The results showed that the glazing thermal performance was critical for energy saving in the building envelope. About 65% of total heat gain was reduced by using semi-transparent BIPV module instead of clear glass throughout a year. The energy saving potential of semi-transparent PV windows was also reported in comparison to the traditional glazing (Li, Lam, Chan, & Mak, 2009; Liao & Xu, 2015). STPV can contribute to better overall building energy performance compared with single and double-pane clear glazing in Hong Kong' climatic condition (Zhang, Lu, Peng, & Song, 2016).

By introducing an air gap with one more layer of glass, single-glazed PV window can be constructed to PV insulated glass unit, which can also be called hollow PV glazing. And this type of PV glazing can save about 25% of building energy in Hong Kong (M. Wang et al.,

2016). Compared with hollow PV glazing, PVDF has more variants due to the controllable air layer, which can be categorized into non-ventilated, natural-ventilated, and ventilated PVDF (J. Peng et al., 2016a; J. Peng, Lu, Yang, & Ma, 2015). 0.4-0.6 m is the suggested width of the air layer for such structure in Berkeley considering power generation, cost, space use and maintenances (J. Peng et al., 2016a). Half the net electricity can be cut down when using PVDF other than traditional glazing. In terms of overall heat transfer coefficient (U-value), the non-ventilated PVDF turns out the lowest one (3.4 W/(m^2·K)) (J. Peng et al., 2015). And the difference in solar heat gain coefficient (SHGC) among three modes of PVDF is not that significant. Ventilated- PVDF produces more electricity as this mode leads to lower solar cells temperature. Another study conducts a comparison between hollow PV glazing and PVDF, and results show that the former performs better in thermal insulation while the latter has lower solar heat gain (M. Wang et al., 2017). It is also evaluated that hollow PV glazing and PVDF use 28% and 30% less energy.

However, a shortcoming of the current PV curtain wall with common double-glazed PV modules lies in the poor thermal insulation performance due to the high solar heat gain coefficient and U-Value (J. Peng et al., 2016b). BIPV modules can still have a thermal conductivity of 1.1 W/m·K, even when inert gas filled up the gap within a double-glazing unit (Anatol C, Francesco F, 2011). The U-value of the hollow PV glazing or double skin façade

using PV blinds is around 2.3 W/(m^2·K) (Luo et al., 2017; M. Wang et al., 2017), which indicates the room for further improvement.

Apart from the U-value and SHGC, the PV module temperature is another point worth investigations. It is known that the power generation performance of a PV module varies inversely with its temperature. Park et al. pointed out that generated eletricity dropped by about 0.5% with 1 ℃ of the temperature rise through experimental studies under both the approximate standard test condition and real outdoor condition (Park, Kang, Kim, Yu, & Kim, 2010). It was also mentioned that the lower temperature of the PV module contributed to more power outputs when the PV module is connected to a cold environment rather than vacuum glazing (Ghosh, Sundaram, & Mallick, 2018). The photovoltaic glazing energy conversion efficiency changes with the temperature of the PV module, as shown in the equation below (Green, Moran, JOHNSTON, Uhler, & Chiu, 1982):

$$\eta_c = \eta_{std} - \beta_c(T_c - T_{c,std}) \tag{2.1}$$

where, η_c is the PV module's energy conversion efficiency at the temperature of T_c (℃); η_{std} is the efficiency at $T_{c,std}$ (℃), the standard condition; and β_c is the temperarure coefficient.

Given the impact on the electricity generation (Park et al., 2010; Sabri & Benzirar, 2014), the temperature of the PV module is a critical parameter to assess its application potential.

Moreover, the internal surface temperature of PV glazing indicates in contact with the indoor environment can influence the resultant cooling or heating load. Also, the less difference between this temperature and indoor temperature, the convective and radiative heat exchange will decrease, and the less discomfort the thermal environment will be (Lyons, Arasteh, & Huizenga, n.d.).

2.3 Vacuum Insulated Windows

The vacuum glazing technology, which was initially proposed by Zoller in 1913 (Zoller, 1924), could minimize conductive and convective heat transfer through the glazing unit by introducing an internal vacuum chamber. Compared with a normal double glazing, the vacuum glazing exhibits superior heat insulation performance, which is identified by its U-values. U-value of the vacuum glazing can be as low as 0.86 W/m^2 K, indicating a much better performance than a double-glazing (P W Griffiths et al., 1998).

Fang Y et al. (Fang et al., 2007) conducted experimental and simulative study to investigate the impact of Low-E coatings on the thermal performance of the vacuum glazing system. In their study, a guarded hot box calorimeter was adopted to test three samples with different emittances (0.04, 0.12, and 0.16). The overall heat transfer coefficient of the whole window varied from 1.15 $W/m^2 \cdot K$ to 1.30 $W/m^2 \cdot K$ with 8.5% uncertainty, which proved the reliability of the simulation results. The findings of this study suggest that single Low-E coating

provided adequate thermal insulation performance of the glazing system, and if the emittance value was as low as 0.02, the further improvement by using two layers of Low-E coating would be limited.

The validated finite volume model was also utilized by Fang Y et al. (Fang et al., 2015) to investigate the enhancement from the Low-E coating in the thermal performance of triple vacuum glazing. The research work studied the impact of changing the number of Low-E coatings in two vacuum chambers and altering the location of the coated vacuum chamber. It was suggested from the study that when using three coatings, the vacuum chamber with two coatings should be facing indoor environment if the weather was more dominated by the cold while that chamber should be facing outdoor in the area with contrary climate. If only two Low-E coatings were used, the thermal performance would be better under the circumstance that separating these two in different chambers other than putting them in just one chamber. Taking initial investment into account, there would be less importance to add the fourth coating in the triple vacuum glazing because of the limited improvement in the reduction of U-value.

Fang Y et al. (Fang, Hyde, & Hewitt, 2013) combined a third glass sheet with a double vacuum glazing to construct a hybrid vacuum glazing. The study presented detailed mathematical model, finite volume model and experimental study and results showed good agreement. The comparison of overall heat transfer performance was made between two

settings of the hybrid vacuum glazing, double vacuum glazing and triple vacuum glazing with 2 and 3 Low-E coatings. The finding indicated that the hybrid vacuum glazing showed better thermal performance when setting the vacuum chamber close to warm side. And both settings of hybrid vacuum glazing had lower U-value than double vacuum glazing did, suggesting the gas-filled cavity indeed helped to insulation. As for the triple vacuum glazing, the U value of center glazing and total glazing were lower than the hybrid vacuum glazing except for one instance, the total glazing with 2 Low-E coatings. However, the author mentioned that the conclusion was drawn under the situation of small size of glazing (400mm×400mm), so the scenario would be different once the dimension changed. The predicted U-value of hybrid vacuum glazing with 3 Low-E coatings was reported as low as 0.33 $W/m^2 \cdot K$, and 0.24 $W/m^2 \cdot K$ for triple vacuum glazing.

Cuce E et al. (Cuce & Riffat, 2015) investigated a vacuum tube window through experimental and numerical approaches. ANSYS FLUENT was adopted to modelling the heat transfer processes inside the window. Designed parameters of the vacuum tube window were studied to find out the solution for the aim of better thermal performance. Involved factors included glass pane thickness, dimensions of tube and argon-filled gap. Experimental chamber tests showed that the U-value was significantly reduced form larger than 2 $W/m^2 \cdot K$ to 0.5 $W/m^2 \cdot K$ when the tube diameter increased from 28mm to 70mm. Numerical study suggested

that smaller tube thickness and argon gap contributed to lower U-value while the variation of pane thickness showed limited impact. 60 mm was reported as the optimal tube diameter to achieve both thermal performance and economy.

In additon to determine the overall heat transfer coefficient, Ghosh A et al. (Ghosh, Norton, & Duffy, 2016) also calculated the dynamic solar heat gain coefficient of the vacuum glazing using the experimental data collected from a test cell. In order to evaluate the thermal and daylight performance, two samples were fabricated within the same size (350mm×210mm), one was double glazing and the other was vacuum glazing. In accordance with the present results, they concluded that 1.4 $W/m^2 \cdot K$ was the average U-value of the vacuum glazing, and the SHGC varied from 0.58 to 0.19, which dropped with increase of the incidence angle. Compared with the double glazing, the vacuum glazing helped to cut down the heat losses while letting similar lightness and same amount of heat pass through to indoor environment. In another work from Ghosh A et al. (Ghosh, Norton, & Duffy, 2017), more attention was paid on the sky clearness index, which was stated with more impact than incident angle on glazing transmittance. The study presented a method to calculate the transmitted solar energy and pointed out that 35% glazing transmittance could be provided if the clearness index of the vacuum glazing was below 0.5.

The U-value of vacuum glazing can reach 0.81 W/(m^2·K) with two layers of low-e coatings (Fang et al., 2014). Triple vacuum glazing can further lower the U-value at the center glazing area to 0.22 W/(m^2·K) (Cuce & Cuce, 2016). Therefore, if the vacuum glazing could be coupled with PV curtain walls in buildings, the heat gain and heat loss could be further reduced. In addition, the vacuum glazing has excellent sound insulation performance owing to its vacuum environment, which is considered an added value for buildings in urban areas.

2.4 Photovoltaics Vacuum Glazing

Given the excellent thermal insulation performance of VG, some researchers have proposed to combine PV with VG, aiming at improving the thermal performance of BIPV applications and related building energy performances. What PV vacuum glazing is called varies from person to person, but it can be roughly divided structurally into PV vacuum glazing with two, three and four layers of glass.

2.4.1 PVVG with four layers of glass

PV laminated glass was firstly coupled with vacuum glazing by a layer of polyvinyl butyral (Zhang, Lu, & Chen, 2017), as shown in the Figure 2.2 below. The sandiwich structure , named vacuum photovoltaic insulated glass unit (VPV IGU) by the authors, had four-layer glasses, and a total thickness of 21 mm, which was thiner than commonly used PV double

glazed insulating glass units (Chow, Li, & Lin, 2010). A triple A class simulator was used to test the electrical characteristics of the PV laminated glass under standard test conditions. The open circuit voltage was 120 V, the short curcuit current was 0.98 A, and the module efficiency is 5.2%. The VPV IGU was horizontally tested outdoors and collected data showed that the average solar irradiation transmittance is merely 0.08. The maximum temperature difference between exterior and interior surface was 30 ℃. The low transmittance and high temperature difference indicated that VPV IGU could block vast majority of solar radiation and heat.

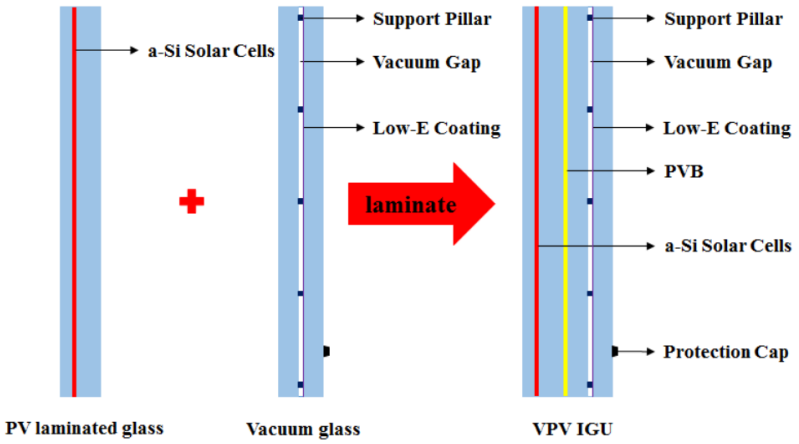

Figure 2.2 Structure of VPV IGU (Zhang et al., 2017)

Later on, small size samples of VPV IGU and double glazing products were tested using small size hot boxes (Figure 2.3) covered by thermal insulation material (Qiu, Yang, & Zhang, 2018). The authors devided the experimental study into three stages. The first stage of the tests was to maintain the temperature difference of exterior and interior surface higer than 5 ℃ and then collect the data of heat flux and temperature in the absence of solar radiation. The U-value was determined as averagely 1.5 W/(m^2·K) using experimental data. By comparison, the U-

value of conventioal double clear glazing was 2.5 W/(m^2·K), which was much higher. The authors pointed out that the center U-value of VPV IGU should be smaller than 1.5 W/(m^2·K) because less heat would be transferred to the center if the scale was lager.

The solar simulator was turned on in second stage to obtain the direct solar transmittance of VPV IGU, double glaizng, PV laminated double glazing and vacuum glazing. Results showed VPV IGU could decrease the direct solar transmittance to below 0.1, although slightly higher, PV double glazing as well kept the value around 0.1, while vacuum glazing had the highest value, beyond 0.6. Moreover, the interior surface temperature of VPV IGU was the lowest, about 10 ℃ lower than that of PV laminated glazing, and approximately 25 ℃ lower than that of vacuum glazing. The results matched those observed in previous study (Zhang et al., 2017), once again demontrating the berrier ability to block solar radiation and heat.

Field test was the last stage to monitor the data of real time temperature and solar radiation for VPV IGU and double glazing. The results of heat flux and interior surface temperature showed that VPV IGU prevented a lot of heat and solar radiation from penetrating compared with double glazing. Apart from experiments, the authors also conducted simulative studies to compare the various performances of installing VPV IGU in different orientations using tools of EnergyPlus and Berkeley Lab WINDOW. Measured physical properties of VPV IGU was inputted into WINDOW to acquire key parameters including U-value, solar heat gain

coefficient (SHGC) and visible light transmittance. The calculated U-value was 0.557 W/(m^2·K), much lower than the experimental result, while the SHGC was 0.143.

Figure 2.3 Small size hot boxes (0.3 × 0.3 × 0.4 m^3) (Qiu et al., 2018)

These parameters was further used in EnergyPlus so as to evaluate the overall energy performance. The south-oriented semi-transparent a-Si PV glazing with 20% transmittance produced the most electricity annually among all orientations in Hong Kong, at around 113.8 kWh per year. The energy saving of the west-oriented vacuum PV glazing was 25.4%, 16.5%, 14.0%, 20.1% and 14.9% compared with the cooling consumption of the room with single-pane clear glazing, double-pane clear glazing, single-pane PV glazing, double- pane PV glazing and vacuum glazing, respectively. The authors suggested that it was better to install VPV IGU on the west, east and south façades to achieve better building energy efficiency, and on the south-oriented façade in order to perform the best overall energy performance.

2.4.2 PVVG with three layers of glass

Another structure of PV vacuum glazing (PVVG) with three layers of glasses (Figure 2.4) was proposed and found having a U-value of 0.8 W/(m^2·K) (Ghosh et al., 2018). The authors claimed that they reported for the first time thermal performance of multicrystalline silicon based semi-transparent (32% PV cell coverage and 33% spectral solar transmittance through non-cover part) PV-vacuum glazing using indoor test cell characterisation. Two different combinations were investigated, the difference was the vacuum glazing either faced external laboratory ambient or internal test cell ambient. Results were compared with similar area semi-transparent PV-double glazing (32% PV cell coverage). To do so, a small-scale test cell dimension of 0.37 m × 0.22 m × 0.26 m was fabricated using 10 mm thick polystyrene to perform indoor characterisation. The ratio of test cell and glazing was 1:1. The thickness of PV-double glazing was 8 mm while the thickness of PVVG was 12 mm. To test the electrical performance, measurements were carried out for 125 min continuous exposure under 1000 W/m^2 indoor simulator radiation. Both types offered equal U-value (0.8 W/(m^2·K)), SHGC (0.42) and transmission (0.33 for non-covered part), while PV cell performance was superior when solar cells faced external laboratory ambient. Compared with PV double glazing, 66% lower U- value and 42% lower solar factor indicated PVVG a suitable candidate for low energy building.

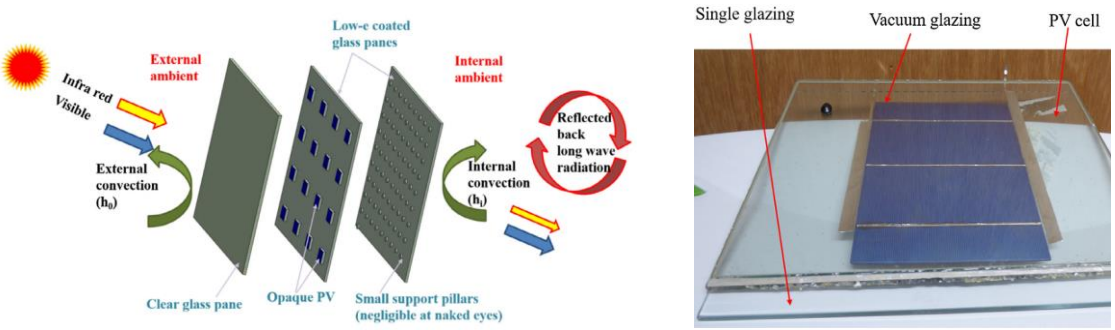

Figure 2.4 Exploded view of semi-transparent PV-vacuum glazing (Ghosh et al., 2018)

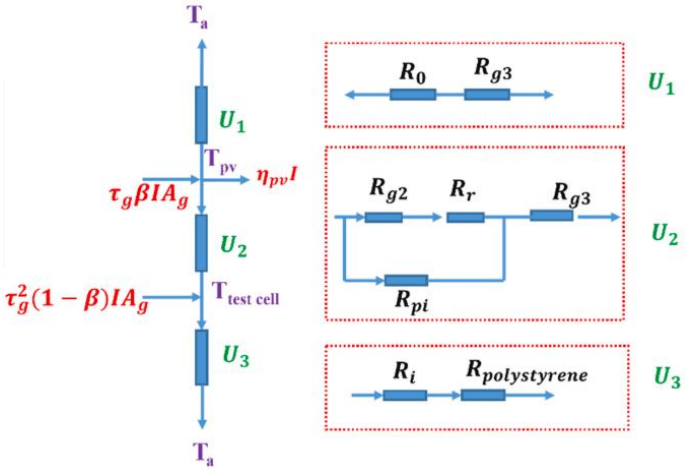

Figure 2.5 Thermal diagram of the BIPV-vacuum glazing (Ghosh, Sarmah, Sundaram, & Mallick, 2019)

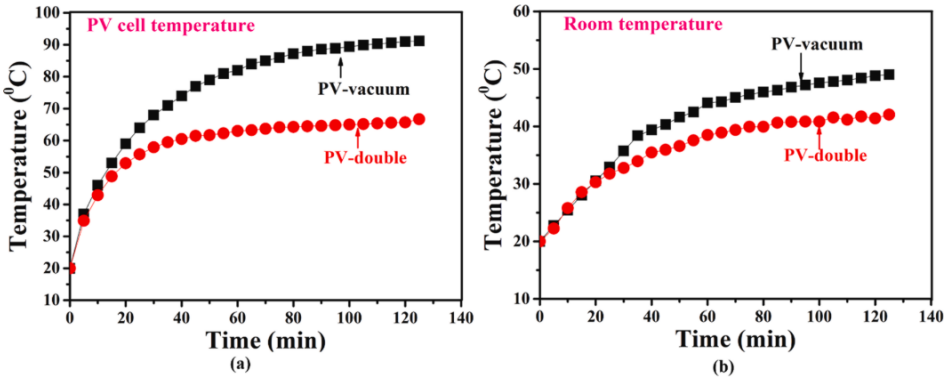

Figure 2.6 Calculated PV cell temperature and test cell temperature for (a) BIPV-vacuum and (b) BIPV-double glazing

The authors also presented numerical studies with a one-dimentional heat transfer model to evaluate the thermal comfort, and found a 39% improvement of indoor thermal comfort when using such PVVG in UK as compared with PV laminated glazing (Ghosh, Sarmah, et al., 2019). The same test cells in previous study were used to collect data of temperature and module efficiency for validating the established model, which was assume to be under quasi-steady state. Figure 2.5 shows the presented thermal diagram of PVVG, which considered heat transfer coefficient as the reciprocal of related resistance. What could be told from the figure is that the long-wave radiation between glass surface and ambient is ignored, only the radiation between PV cell and vacuum glass was considered by the authors. Results shown in Figure 2.6 indicated that under 1000 W/m^2 continuous exposure from constant indoor solar spectrum, PV cell temperature was much higher in PVVG than in PV laminated glazing. The authors explained that the excellent heat insulation property of vacuum glazing was the main cause. It was also predicted that vacuum glass facing external ambient was suitable for the UK climate whilst vacuum glass facing internal room ambient was applicable for Indian climate. Another study leaded by the same authors mainly focused on colour properties and glazing factors, through which they found that the multicrystalline based semi-tranparent PVVG had high correlated colour temperature and colour rendering index, indicating quality of entering

daylight (Ghosh, Sundaram, & Mallick, 2019). And once again the authors claimed that PVVG had lower SHGC compared to vacuum and single glazing.

2.4.3 PVVG with two layers of glass

A research reports a streamlined structure which merely includes two glass panes to combine PV and VG, as shown in Figure 2.7 (Jarimi, Lv, Omar, Zhang, & Riffat, 2020). It is manufactured by attaching the thin film PV layer to the interior surface of tempered glass and supporting a 0.3 mm vacuum gap between tempered glass and Low-E coated glass with evenly distributed aerogel vacuum pillars. Such a simplified combination of the vacuum glazing and solar cell has an equivalent overall heat transfer coefficient compared with the four-pane structure, which is determined as 0.6 W/(m^2·K) (Jarimi et al., 2019). The whole thermal analysis is mainly established on the basis of the production of the heat transfer coefficient and the temperature difference, as well as the transmitted and absorbed solar radiation. As for the heat transfer within the vacuum gap, a total heat transfer coefficient is used to represent the radiation and conduction through vacuum pillars. However, no detailed heat conduction calculation is performed for the vacuum pillar array and the stress constraints for the thin-film cells are not specified. It is worthwhile to further discuss whether photovoltaic cells in this simplified structure have heat dissipation difficulty under solar radiation, and their power generation efficiency compared to the four-pane structure.

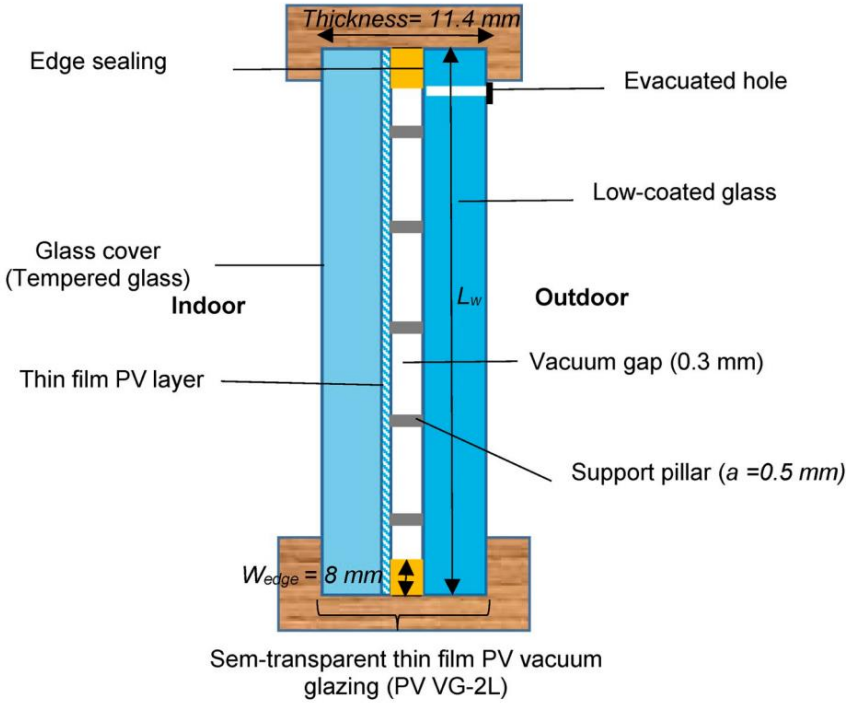

Figure 2.7 The photovoltaic vacuum glazing with two glass layers (Jarimi et al., 2020)

2.5 Research Gaps

The literature review has indicated that photovoltaic vacuum glazing can offer several benefits, such as generating electricity, thermal insulation, and reducing the solar heat gain. However, the research about composite photovoltaic vacuum glazing is still rare, no field test has been conducted to investigate the practical performance of the novel structure. Researchers has improved the thermal performance of photovoltaic laminated glazing with the air cavity, but no work has ever mentioned to further integrate the air cavity into photovoltaic vacuum glazing. There is a lack of systematic study on the overall energy performance of photovoltaic

vacuum glazing for low-energy building. The research gaps based on the literature review are illustrated as follows:

1) The thermal-power performance and energy saving potential of the photovoltaic vacuum glazing requires further investigation with a comprehensive whole building simulation. The applicability of such PV envelope systems in diverse meteorological conditions has not been thoroughly discussed and its integration with other architectural design parameters has not been sufficiently addressed.
2) Existed numerical model to predict the thermal behavior of composite photovoltaic vacuum glazing was built based on steady state and one dimension without a clear and detailed analysis on the heat flow through the whole structure. There is a lack of a 3D thermal model to appropriately describe the whole heat transfer. And few studies have addressed the solar heat gain coefficient, even though it is a very important parameter for PV vacuum glazing.
3) No research has been found that studied the integration of air cavity with photovoltaic vacuum glazing. And the impact from design factors like thermal properties, vacuum pillar dimension and separation, low-e coating and air cavity width have not been investigated. The overall performance of composite photovoltaic vacuum glazing with or without intermediate air cavity also needs investigation.

4) Currently indoor tests are the main approach to find out the thermal and electrical performance of photovoltaic vacuum glazing, and limited work has only tested the horizontally placed samples. Trials have not been done to fabricate the large-scale photovoltaic vacuum glazing and measure the real time data for the practical performance analysis.

5) Current studies merely focus on the comparison between PV vacuum glazing and double glazing. This indicates a need to compare the overall performance of hollow PV vacuum glazing with vacuum glazing, hollow PV glazing and PV vacuum glazing in diverse orientations and climates.

2.6 Objectives and Methodology

Integrating BIPV to replace conventional double glazing has been reported effective to save about 16% building energy with the see-through amorphous silicon (a-Si) solar cells (Zhang et al., 2016). Recent research has reported another glazing combining photovoltaic with vacuum glazing could decrease the overall heat transfer coefficient to a promising low value of 0.8 W/m^2 K (Ghosh et al., 2018), indicating more building energy saving. By contrast, the former structure of semi-transparent BIPV window had an overall heat transfer coefficient of 5.54 W/m^2 K (Zhang et al., 2016), much higher than the combination of photovoltaic and vacuum glazing. Given the excellent thermal performance, the research of solar photovoltaic

integrating vacuum glazing is still in early stage and deserves more detailed and in-depth research. Therefore, the purposes of this thesis comprise of:

1) To investigate the overall energy performance of the photovoltaic vacuum glazing using building energy simulation software and find out the building energy saving potential of integrating the photovoltaic vacuum glazing with passive building design.

2) To propose a novel structure integrating an additional air layer with the photovoltaic vacuum glazing (PVVG) and compare this composite hollow photovoltaic vacuum glazing (HPVVG) with existing photovoltaic vacuum glazing in terms of both thermal and electrical performance.

3) To build a three-dimensional heat transfer model for predicting the temperature distribution of different types of photovoltaic vacuum glazing (including both HPVVG and PVVG with diverse configurations) and analyze the impact of critical design factors on the overall heat transfer coefficient (U-value).

4) To establish a mathematical heat transfer model for evaluating the U-value, solar heat gain coefficient of different types of photovoltaic vacuum glazing and analyze the hourly heat gain and heat loss.

5) To set up experimental apparatus and collect data when photovoltaic vacuum glazing receives zero and real-time sunlight and validated the mathematical heat transfer model.

The annual overall performance of different types of photovoltaic vacuum glazing can be predicted in different climate zones using the validated model.

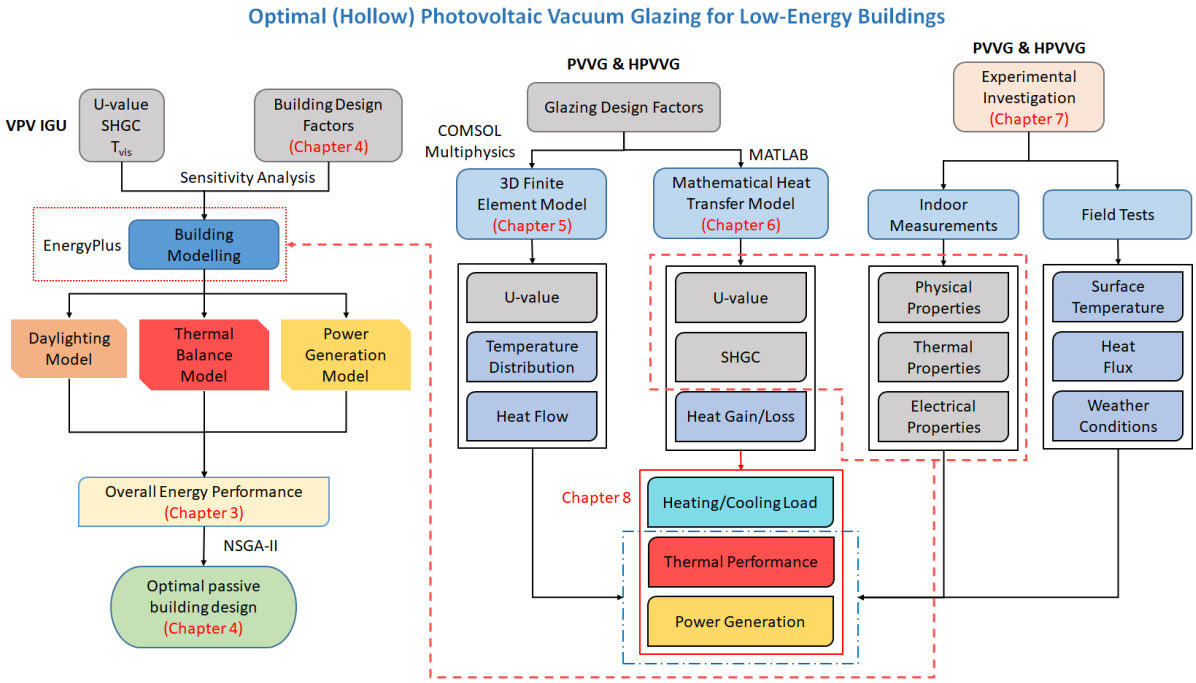

Figure 2.8 Research flow chart

The present study is designed to determine the optimal composite PV vacuum glazing for low-energy buildings. The methodology framework shown in Figure 2.8 mainly involves the development of a modelling platform by combining different simulation tools, statistical analysis methods and optimization algorithms, the establishment of a finite element model and a mathematical model, and the experimental investigation.

First of all, this study presents a comprehensive investigation of the thermal, lighting, and power performance of a novel vacuum photovoltaic insulated glass unit (VPV IGU) as well as an integrated design optimization of photovoltaic envelope systems. A prototype office

building model with a curtain wall design is first constructed in EnergyPlus to compare the heat gain, heat loss, thermal load, lighting energy and PV generation for different curtain walls. Furthermore, screening and variance-based sensitivity analyses are conducted to prioritize building integrated photovoltaic design parameters with respect to specific weather conditions. The selected important design parameters are then optimized with the non-dominated sorting genetic algorithm-II (NSGA-II) to determine the optimal passive building design with the application of PV vacuum glazing.

Then, this study proposes an integrated photovoltaic vacuum glazing unit with an intermediate air cavity and a calibrated modelling approach to quantify its thermal properties and evaluate the heat transfer performance. Theoretical analyses of the heat transfer process are conducted with reasonable hypotheses and traceable boundary conditions. Three-dimensional heat transfer models are then established and cross-validated against previous publications. The detailed validation demonstrates the reliability of the developed complex models under different circumstances. Furthermore, four photovoltaic vacuum glazing configurations are compared in terms of the temperature distribution and overall heat transfer coefficient.

This study also seeks to provide an approach to evaluate the U-value and solar heat gain coefficient of photovoltaic glazing with different structures and identify the optimal one for

various climate zones in terms of the thermal and power performance. A comprehensive heat transfer analysis is presented, and a mathematical heat transfer model is established and validated against published references. For further validation with experimental data, a test rig is built for both indoor and outdoor experiments to study the thermal and electrical performance of different photovoltaic glazing. Physical parameters including thermal conductivity, optical and electrical properties are measured. Hollow photovoltaic glazing, photovoltaic vacuum glazing and hollow photovoltaic vacuum glazing are evaluated through experiments and numerical simulations, with double glazing and vacuum glazing as the baselines. The U-value and solar heat gain coefficient will then be obtained for different glazing, and the comprehensive comparison will as well be conducted considering the detailed impact of the Low-E coating, and variation of orientations and climates, to decide the proper composite PV vacuum glazing for low-energy buildings.

CHAPTER 3 DEVELOPMENT OF SIMULATION MODELS FOR ANALYZING THE ENERGY SAVING POTENTIAL OF PHOTOVOLTAIC VACUUM GLAZING

This chapter is designed to explore the energy saving potential of applying photovoltaic vacuum glazing into buildings, which is also a preliminary investigation and a benchmark for the further optimization study with passive building design in the following Chapter 4. Overall building energy performance is analysed considering the heat gain and loss through windows, electricity used for lighting, equipment, cooling and heating, and photovoltaic power generation.

3.1 Building modelling

The PV vacuum glazing and other alternative glazing materials are first composed in WINDOW and then incorporated with EnergyPlus to perform dynamic building performance modelling.

3.1.1 Simulation tools

EnergyPlus 8.8.0 serves as the major simulation tool to evaluate both building energy consumption and photovoltaic power generation. It has been broadly recognized as a robust

building performance prediction tool, whose accuracy has been validated by multiple existing studies (Delgarm, Sajadi, Kowsary, & Delgarm, 2016; Khoroshiltseva, Slanzi, & Poli, 2016). Building geometries, thermal zones, operation schedules, internal loads, illumination and HVAC systems as well as power generators are modelled by inter-connected submodules of EnergyPlus. Energy meters are then used as post-processors of on different categories of energy demand and supply.

WINDOW 7.5 holds a vast database of miscellaneous windows composed of single or multiple layers with difference choices of frames. It can generate window properties including U-factor (or U-value), SHGC (solar heat gain coefficient), and visible light transmittance. Among these three parameters, U-value describes the overall heat transfer, with a lower value indicating a better thermal insulation performance (Cuce, 2018). SHGC represents the percentage of incident irradiance which eventually penetrates the glazing, through either direct transmittance or secondary inward radiation from the part absorbed by the glazing panel (Marinoski, Güths, Pereira, & Lamberts, 2007). The visible light transmittance (VT) refers to how much visible light passes through a window, having an immediate impact on the daylight and visual comfort performance (Zhang & Lu, 2017). For clear glazing, the light-to-solar gain ratio (LSG), presented as VT/SHGC, is generally around 1.0. However, spectrum selective glazing can increase this value up to 3.0, making it an important variable for balancing indoor

daylight and thermal performances (Alvarez et al., 2004; Gueymard & DuPont, 2009; Omar & Al-Ragom, 2002). The active PV module area (PVA) on the window is then determined to vary with VT as a dependent design variable.

Table 3.1 shows thermal and optical parameters of curtain wall glasses adopted in four different simulation models.

Table 3.1 Settings of all windows in different models

Model	**U-factor(W/m^2-K)**	**SHGC**	**VT**
NDP	2.63	0.703	0.786
NP	2.63	0.703	0.786
STPV	5.497	0.471	0.153
VPV	0.557	0.143	0.120

Windows in former three models are derived from the glazing system library in WINDOW, while the property of vacuum photovoltaic insulated glass unit, shortly named as photovoltaic vacuum glazing (PVVG) in the remain part of this thesis, is obtained from previous outdoor and indoor measurements (M. Wang et al., 2016; Zhang et al., 2017). Model NDP (without PV module and daylight control) and Model NP (without PV module and with daylight control) share the same typical double pane clear glazing. Model VPV (with vacuum PV glazing) is characterized by the lowest SHGC and U-value, while model STPV (with single-glazed semi-

transparent PV) presents the worst-case in the overall heat transfer performance (i.e., U-value). An extremely low LSG of 0.325 indicates the poor thermal and daylight performance of STPV.

3.1.2 Weather conditions

Because vacuum glazing is usually not openable especially in a commercial building design, its application in temperate zones is restricted when natural ventilation strategies are usually adopted to modulate indoor thermal comfort (X. Chen & Yang, 2017, 2018). Therefore, the PVVG curtain wall system is only examined in a cooling dominated climate in Hong Kong (HK) and a heating dominated climate in Harbin (HB). The two cities are representing the hot summer cold winter and severe cold zones of China with abundant solar radiation resources. The typical weather data of Hong Kong takes the form of IWEC (International Weather for Energy Calculations), while that of Harbin comply with the CSWD (Chinese Standard Weather Data) format. The major difference between the two climates lies in the outdoor dry bulb temperature and solar radiation as shown in Figure 3.1. The apparently lower outdoor temperature from October to April leads to the heating-dominated condition in HB, while more solar resources are available in Harbin especially in the summer period due to longer daytime and less cloudy/rainy days.

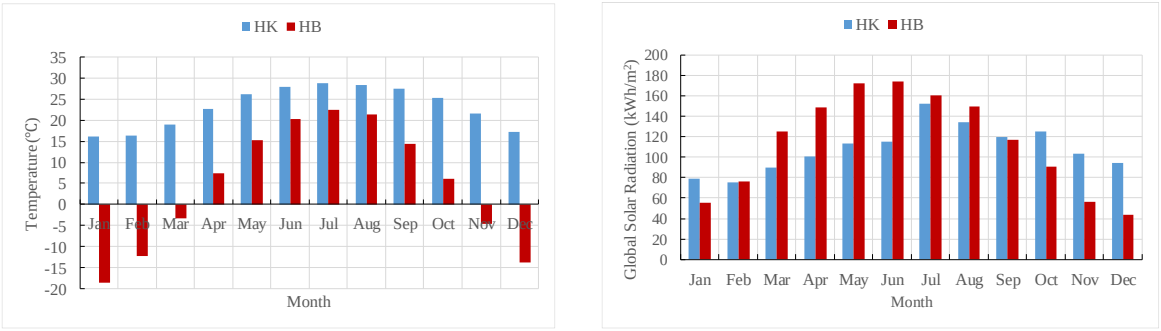

a. Monthly dry bulb temperature

b. Monthly solar radiation

Figure 3.1 Weather conditions in Hong Kong and Harbin

3.1.3 Model setting

The building model with curtain wall systems was developed from the commercial prototype buildings covering 80% of the total floor area in U.S. Original model settings are referenced to ANSI/ASHRAE/IES Standard 90.1, while they are modified according to the Building Energy Code issued by EMSD of HKSAR and BEAM Plus guidelines from the Hong Kong Green Building Council. As shown in Figure 3.2, the typical floor, whose total floor area is 540 m^2 and height is 3 m, is divided to five independent air-conditioning zones, including four perimeter zones facing different orientations and one internal zone (i.e., core zone). The area of this internal zone takes up 40.47% of the total floor area. The window to wall ratio (WWR) of all perimeter zones is evenly set to 83.33%, representing the scenario of curtain walls. In addition to basic building information, the sources of miscellaneous internal gains are

presented in Table 3.2, including the occupancy, lighting, electric equipment and outdoor air flow.

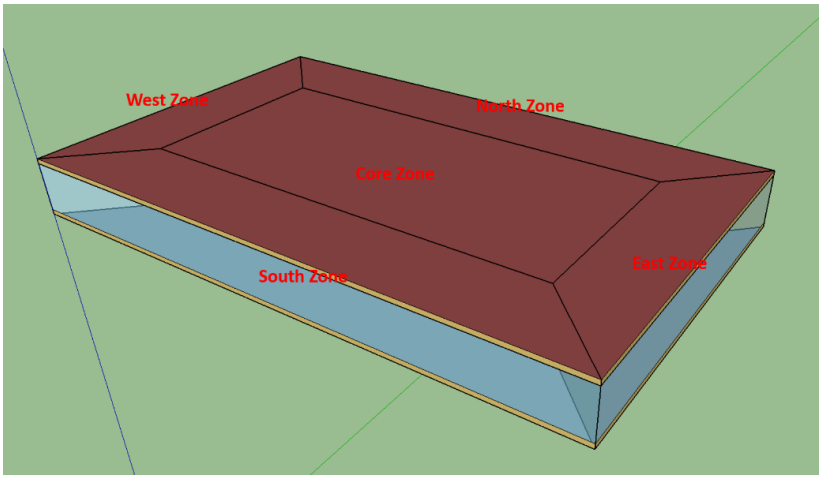

Figure 3.2 Typical floor of the building model

Table 3.2 Basic parameters in all simulation models

Type	**Data**
Occupancy	8 m^2/person
Lighting	12 W/m^2
Equipment	10 W/m^2
Outdoor air flow	0.008 m^3/s·person

The ideal loads air system (IdeaLoadsAirSystem module in EnergyPlus) is adopted to provide required heating and cooling with 100% energy conversion efficiency as a simplified HVAC system to maintain the research focus on the influence of the building envelope. The cooling and heating demand of the building are obtained with HVAC setpoints kept at 24 ℃

and 21 ℃ respectively. The cooling period is assumed to be from May to September, while the rest time of a typical year is considered as the heating period in the simulation. Infiltration with a constant air change rate and availability schedule is assumed for all four perimeter zones.

The lighting dimming control is used in Model VPV, Model NP and Model STPV, where a reference illuminance level over 300 Lux is considered sufficient for utilizing natural lighting (Nabil & Mardaljevic, 2006). The position and the quantity of the reference point depend on the different lighting needs of the working situation. In this simulation study, only one reference point is set at the middle of each external zone (i.e., 2 m away from the external facade).

Power generation from PV curtain wall systems are predicted with implanted generator models. Since the Equivalent One-Diode and Sandia model require more detailed experimental data which cannot be confirmed in the early design stage, the Simple model is selected to estimate PV energy supplies based on the assumption of an average efficiency standard test conditions (STC) as specified in Table 3.3 (M. Wang et al., 2017; Zhang et al., 2016). The annual electricity and peak power generation can be quickly obtained by this simplified model, which can increase the calculation efficiency in the initial design. Apart from PV panels applied on windows, 90% of opaque facade areas are assumed to be coupled with monocrystalline silicon photovoltaic panels with a conversion efficiency of 15% (Jelle et al., 2012).

Table 3.3 Photovoltaic parameters

Model	Conversion Efficiency	Reference
STPV	5.9%	(X. Chen & Yang, 2018)
VPV	6.3%	(Omar & Al-Ragom, 2002)

3.2 Thermal and Power Generation Properties

This section mainly demonstrates the thermal and power generation properties of the vacuum PV glazing in comparison with other available glazing materials in the building industry. The heat transfer through windows, lighting energy, HVAC demand and power generation in different modelling scenarios are analysed and discussed.

3.2.1 Heat gain and loss through windows

The heat gain and loss through windows in the two climatic conditions are first predicted by EnergyPlus. As shown in Figure 3.3, the prototype office building gains more heat through windows in Hong Kong than in Harbin. With the same settings of window properties, Model NDP and Model NP exhibit similar heat gain levels in both climates. A remarkable reduction in the heat gain can be observed when PV glazing is adopted in Model VPV and STPV. Model VPV gets the lowest heat gain among the four models, leading to a reduction of 81.63% in

Hong Kong and 75.03% in Harbin compared with Model NDP. This result validated the excellent thermal performance of PVVG in isolating solar radiation.

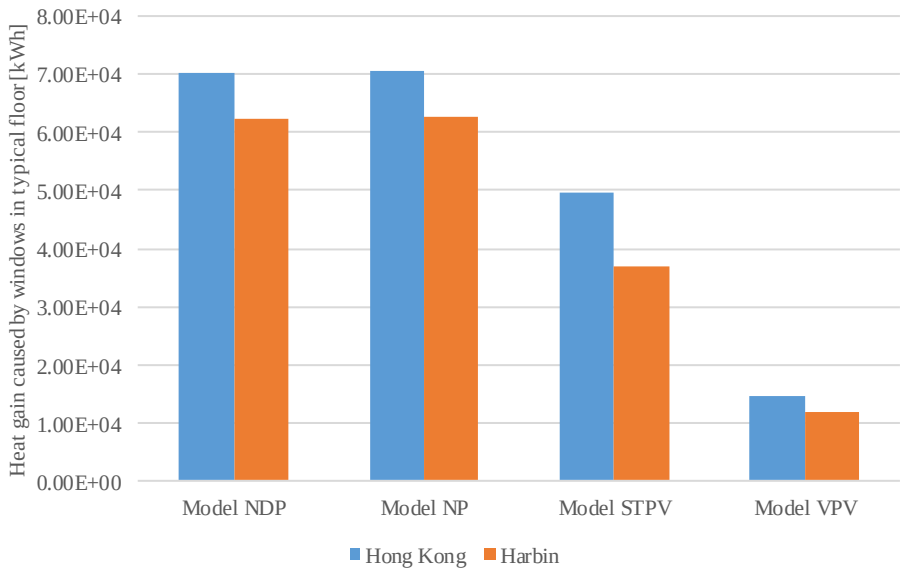

Figure 3.3 Heat gain through windows in typical floor

As for the heat loss through windows, Figure 3.4 clearly indicated that the office building in Harbin is subject to more heat losses due to lower outdoor temperatures through most time of a typical year. The difference of heat losses between two climates is much more conspicuous than that of heat gains. Similar to heat gain conditions, heat losses of Model NDP and Model NP are very close, indicating a minor influence of the daylight control strategy on the indoor thermal environment. Compared with Model NDP, Model VPV achieved a 31.94% and 32.03% reduction of the heat loss in Hong Kong and Harbin respectively, where the excellent thermal performance of PVVG is highlighted again. However, it is noteworthy that Model

STPV lost more heat than Model NDP and Model NP, possibly caused by its relatively higher U-value.

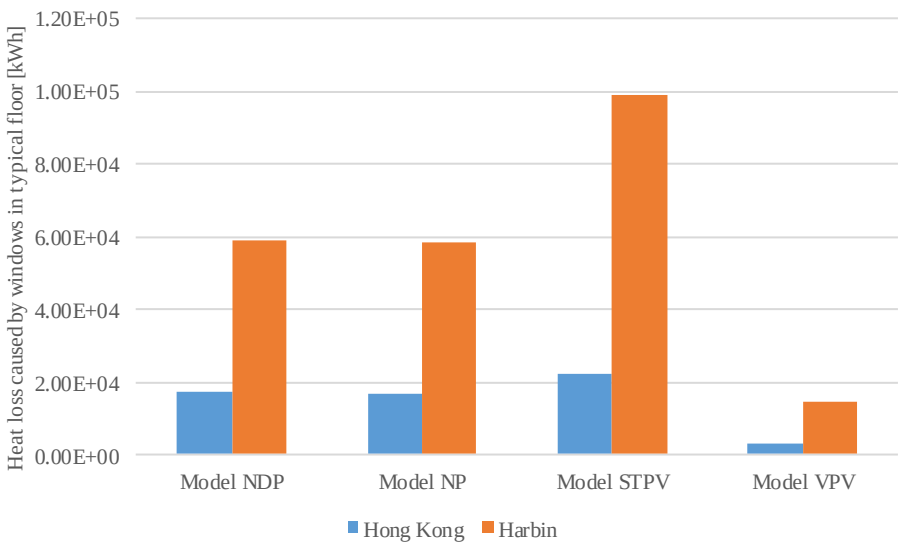

Figure 3.4 Heat loss through windows in typical floor

3.2.2 Lighting and equipment electricity use

Lighting energy consumption of the four models in Hong Kong and Harbin is presented in Figure 3.5. It can be found that Model NDP consumes the highest lighting energy in the two climates, because no daylight control is adopted for energy saving. According to the graph, Model NP, Model STPV and Model VPV consume more energy in Harbin, because of less available daylight access at higher latitudes. Among these three models, a slightly growing tendency can be observed in lighting energy use because PV windows impaired the visible light transmittance. Comparing all models, it can be found that the setting of daylight controls can contribute to an energy saving up to 9.32% (maximum difference between Model NP and NDP).

When it comes to the demand of miscellaneous equipment, all four models share the same schedule and peak power setting, leading to an equal annual consumption. Specific data will be given in the following analysis and tabular summary.

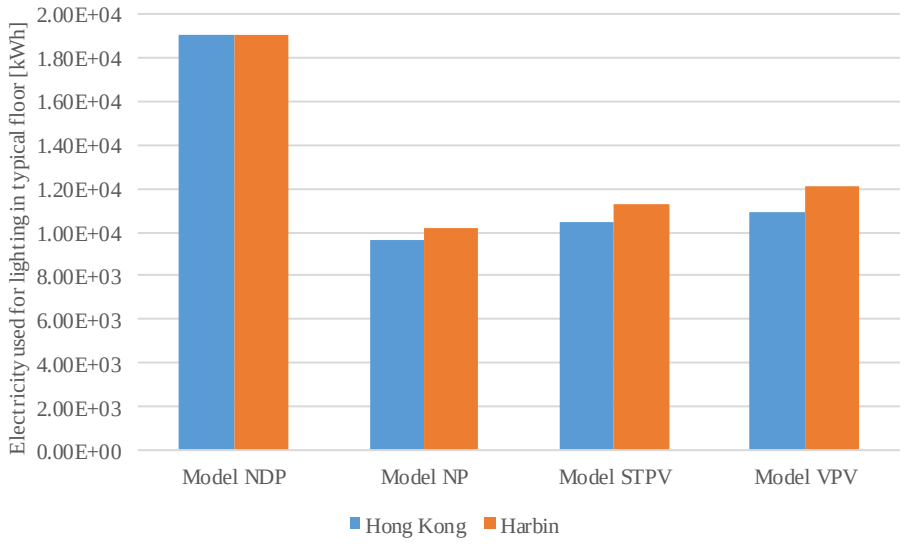

Figure 3.5 Electricity used for lighting in typical floor

3.2.3 Heating electricity use

Heating energy consumption in Hong Kong and Harbin is presented in Figure 3.6, where the building in Hong Kong has almost zero heating demand due to its warm and short winter. Although it might be hard to tell from the figure, the heating energy use in two cities has identical trend in which Model STPV consumes the most energy and Model VPV consumes the least. The best heat insulation performance of Model VPV, represented by its lowest U-value, is identified as the main contributor to the heating energy reduction. In addition, the

heating energy in Model NP slightly exceeded that in Model NDP, because the daylight control also decreased the internal gain from lighting facilities.

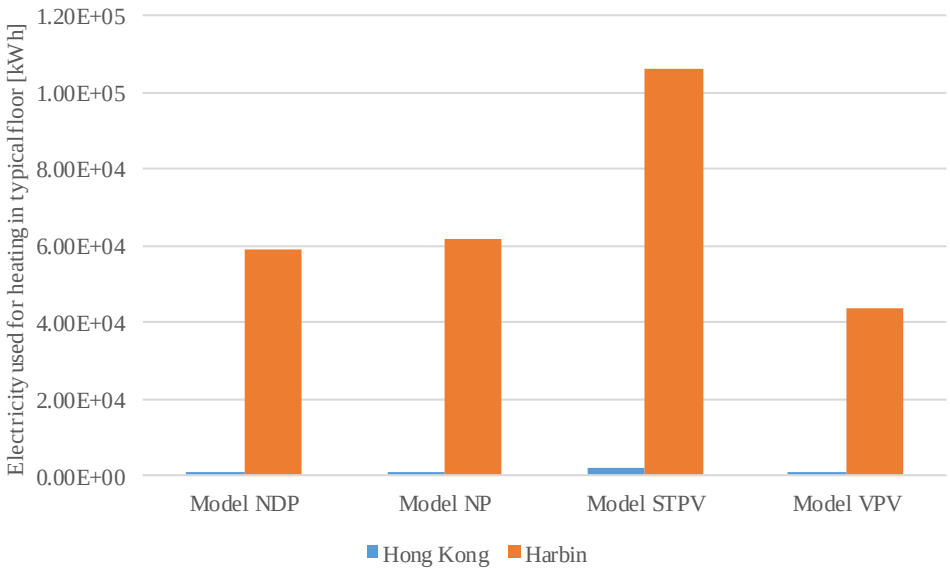

Figure 3.6 Electricity used for heating in typical floor

3.2.4 Cooling electricity use

On the contrary, building models in Hong Kong consume more cooling energy than Harbin, with a smaller gap between the two cities compared to Figure 3.6. The cooling consumption of each model in Hong Kong almost tripled that in Harbin. Figure 3.7 shows a gradual reduction of the cooling energy among the four models, leading to a decrease more than 50% in Harbin. The reduction can be mainly attributed to the daylight dimmable control and low SHGC. The daylight control lowered the cooling demand by removing the lighting heat gain, which can be clearly observed by comparing Model NDP and Model NP. Low SHGC of PV glazing contributes to the cooling load reduction by restricting the penetration of solar

radiation. Similar to the scenario of heating energy, Model VPV is predicted with the lowest cooling energy consumption.

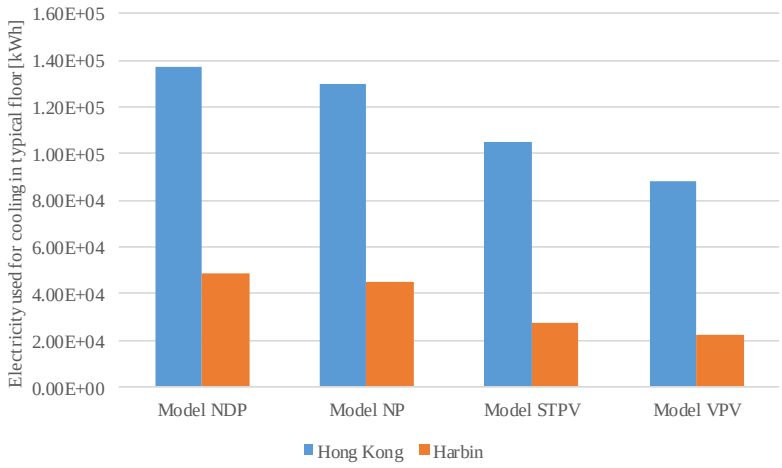

Figure 3.7 Electricity used for cooling in typical floor

3.2.5 PV power generation

Figure 3.8 compares the power generation of all vertical façades in models with PV glazing in Hong Kong. Model VPV produces slightly more electricity than Model STPV, which can be seen in each façade as per the bar chart. This trend is also shown in Figure 3.9 for building models in Harbin. Model STPV generates slightly less electricity due to its lower power conversion efficiency. South-facing PV glazing always yields the most electricity among four building facades across the two climates. Especially in Harbin, the output of south façade almost takes up half of the total power generation. The difference between Hong Kong and Harbin appears among north, west and east facades. In Hong Kong, the disparity of the electricity yield between these three facades is quite small, whereas it is more apparent in

Harbin. Besides the south façade, the west façade ranks second in power generation which is followed by the east and north façade in sequence. This is mainly caused by the variety in both the global solar radiation and solar altitude between the two climates.

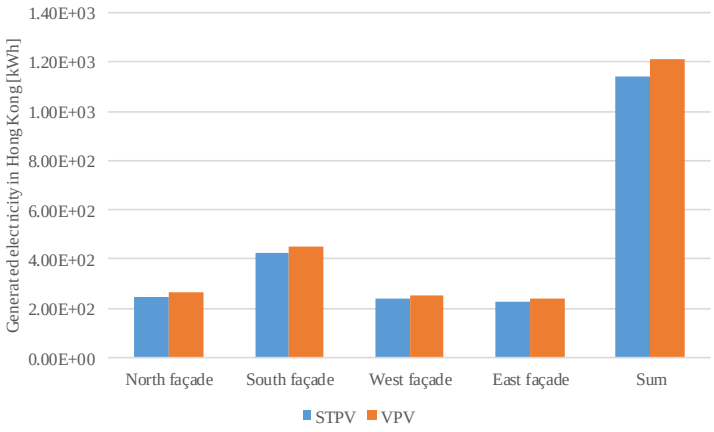

Figure 3.8 Generated electricity in Hong Kong

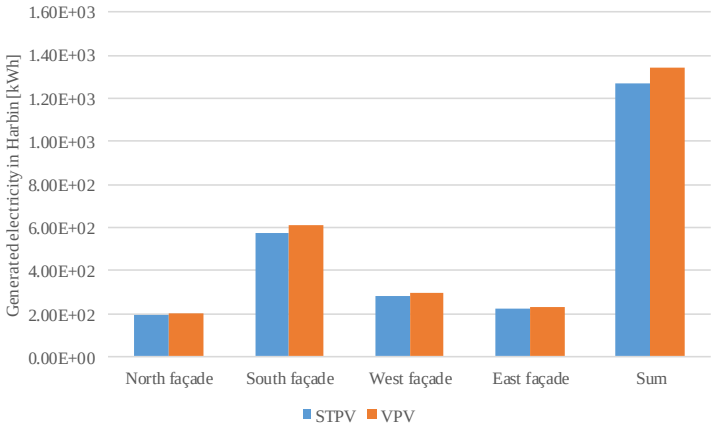

Figure 3.9 Generated electricity in Harbin

3.3 Overall building energy performance

The total building energy demand is calculated by summing up lighting, equipment, heating and cooling loads, which are illustrated in Table 3.4 and If power generation is

considered when calculating the net purchased energy as per Table 3.6, the energy saving of Model STPV and Model VPV can be further increased. On top of the demand reduction, the total energy use can be reduced by up to 37.79% and 39.82% in Hong Kong and Harbin. PVVG is therefore proved to be slightly more suitable for replacing the traditional double-pane clear glazing in cold areas like Harbin. On the contrary, the STPV curtain wall still consumes more net purchased energy in Harbin because its power generation cannot neutralize the additional building demand.

Table 3.5. The daylight control brings about nearly 9.32% and 6.58% lighting energy saving in Hong Kong and Harbin. Although Model STPV achieved energy saving (i.e., 21.82% compared with Model NDP) in Hong Kong, it increased the total demand by 12.11% in Harbin. Model VPV, however, achieved the most saving of 31.94% and 32.03% compared to Model NDP in both climates. The application of PVVG curtain wall is preferable for reducing energy demands even when the electricity production is not included.

Table 3.4 Building Energy Consumption of each model in Hong Kong

Energy Uses [kWh]	**Lighting**	**Equipment**	**Heating**	**Cooling**	**Sum**	**Consumption Saving**
Model NDP	19046.02	24229.80	324.74	137353.27	180953.83	-
Model NP	9657.97	24229.80	466.72	129729.55	164084.04	9.32%

Model STPV	10491.29	24229.80	1681.78	105072.47	141475.34	21.82%
Model VPV	10945.33	24229.80	169.20	87813.58	123157.91	31.94%

If power generation is considered when calculating the net purchased energy as per Table 3.6, the energy saving of Model STPV and Model VPV can be further increased. On top of the demand reduction, the total energy use can be reduced by up to 37.79% and 39.82% in Hong Kong and Harbin. PVVG is therefore proved to be slightly more suitable for replacing the traditional double-pane clear glazing in cold areas like Harbin. On the contrary, the STPV curtain wall still consumes more net purchased energy in Harbin because its power generation cannot neutralize the additional building demand.

Table 3.5 Building Energy Consumption of each model in Harbin

Energy Uses [kWh]	**Lighting**	**Equipment**	**Heating**	**Cooling**	**Sum**	**Consumption Saving**
Model NDP	19046.02	24229.80	59047.98	48865.83	151189.63	-
Model NP	10179.87	24229.80	61951.93	44876.99	141238.59	6.58%
Model STPV	11274.69	24229.80	106366.17	27628.59	169499.25	-12.11%
Model VPV	12098.90	24229.80	43815.53	22625.94	102770.17	32.03%

Table 3.6 Overall energy use in Hong Kong and Harbin

City	**Subcategory**	**Model NDP**	**Model NP**	**Model STPV**	**Model VPV**
HK	Total electricity use	180953.83	164084.04	141475.34	123157.91

	Electricity production	-	-	9985.82	10592.80
	Purchased electricity	180953.83	164084.04	131489.52	112565.11
	Saving percentage	-	9.32%	27.34%	37.79%
HB	Total electricity use	151189.63	141238.58	169499.25	102770.17
	Electricity production	-	-	11106.12	11781.20
	Purchased electricity	151189.63	141238.58	158393.13	90988.97
	Saving percentage	-	6.58%	-4.76%	39.82%

The purchased electricity of each model in the two cities is presented in Figure 3.10. The total electricity shows a monotonous descending tendency in Hong Kong, but such trend is interrupted by Model STPV in Harbin for above mentioned reasons.

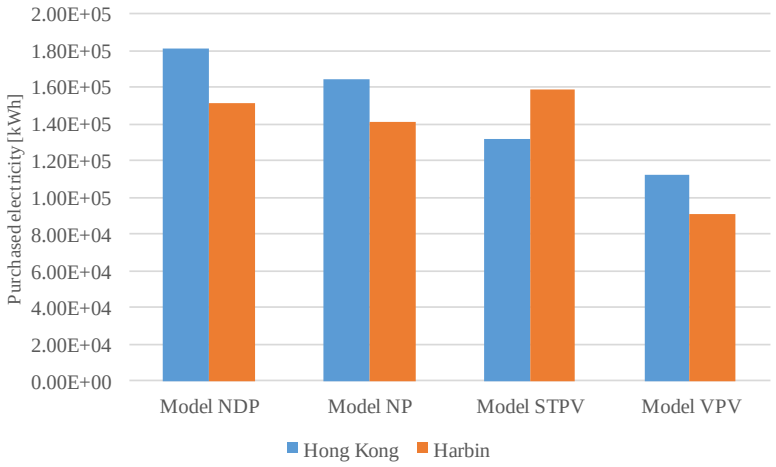

Figure 3.10 Purchased electricity in the building models for the two climates

3.4 Summary

This chapter investigated the energy-saving potential and applicability of a novel PV

vacuum glazing in high-rise commercial buildings under diverse climatic conditions. Hong Kong and Harbin are selected as representative cities in hot summer warm winter and severe cold areas for modelling experiments. Comparisons of building thermal and energy performances were conducted with different curtain walls and control strategies.

The PV vacuum glazing can reduce up to 81.63% and 75.03% of heat gain in Hong Kong and in Harbin compared to the baseline window system. Meanwhile, heat loss can be decreased by 31.94% and 32.03% in the two climatic areas. Although the conventional semi-transparent PV (STPV) also performed well in reducing heat gain, it caused extra heat loss especially in cold areas. Above differences highlighted the excellent thermal insulation performance of the vacuum glazing in minimizing convective and radiative heat transfers.

When comparing buildings with PVVG (i.e., Model VPV) to buildings without the PV glazing and daylight control (i.e., Model NDP), approximately 32% reduction of the energy demand can be observed in both Hong Kong and Harbin. Furthermore, PV power supplies can further increase the saving of total energy use to 37.79% and 39.82% in the two areas. It can be also found that daylight controls can contribute to an energy conservation up to 9.32% for indoor lighting. All simulation models share the same energy consumption in equipment because of the uniform setting. On the contrary, the conventional STPV curtain consumed more net purchased energy in cold areas because its power generation cannot neutralize its addition

to building demands.

CHAPTER 4 OPTIMIZATION OF BUILDING ENERGY PERFORMANCE UTILIZING PHOTOVOLTAIC VACUUM GLAZING IN PASSIVE BUILDING DESIGN

To further validate the applicability of PVVG and maximize overall building energy performance, an integrated sensitivity analysis and design optimization is conducted by addressing major architectural design factors in the prototype high-rise commercial building.

4.1 Building Design Optimization

High-rise commercial buildings in Hong Kong usually adopts curtain wall as the external building envelope. To maximize the overall energy efficiency of PV curtain wall systems, extensive sensitivity analyses (SA) and optimizations are necessary for facilitating the resource allocation and decision-making to design low-energy buildings. Global sensitivity analysis with screening-based and variance-based methods are proved to be suitable for non-linear and non-additive building models with complicated envelope designs (Tian & Wei, 2013). Morris is a classic screening-based SA approach, where the relative importance of design factors can be qualified with a small sampling dimension (Campolongo & Saltelli, 1997; Menberg, Heo, & Choudhary, 2016). Silva et al. conducted an initial sensitivity analysis with Morris for a multi-criteria decision-making process to improve building energy and thermal performances

(Santos Silva et al., 2016). The non-linear effect and relative importance of design factors were successfully identified for the factor prioritizing and fixing. The Fourier Amplitude Sensitivity Test (FAST) method, on the other hand, can quantify the influence of each design factor on the model output (X. Chen, Yang, & Sun, 2017; Van Hooff, Blocken, Timmermans, & Hensen). Mechri et al. conducted the analysis of variance (ANOVA) for the energy performance of an office building regarding the building compactness, orientation, envelope thermal properties and local shadings (Mechri, Capozzoli, & Corrado, 2010). The methodology was proved useful for architects to evaluate the exact impact of each design strategy. ANOVA with FAST was applied to quantify the influence of design parameters over the available solar radiation on building facades. The building location, orientation and shading feature were determined to be the top three factors responsible for the major uncertainty of solar fractions.

The identified key design factors can then be subject to an integrated optimization of the overall building energy performance by simultaneous considering the lighting, cooling, heating, and PV energy. Ascione et al. conducted a two-stage cost-optimal analysis of energy retrofit measures with the combination of EnergyPlus and MATLAB (Ascione, Bianco, De Stasio, Mauro, & Vanoli, 2016). The energy retrofit measures mainly focus on the thermal properties of external building envelope and energy recovery systems. The developed multi-stage optimization approach was also applied in the design of a net-zero energy building in the

Mediterranean climate, where the property of building geometry and phase changing materials were also investigated (Ascione, De Masi, de Rossi, Ruggiero, & Vanoli, 2016). Multi-objective optimizations involving the lighting, cooling and heating loads were conducted based on both the swarm intelligence and genetic algorithm (Carlucci, Cattarin, Causone, & Pagliano, 2015; Méndez Echenagucia, Capozzoli, Cascone, & Sassone, 2015). These studies also investigated the influence of window thermal and geometric properties under different climatic conditions. Apart from building energy and economic indices, indoor environmental performances including the thermal comfort, visual comfort and air quality were also investigated by a multi-objective optimization with the combination of GenOpt and EnergyPlus. Multi-dimensional Pareto optima were obtained to offer design alternatives for decision-makers to reach the final design solution. Adaptive variation of optimization settings was also conducted to derive the most suitable configuration of genetic algorithms (X. Chen, Yang, & Zhang, 2018). In addition, surrogate models of traditional simulation tools were incorporated into the optimization process to significantly improve the computation efficiency. Extensive modelling experiments can then be completed within a short time period for a swift decision-making in an early design stage (X. Chen & Yang, 2017).

4.2 Integrated sensitivity analysis and design optimization

To further achieve a holistic design optimization process for daylight, thermal performance and power generation of PV envelope systems, a joint parametric optimization platform is developed with the combination of EnergyPlus and R programming. The probability distribution function is first determined for all related architectural design parameters and a correlation test is conducted to identify the appropriate sensitivity analysis methods. Morris and FAST methods are then conducted to qualify and quantify the significance of design factors in non-linear or non-additive models.

Morris is a popular screening-based SA method to qualify the relative importance between design factors by statistics developed from the Elementary Effect (Saltelli, Tarantola, Campolongo, & Ratto, 2004):

$$EE_i(x) = \frac{\left[y(x_1, x_2, \cdots x_{i-1}, x_i + \Delta, \cdots x_k) - y(x)\right]}{\Delta} \tag{4.1}$$

Morris can explore the input design space efficiently with a randomized "one factor at a time" modelling experiment. The mean μ (stands for the main effect of input variables) and standard deviation σ (stands for the non-linearity and interaction with other variables) of the Elementary Effect are then defined as sensitivity measures:

$$\mu = \sum_{i=1}^{r} EE_i / r \tag{4.2}$$

$$\sigma = \sqrt{\sum_{i=1}^{r} (EE_i - \mu)^2 / r} \tag{4.3}$$

The variance-based method is then conducted to quantify the sensitivity indices and validate the ranking of importance obtained from Morris. The total variance of the output is decomposed as Eq. (4):

$$V(Y) = \sum_{i=1}^{k} V_i + \sum_{j>i}^{k} V_{ij} \cdots + V_{12\cdots k} \tag{4.4}$$

The relationship between different orders of sensitivity indices can be obtained from:

$$1 = \sum_{i=1}^{k} S_i + \sum_{j>i}^{k} S_{ij} + \cdots + S_{12\cdots k} \tag{4.5}$$

where S_i is called the first-order sensitivity index which is used to prioritize different design inputs. The total sensitivity index summarizing all orders of sensitivity indices are expressed by Eq. (6).

$$S_{Ti} = S_i + \sum_{j\neq i}^{k} S_{ij} + \cdots + S_{i\cdots j\cdots k} \tag{4.6}$$

Based on selected important design parameters from SA, a multi-objective optimization with NSGA-II is applied to explore the optimum design for specific outdoor weather conditions. The crossover and mutation probability are set to be 0.9 and 0.355 according to a previous modelling experiment conducted by the authors (X. Chen et al., 2018). The population size is determined as 18, twice the dimension of input variables. To obtain a single final solution, the weighted sum method is adopted by allocating equal weightings to all energy aspects (i.e., the

lighting, cooling, heating demand and PV generation supply) with the net building energy consumption as the univariate optimization target.

4.3 Design input intercorrelations

Before conducting the sensitivity analysis, the distribution of building envelope design parameters is first determined as Table 4.1.

Table 4.1 Value ranges of design parameters

Design parameter	**Acronym**	**Value range**	**Baseline value**
Building Orientation (°)	BO	0~180°	0
Wall Specific Heat (J/kg·K)	WSH	800~2000	840
Visible Light Transmittance	VT	0.24~0.9	0.786
Wall Thermal Resistance (m^2·K/W)	WTR	0.09~6.25	0.136
Light to Solar Gain Ratio	LSG	1.0~2.4	1.118
Window to Wall Ratio	WWR	0.1~0.8	0.833
Window U-value (W/m^2·K)	WU	0.2~6	2.630
Overhang Projection Fraction	OPF	0.0~0.6	0.000
Infiltration Air Changes per Hour	IACH	0.05~1.5	0.600

The building orientation (BO), wall specific heat (WSH), visible light transmittance (VT), wall thermal resistance (WTR), light to solar gain ratio (LSG), window to wall ratio (WWR), window U-value (WU), overhang projection fraction (OPF), and infiltration air changes per hour (IACH) are chosen as model inputs distributed uniformly in specified ranges based on existing literatures and sustainable building guidelines (X. Chen & Yang, 2018). The benchmarking value of each design parameter (i.e., in Model NDP) is presented for comparative analyses.

The correlation between 9 design parameters is first analysed with colour-painted ellipse and rectangular areas in the upper and lower parts of the matrix shown in Figure 4.1 Correlogram of design input intercorrelationsFigure 4.1. The blue proportion filling the ellipse in clockwise directions means positive reciprocity between two corresponding factors, while the red one filling anti-clockwise directions indicates negative correlation. Darker colours and higher saturation signify stronger correlations. Rectangles at lower left half of the figure indicate the same relationship as those ellipses. As a result, WWR and ICAH have the strongest positive reciprocity while BO and WTR have the strongest negative correlation. These inter-correlations and covariate characteristics indicated that linear regression analysis is not suitable for this sensitivity analysis, so that Morris and FAST methods are used instead.

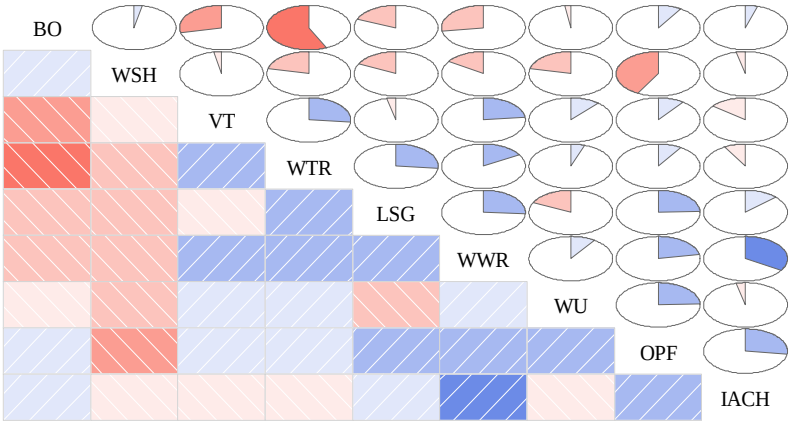

Figure 4.1 Correlogram of design input intercorrelations

4.4 Qualitative analysis of design input

Sensitivity analysis with 100 modeling experiments was first conducted with the Morris method. A scatter plot with three reference lines is illustrated as Figure 4.2, which describes the relationship between the model input and output. Based on the absolute value of μ, WWR (window to wall ratio) and VT (visible light transmittance) can be identified as the two most influential design factors in Hong Kong. WWR lies between the line σ/μ=0.5 and σ/μ=0.1, indicating a monotonic relationship with the total building energy consumption. VT lies between the line σ/μ=0.5 and σ/μ=1.0, is thus considered almost monotonic with the model response (Garcia Sanchez, Lacarrière, Musy, & Bourges, 2014; Menberg et al., 2016). Following these two factors, LSG (light to solar gain ratio) and WU (window U-value) are also identified as significant parameters by their relatively high μ values. OPF (overhang projection fraction) also seems to have an important role in the building design but its exact impact on the

energy usage needs further quantitative analysis. Remaining factors gathering around the corner of the chart (i.e., WTR, IACH, BO and WSH) are therefore of minor importance to the model response judging by their low μ and σ values.

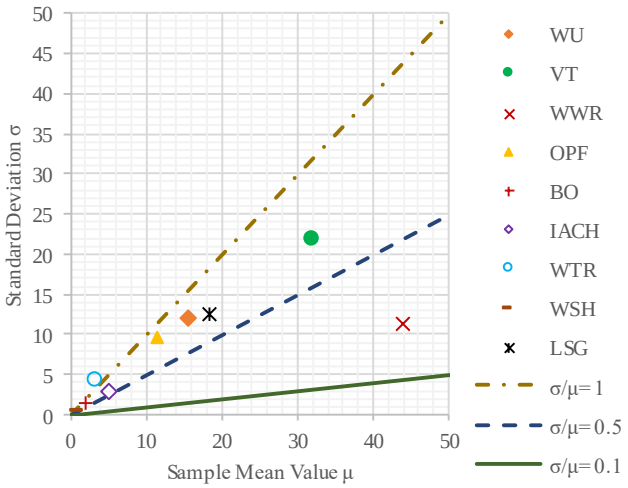

Figure 4.2 Morris indices in Hong Kong

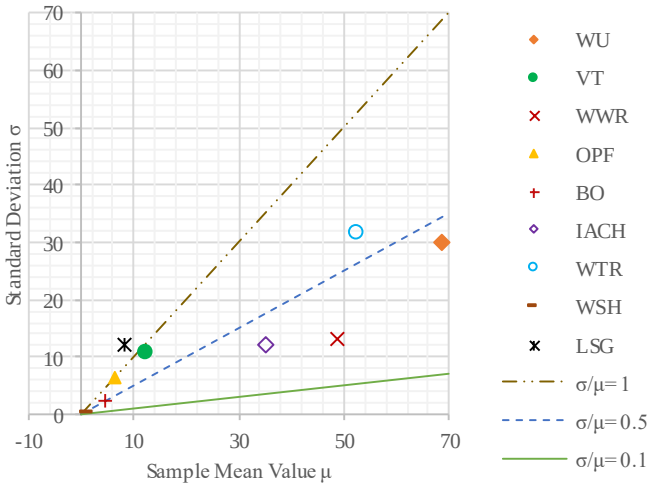

Figure 4.3 Morris indices in Harbin

Except WTR, which lies above the line σ/μ=1.0 and holds a non-linear and non-monotonic relationship with the model response, most factors are almost monotonically correlated with

the building energy consumption. Furthermore, given the fact that no design parameter lies under the line $\sigma/\mu=0.1$, the model output is clearly not linearly correlated with any design input, so that the most commonly used linear regression analysis is again proved to be not suitable for this SA. The above qualitative SA can be easily obtained with merely 100 simulation runs but cannot decide the exact contribution of each design factor to the variation of building energy consumption, leading to the necessity of further quantitative analyses.

Unlike Hong Kong, Morris indices in Harbin, as shown in Figure 4.3, identified WU, WTR, WWR and IACH as the top four influential design parameters in sequence. Among these four factors, WTR (wall thermal resistance) has an almost monotonic relationship while the others have monotonic relationship with the model response. Besides the window geometry (WWR) and its thermal property (WU), wall insulation (WTR) and airtightness (IACH) are also considered to have significant impact on the building energy consumption in cold areas.

4.5 Quantitative analysis of design input

To quantify the exact impact from each design input, first-order sensitivity indices based on FAST are presented in Figure 4.4 and Figure 4.5 below with more than 5000 simulation runs in each climate (Mechri et al., 2010). It can be seen from Figure 4.4 that WWR ranks first among all design factors with a contribution of 47.43% to the variation of building energy consumption. The second important factor is VT, which is followed by LSG and WU,

accounting for 20.72%, 7.68% and 3.87% of the variation in the model response respectively. The above ranking consolidated the previous qualitative results shown in Figure 4.2. It is also illustrated that OPF only contribute to 1.14% of the explainable variation of the model response. Other factors including IACH, WTR, WSH and BO, however, have a total contribution less than 1%. In addition, interactive impacts of all design factors add up to a total contribution of 18.74%.

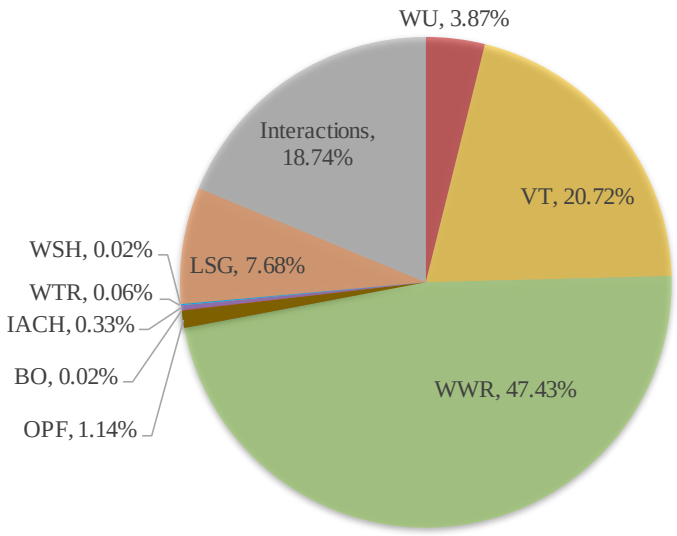

Figure 4.4 First-order sensitivity indices in Hong Kong

Figure 4.5 also validated that the four crucial factors (i.e., WU, WTR, WWR and IACH) identified from Figure 4.3 also account for the major variation of building energy consumption in Harbin. The total contribution of the other design factors and their interactions is reduced to 13.59%. It is noteworthy that WU makes an independent contribution of 32.26% to the building energy performance in Harbin, which is much larger than the 3.87% contribution in Hong Kong.

It can be concluded that thermal insulation using vacuum glasses is a more effective strategy in cold areas.

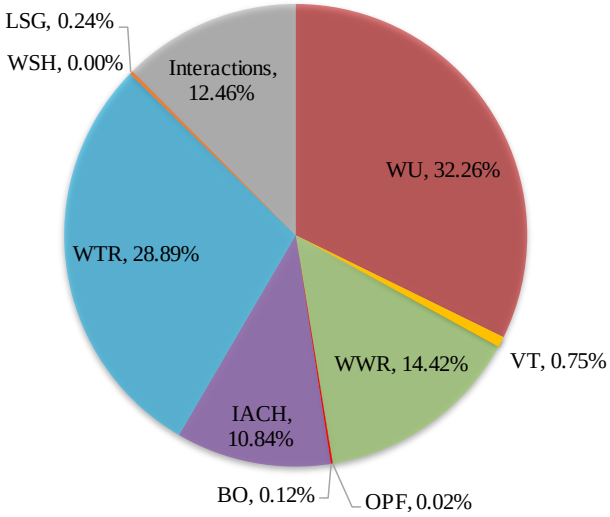

Figure 4.5 First-order sensitivity indices in Harbin

From above Morris and FAST indices, we can find that five design factors in each climate make minor independent contribution to building energy consumption. However, to completely exclude them form key design factors, total-order indices have to be calculated to take their interactive effects into account. Based on 1000 bootstrap replications, FAST total-order indices are estimated with standard errors and 95% confidence intervals. OPF, BO, IACH, WTR and WSH were validated as insignificant desgin factors with possible zero total-order indices in Hong Kong, while VT, LSG, OPF, BO and WSH were screened out in Harbin based on the same standard. These eliminated factors have ingorable influence over building energy consumption, so that they can be excluded from the optimization problem space in the primary building design. This practice is considered appropriate for architects and engineers when a

high-efficiency design optimization is preferred for early decisions. Hence, four key design factors in each climate are selected for a simplified optimization approach (SOPT) in both Hong Kong and Harbin, while a comprehensive optimization approach (COPT) involving all 9 factors is used as the reference case for comparison.

4.6 Design optimization and decision-making

This section presents detailed comparisons between all design optimization approaches including SOPT and COPT. As mentioned above, SOPT optimizes only four significant design inputs while model COPT optimizes all factors. The difference is that WWR, VT, LSG and WU are involved in SOPT of Hong Kong, but these factors are changed to WU, WTR, WWR and IACH in SOPT of Harbin. Through NSGA-II and the weighted sum method, final optimum designs are summarized in Table 4.2. In the case of Hong Kong, both optimum solutions are characterized by high WU of 5.194 and 5.747 and low SHGC of 0.109 and 0.112, which fit in with typical thermal properties of STPV. In contrast, optimum solutions in Harbin require low U-value between 0.211 and 0.345 and relatively higher SHGC between 0.263 and 0.703, which make vacuum glasses more applicable. In addition, a small window to wall ratio between 0.107 and 0.132 are preferred in both models so that curtain walls are not recommended for energy-saving envelope designs.

Table 4.2 Values of factors after optimization

Area	Model	BO	WSH	VT	WTR	LSG	WWR	WU	OPF	IACH
HK	Model SOPT	0.000	840.000	0.257	0.136	2.297	0.132	5.747	0.000	0.600
	Model COPT	71.000	1465.000	0.251	1.147	2.297	0.131	5.194	0.004	1.396
HB	Model SOPT	0.000	840.000	0.786	2.036	1.118	0.110	0.211	0.000	0.059
	Model COPT	359.000	1188.000	0.572	2.417	2.172	0.107	0.345	0.332	0.072

Error! Not a valid bookmark self-reference. and Table 4.4 show the energy consumption data per floor area of all building models. As per **Error! Not a valid bookmark self-reference.**, Model VPV in Hong Kong can save up to 37.79% total energy compared with Model NDP, which is the ideal scenario without the integrated design optimization. 10.93% and 14.32% more electricity can be reduced after the simplified and comprehensive optimization on top of Model VPV. Approximately 50% reduction of purchased electricity can be achieved by lowering building demands and increasing power supplies in both SOPT and COPT. The difference between total energy consumption of Model SOPT and Model COPT is within 5%, which means the simplified design optimization approach is capable of delivering an acceptable solution in the early design stage (X. Chen, Yang, & Sun, 2016).

Table 4.3 Energy uses of all models in Hong Kong

Energy Uses [kWh]	**Model NDP**	**Model NP**	**Model STPV**	**Model VPV**	**Model SOPT**	**Model COPT**
Lighting	35.27	17.89	19.43	20.27	19.48	19.52
Equipment	44.87	44.87	44.87	44.87	44.87	44.87
Heating	0.60	0.86	3.11	0.31	4.15	1.30
Cooling	254.36	240.24	194.58	162.62	144.14	137.12
Total use	335.10	303.86	261.99	228.07	212.64	202.82
Generated power	-	-	18.49	19.62	40.79	42.33
Purchased electricity	335.10	303.86	243.50	208.45	171.85	160.48
Total saving	-	9.32%	27.34%	37.79%	48.72%	52.11%

In Harbin's case, all models in Harbin use the same amount of equipment energy and Model NP is the one with least lighting energy consumption. In the SOPT approach, the optimum solution saves additional 20.98% total building consumption compared with Model VPV, despite a minor increase in lighting and heating energy. The difference between SOPT and COPT is further reduced to 1.18%, leading to a total energy saving up to 61.98% compared with Model NDP. This minor disparity between SOPT and COPT validated again the

robustness of the simplified optimization approach in the initial building design. The increased total energy saving in Harbin also confirmed the conclusion by Ghosh et al. that vacuum glazing performs better in cold climate region where a low U-value is highly recommended (Ghosh et al., 2016).

Table 4.4 Energy uses of all models in Harbin

Energy Uses [kWh]	**Model NDP**	**Model NP**	**Model STPV**	**Model VPV**	**Model SOPT**	**Model COPT**
Lighting	35.27	18.85	20.88	22.41	19.87	20.57
Equipment	44.87	44.87	44.87	44.87	44.87	44.87
Heating	109.35	114.73	196.97	81.14	42.02	45.76
Cooling	90.49	83.11	51.16	41.90	47.84	40.42
Total use	279.98	261.55	313.89	190.32	154.59	151.61
Generated power	-	-	20.57	21.82	44.84	45.16
Purchased electricity	279.98	261.55	293.32	168.50	109.75	106.44
Total saving	-	6.58%	-4.76%	39.82%	60.80%	61.98%

4.7 Summary

Thus far, the chapter performed design optimizations to achieve optimal PV envelope designs based on factor-prioritizing and factor-fixing results. Main conclusions are drawn as below:

Sensitivity analyses with Morris and FAST were conducted to qualify and quantify the influence of design parameters on the net building energy consumption. Window dimensions and physical properties are proved to be significant factors for the PV envelope design in Hong Kong. However, the wall thermal insulation (i.e., WTR) and airtightness (i.e., IACH) substitute for the visible lighting transmittance (VT) and light-to-solar gain ratio (LSG) as key design factors in Harbin. The ranking of key design factors by the qualitative approach was completely consistent with that obtained by the quantitative approach. The insignificant design factors were also excluded from optimization problem space by bootstrapped FAST total-order indices.

Both the simplified optimization (SOPT) based on key design factors and comprehensive optimization (COPT) based on all factors were conducted to derive the optimum solution for PV envelope designs in the two climatic conditions. The difference of net energy saving with both optimization approaches was within 5%, indicating that high-efficiency SOPT is suitable and reliable for initial design pursuing a swift decision-making process. Up to 52.11% and 62.98% energy conservation can be achieved with reference to the benchmarking building

design.

The integrated design optimization validated that PVVG is more suitable for application in cold areas, where a low U-value between 0.211 and 0.345 is recommended. In addition, a small window to wall ratio between 0.107 and 0.132 is preferred in both climates so that large-area curtain walls are not recommended for optimal envelope designs, when energy saving is the priority of a green building project. The systematic approach in this study can also be utilized to provide detailed user guidelines for building integrated PV applications.

This chapter not only discussed the applicability of the novel vacuum PV glazing in different climates but also proposed an integrated design optimization framework for its application in high-rise buildings. This approach can be used to identify potential energy efficient measures in a new construction or renovation project of the green building industry. The main findings can be used to develop energy assessment benchmarks for commercial buildings, where the net-zero energy target can be further approached by jointly considering the synergy of passive architectural design and PV envelope systems.

CHAPTER 5 SIMULATION STUDY ON THE OVERALL HEAT TRANSFER CHARACTERISTICS OF PHOTOVOLTAIC VACUUM GLAZING

This chapter proposes an integrated photovoltaic vacuum glazing unit with an intermediate air cavity and a calibrated modelling approach to quantify its thermal properties and evaluate the heat transfer performance. Theoretical analyses of the heat transfer process are conducted with reasonable hypotheses and traceable boundary conditions. Three-dimensional heat transfer models are then established and cross-validated against previous publications. Furthermore, four photovoltaic vacuum glazing configurations are compared in terms of the temperature distribution and overall heat transfer coefficient (i.e., U-value).

5.1 Thermal performance modelling

COMSOL Multiphysics ("COMSOL Multiphysics," n.d.), a powerful software tool based on finite element method, is chosen to simulate the complex heat transfer process of compositive PV vacuum glazing. This platform has been used to conduct PV system related research (Du, Tao, Liu, Jiang, & Huang, 2017; Jha & Tripathy, 2019) with a demonstrated modelling accuracy. Du et al. (Du et al., 2017) built thermal models in COMSOL Multiphysics to investigate the difference of using polymer and glass layers behind the solar cell. The model

was validated by experiments and the temperature distribution showed good agreement. The same tool was used by Jha and Tripathy (Jha & Tripathy, 2019) to describe the thermal behavior of the PV panel and it is indicated that the finite element model showed higher accuracy in temperature predictions than the nominal operating cell temperature model. Therefore, a 3D model is established on this platform to represent the compositive structure and simulate the heat transfer by coupling physics interfaces of heat transfer in solids and surface to surface radiation. The former involves thermal conduction, convection as well as the radiation between a certain surface and the ambient, while the latter mainly deals with radiative heat exchange between surfaces.

5.1.1 Heat transfer analysis

Due to the complex structure of PVVG, it is difficult to precisely evaluate its thermal performance as many factors need rigorous definitions. Taking PVVG with three layers of glasses as an example shown in Figure 5.1, the complex heat transfer process can be divided into five parts: (1) The front glass sheet: the conductive heat transfer through the glass sheet, convective heat transfer between ambient air and the external surface, the short-wave radiation (solar radiation) and long-wave radiation between the external surface and the ambient; (2) The layer of solar cell and EVA: conductive heat transfer through solar cell and EVA; (3) The

middile glass sheet: the conductive heat transfer, radiative heat transfer between two inner surfaces of the vacuum gap; (4) The vacuum pillars: the conductive heat transfer through the pillar array; (5) The back glass sheet: the conductive heat transfer, radiative heat transfer between two inner surfaces, convective heat transfer and long-wave radiation between indoor air and the internal surface.

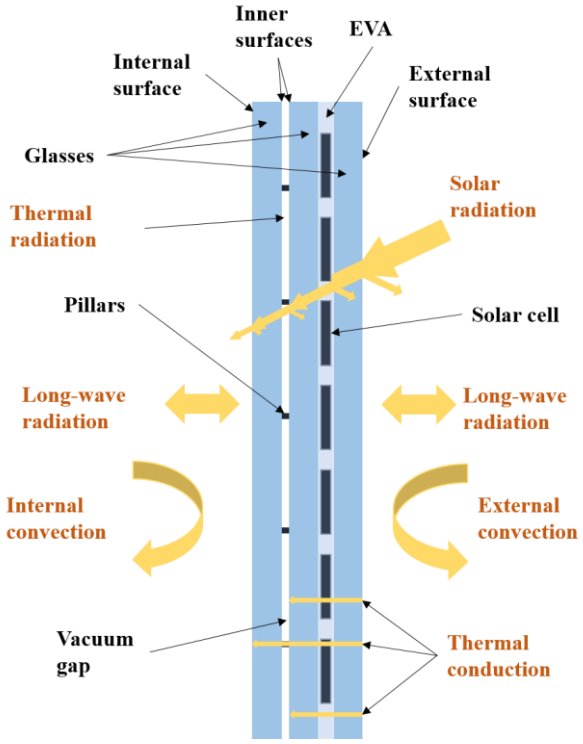

Figure 5.1 The complex heat transfer through the PV vacuum glazing with three layers of glass

The above illustrative model is set up with below assumptions: neglecting the radiative heat transfer between the cylindrical surfaces of the pillar array and two inner glass surfaces; ignoring the conductive and convective heat transfer of residual air in the vacuum gap; assuming only one integral layer to represent solar cells and EVA; considering merely the

central area of the glazing excluding the sealant and frame. Similar hypotheses can also be found in references (Du et al., 2017; Fang et al., 2013; Zhiming Han et al., 2012). From the analysis above, the thermal performance of PV vacuum glazing can be affected by factors including the thermophysical properties, dimension of components, seperation of vacuum pillars, the use of low-e coatings and the PV module design. The effect of these factors is also analyzed in this chapter.

5.1.2 Heat transfer model

The 3D heat transfer models are established in COMSOL Multiphysics based on three general patterns of the heat transfer. The conductive heat flux q_{cond}, convective heat flux q_{conv} and radiative heat flux q_{rad} can be described by Eq. (5.1-5.3):

$$q_{cond} = -k\nabla T \tag{5.1}$$

$$q_{conv} = -h(T_{ext} - T) \tag{5.2}$$

$$q_{rad} = -\varepsilon\sigma(T_{amb}^4 - T^4) \tag{5.3}$$

where k is the thermal conductivity (W/(m·K)); ∇T is the temperature gradient; h is the heat transfer coefficient (W/(m^2·K)); T_{ext} is the temperature (K) of the external fluid outside the surface; ε is the surface emissivity; σ is the Stefan-Boltzmann constant (W/(m^2·K^4)); and T_{amb} is the temperature (K) of the ambient that can be the surroundings or the opposite surface.

The temperature distribution of different glazing, including the temperature of the internal surface and PV module, can then be predicted by heat transfer models. Furthermore, the overall heat transfer coefficient (U-value) is evaluated by Eq. (5.4-5.5) with the acquired temperature distribution and heat flux. U-value has also been presented as an important indicator for evaluating the thermal performance of PV glazing system (J. Peng, Lu, & Yang, 2013) as well as the vacuum glazing(Ghosh et al., 2016).

$$U = \frac{Q_{int}}{T_{in} - T_{out}} \tag{5.4}$$

$$Q_{int} = A(q_{conv} + q_{rad}) \tag{5.5}$$

where Q_{int} is the heat flux transferred from the internal surface to the indoor environment (W); T_{out} is the outdoor temperature (℃); T_{ind} is the indoor temperature (℃) and A is the area (m^2) of the internal surface of PV vacuum glazing.

As the influence from the sealant and frame is out of the scope of this work, the calculated U-value should be the overall heat transfer coefficient of the central window area. To exclude the impact from the glazing edge, a 3D geometric model with only one vacuum pillar is established as shown in Figure 5.2 for vacuum glazing. This approach is deemed adequate to predict the thermal responses of vacuum glazing given its symmetric structure, and has been adopted in exsiting research to reduce the compution time (Fang et al., 2013).

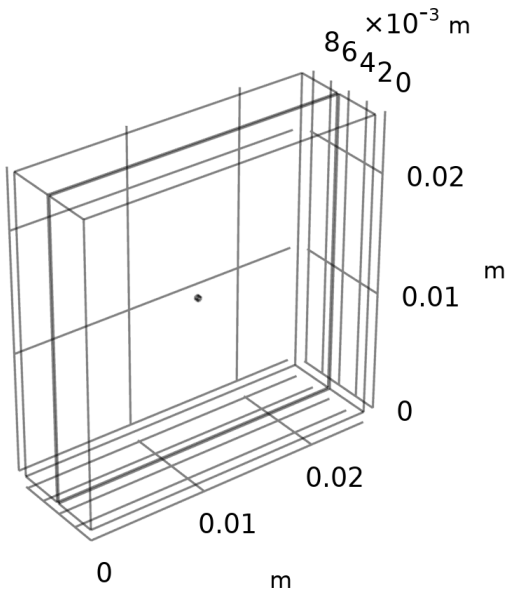

Figure 5.2 The 3D geometric model of vacuum glazing

5.1.3 Boundary conditions

This chapter aims at describing the thermal response of PV glazing under the steady state, which is as well the experimental condition to determine the overall heat transfer coefficient (U-values) (Fang, Eames, Norton, & Hyde, 2006; Ghosh et al., 2016). Similar settings of the winter condition proposed by ASTM C1199 (similar in ASHRAE handbook) are adopted to determine U-values of various fenestration products (ASHRAE, 2017). Generally, the guarded hot box calorimeter is established to keep different temperatures on both sides of the installed target glazing. Table 5.1 shows the detailed information of boundary conditions for the heat transfer models in Section 4 and 5. In this study, the heat transfer is modelled in the enclosed hot box environment, so that no solar radiation is involved. It is also noteworthy that the U-

value is assumed to be the thermal transmittance without solar radiation as suggested in ISO 15099:2003.

Table 5.1 Winter condition for the calorimetric hot box to determine the U-value

Winter condition (ASTM C1199)	
Indoor side:	Outdoor side:
$T_{in} = 21.2 \pm 0.3℃$	$T_{out} = -17.8 \pm 0.3℃$
$h_{in} = \frac{7.7W}{m^2K} \pm 5\%$	$h_{out} = \frac{30W}{m^2K} \pm 10\%$

5.2 Thermal performance of composite glazing

According to the winter condition specified in ASTM C1199, this section compares the thermal performance of the existing VPVG and proposed hybrid VPVG integrated by an air cavity (i.e., VPVDG). VPVDG has the same setting as VPVG except that the 12 mm wide cavity is filled with air with an extra glass layer. Only two surfaces facing the vacuum gap are coated ($\varepsilon = 0.03$). Section 3.2 has discussed one configuration of VPVG whose vacuum gap faces the outdoor environment (i.e., cold side). This section also discussed an inversed configuration of PVVG and PVVDG, where the PV module is placed in front of the vacuum gap and faces the outdoor environment. Four models are established to compare the temperature of the "PV layer" as well as the U-value of whole composite glazing. The geometric models of these glazing units are illustrated in Figure 5.3, which highlighted the

coated surfaces in circles as surface 1 and 2 in Figure 5.3(a), (b), (c) and surface 3 and 4 in Figure 5.3(d).

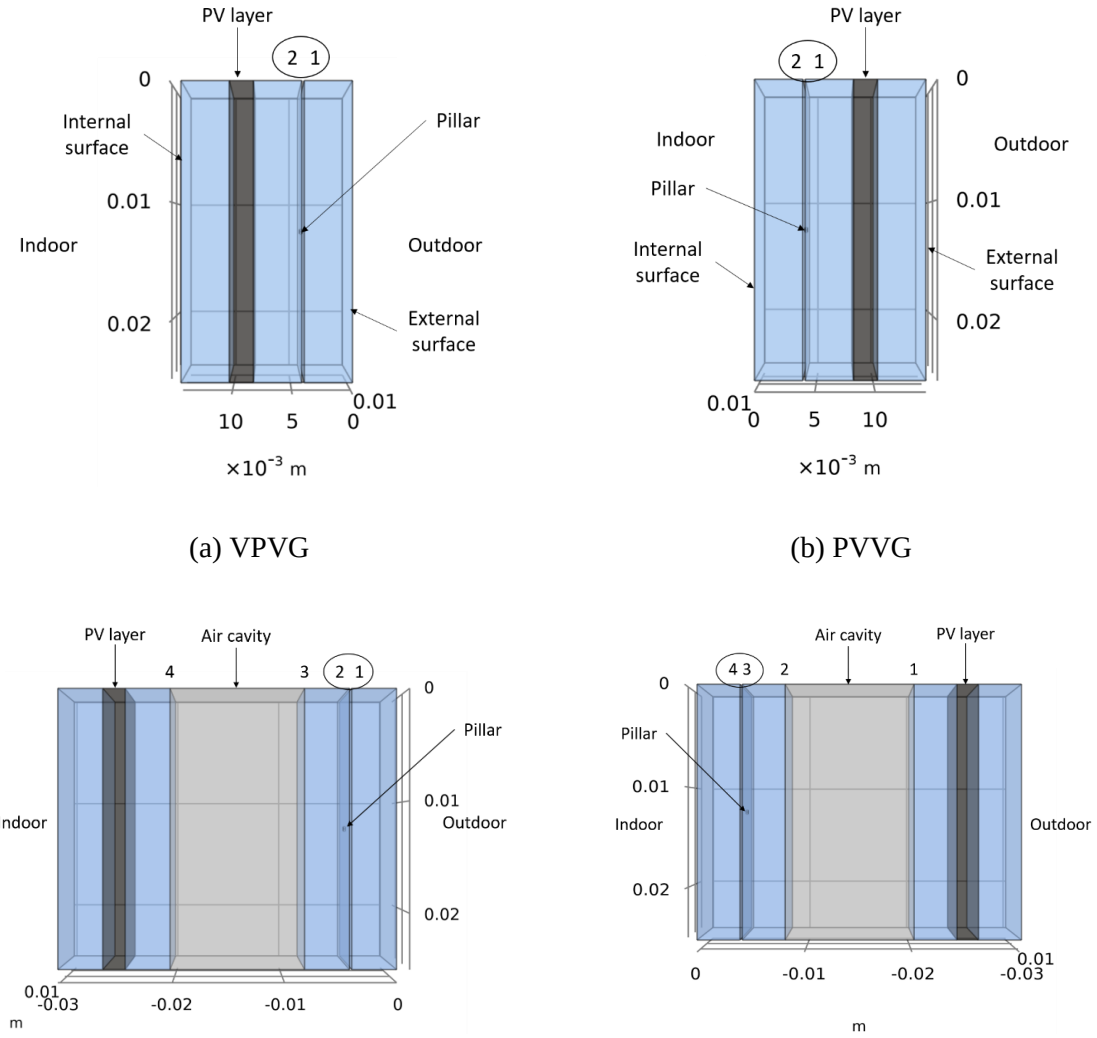

(a) VPVG (b) PVVG

(c) VPVDG (d) PVVDG

Figure 5.3 The geometry models with one vacuum pillar in the centre

5.2.1 Model validation

To validate the proposed method, comparisons have been conducted based on extracted data from published articles. The validation involves different glazing types, including vacuum

glazing (VG), PV laminated glazing (PVLG), PV double glazing (PVDG) and PV vacuum glazing (PVVG). The comparisons between heat transfer modelling results and previous publications can demonstrate the accuracy of the proposed method as well as its competence in predicting thermal performances of different windows.

A guarded hot box was constructed for experimental validation of a finite element model (Fang et al., 2006), involving the comparison between a float glass and VG with different sealant widths. The author investigated the influence of low-e coatings and acquired numerical and experimental U-values of VG (Fang et al., 2007). Table 5.2 summarizes the comparison between the testing and modeling results from the above two references and simulation results with COMSOL Multiphysics.

Judging from the detailed comparison in Table 5.2, modelling results of Case 1 and 2 show better consistency with those reported (Fang et al., 2006). Modelling results of this study also show a slight increase as validated by variation of experimental results from Case 1 to Case 2. For the Cases 3-5, the main difference is the emissivity of low-E coatings applied to VGs. Modeled U-values in this study again show the same decreasing tendency with reduced emissivity as those reported (Fang et al., 2007). The related input parameters to reference models are illustrated in Table 5.3.

Table 5.2 The comparison between this modelling approach and published works

Reference	Case	Glazing	U-value in references (W/(m²·K))		U-value in this study (W/(m²·K))
			Modelling	Experiment	Modelling
(Fang et al., 2006)	1	VG-1	1.0	0.97±0.08	0.95615
	2	VG-2	0.9	1.06±0.09	0.97699
(Fang et al., 2007)	3	VG-A	1.06	1.07±0.09	1.1898
	4	VG-B	0.97	1.00±0.09	1.1434
	5	VG-C	0.85	0.87±0.07	0.99849

Table 5.3 Model input according to References (Fang et al., 2006, 2007)

Parameters	VG-1	VG-2	VG-A	VG-B	VG-C
T_{in}(℃)	27.6	37.1	21.1	21.1	21.1
h_{in}(W/(m²·K))	3.31	3.22	8.3	8.3	8.3
T_{out}(℃)	5.5	12.4	-17.8	-17.8	-17.8
h_{out}(W/(m²·K))	6.02	4.71	30	30	30
t_g(mm)	4	4	4	4	4
ε	0.16, 0.16	0.16, 0.16	0.16, 0.16	0.12, 0.16	0.04,0.16
s_p(mm)	25	25	25	25	25
d (mm)	0.4	0.4	0.32	0.32	0.32
H(mm)	2	2	0.12	0.12	0.12

Apart from the U-value, the measured surface temperature of tested samples was also presented (Fang et al., 2006), which is listed in Table 5.4 together with the modeling results in this study. It is found that the developed heat transfer model can accurately predict the glazing surface temperature. The maximum difference between experimental and modelling results is 1.27℃, with a relative error of 3.8%. As a result, the developed heat transfer model is successfully cross-validated with a high reliability in predicting the temperature distribution and U-value.

Table 5.4 The comparison of temperature from Reference (Fang et al., 2006) and simulation results in this study

Reference	Case	Glazing	External Surface Temperature		Internal Surface Temperature	
			Experiment	Simulation	Experiment	Simulation
(Fang et al., 2006)	1	VG-1	24.2℃	25.093℃	7.6℃	7.574℃
	2	VG-2	33.1℃	34.369℃	15.5℃	15.021℃

Compared with the structure of PVLG, PVDG has a 12 mm air cavity and one more glass sheet with varied thickness of each layer. As for PVVG, the glass sheet before the PV module is replaced by a vacuum glazing unit. As only limited parameters are provided (Ghosh et al., 2018; Sánchez-Palencia, Martín-Chivelet, & Chenlo, 2019), the environment temperature and

heat transfer coefficient given in Table 5.1 will be utilized in this simulation. Additional model inputs are listed in Table 5.5.

Table 5.5 Model inputs for PVLG, PVDG and VPVG in addition to ASTM C1199

Parameters	**PVLG**	**PVDG**	**PVVG**
ε	0.84, 0.84	0.05, 0.88	0.03, 0.03
$t_g(mm)$	6	4	4
$k_g(W/mK)$	0.76	1	1

For Case 6 and 7, it could be found in Table 5.6 that modeling results of PVLG and PVDG in this study are closer to values in existing references (J. Han, Lu, & Yang, 2010; Liao & Xu, 2015). The thermal transmittance of PVDG is lower than PVLG because of the existence the air cavity. The air with lower thermal conductance contributes to less heat passing through the glazing. As for the last case, PVVG, good agreement is as well shown between experimental and simulative studies. The simulative U-value is obtained based on the condition that the inner surfaces in vacuum gap are both coated with a low-e coating ($\varepsilon = 0.03$).

Based on the comprehensive comparisons with previous works, the proposed method can achieve adequate accuracy in predicting the temperature distribution and U-value for different

glazing configurations. The reliable heat transfer model can then be used to compare different composite PV vacuum glazing and investigate the potential influence of various design factors.

Table 5.6 The comparison between simulative approach and published works (Ghosh et al., 2018; J. Han et al., 2010; Liao & Xu, 2015)

Reference	Case	Glazing	U-value ($W/(m^2 \cdot K)$) in references	U-value ($W/(m^2 \cdot K)$) in this study
(Liao & Xu, 2015)	6	PVLG	5.18	5.003
(J. Han et al., 2010)	7	PVDG	2.46	2.243
(Ghosh et al., 2018)	8	PVVG	0.8	0.878

5.2.2 VPVG and PVVG modeling results

Figure 5.4(a) shows the temperature distribution of the whole structure of VPVG under the winter condition. Apparently, the front glass sheet has the lowest temperature (-16.81 ℃) when facing the cold outdoor environment. For the inner surface in the vacuum gap, it can be clearly seen in Figure 5.4(b) that the temperature around the vacuum pillar is lower than other

areas because it has direct contact with the colder outside glass panel of VG (i.e., the cold bridge effect). Under this circumstance, the PV module temperature (18.32 ℃) is much higher than that of the vacuum pillar (1.03 ℃). The temperature difference between the external and internal surface is 35.23 ℃, indicating an outstanding thermal insulation performance. The internal surface temperature can be kept at 18.46 ℃ while the outdoor environment only has a temperature of -17.8 ℃. The U-value of VPVG is also as low as 0.878 W/(m^2·K).

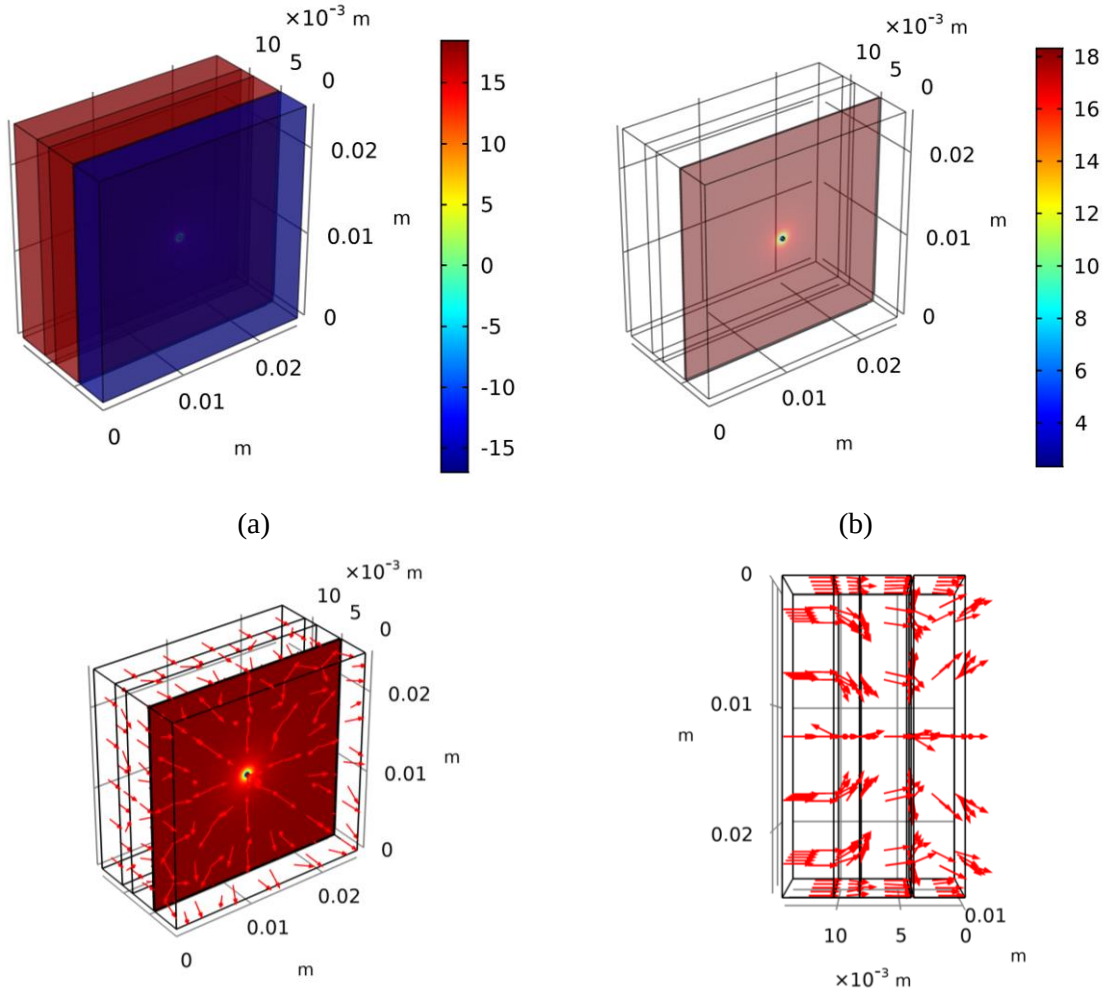

Figure 5.4 Temperature distribution and heat flow direction of VPVG

The arrows in Figure 5.4(c) and (d) illustrate the direction of heat flow passing through the whole structure of VPVG. The heat flow starts from the innermost glass facing the indoor environment and is conducted to the middle glass sheet, where the arrows gradually concentrate towards the central vacuum pillar and then spread out in the last glass sheet.

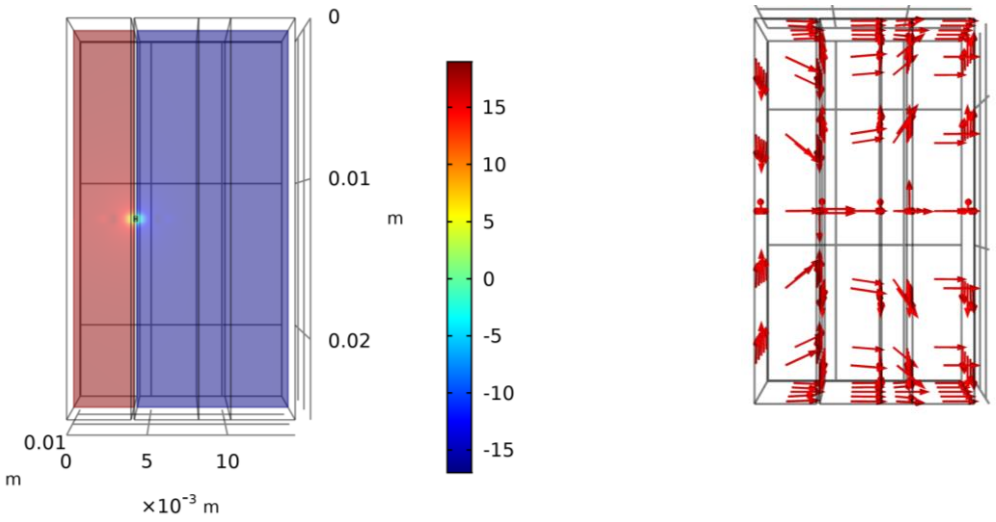

(a) (b)

Figure 5.5 Temperature distribution and heat flow direction of PVVG

Regarding PVVG, the temperature distribution is reversed as the PV module is facing the cold side. As shown in Figure 5.5(a), the temperature around the vacuum pillar is 0.82 ℃, much higher than the temperature of the PV module (-16.63 ℃). The arrows in Figure 5.5(b) also show a similar heat flow pattern which concentrates to the vacuum pillar at first but start spreading in the vacuum glazing part. The U-value of PVVG under the winter condition is as well 0.878 W/(m^2·K), the same as VPVG, which echoes with the result from reference (Ghosh et al., 2018). Compared with VPVG, the PV module temperature is much lower in PVVG and

can therefore prevent the decline of its conversion efficiency. In addition, placing the PV module in front of vacuum glazing can harvest more solar radiation. Given above reasons, PVVG is more suitable for applications in the cold climate than VPVG.

5.2.3 VPVDG and PVVDG modelling results

The main difference between VPVDG and VPVG is the air cavity located between vacuum glazing and PV glazing, just as the situation between PVVDG and PVVG. A study from Aydin (Aydin, 2000) emphasized that the convective heat transfer would become comparable if the air gap width exceeded 15 mm in double glazing, otherwise the conduction dominates other patterns of the heat transfer. As the air cavity width is only 12 mm, it is assumed that the air is not circulating in the air-tight cavity under the steady state and the influence of convection is ignored in this study. Thus, the heat is transferred within the cavity mainly by two patterns, i.e., heat conduction through the air and radiation between inner surfaces. Figure 5.6 shows the temperature distribution and heat flow direction of VPVDG and PVVDG. The similar temperature distributions can be found between VPVG and VPVDG as well as between PVVG and PVVDG. It can be distinguished by the arrows that the heat flow at the front glass differs because of the reversed configurations of PVG and VG.

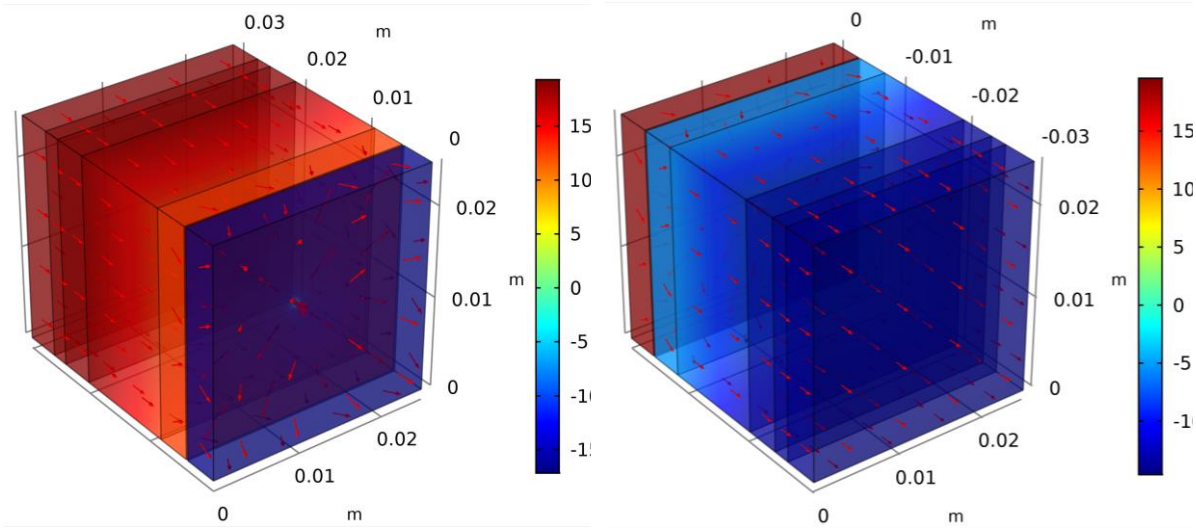

(a) VPVDG (b) PVVDG

Figure 5.6 Temperature distribution and heat flow direction of VPVDG and PVVDG

Since the air acts as a thermal insulation medium, the PV module has a higher temperature (19.01 ℃) in VPVDG compared with that of VPVG for less heat losses. Although a higher temperature may impair the efficiency of power generation, the small temperature difference of 0.68 ℃ can almost be ignored. Considering the difference of U-values shown in Table 5.7, VPVDG should be preferred over VPVG. As for the comparison between the other two configurations, the PV module temperature -16.93 ℃ of PVVDG is slightly lower than that of PVVG. What is more, the U-value of PVVDG (0.650 W/(m^2·K)) turns out to be the lowest and proves that this structure shows the best thermal performance. The additional air cavity with a width of 12 mm helps to decrease the U-value from 0.878 W/(m^2·K) to 0.670 W/(m^2·K) comparing the case of VPVG and VPVDG, and from 0.877 W/(m^2·K) to 0.650 W/(m^2·K) for PVVG and PVVDG. The performance improvement is up to 23.7% and 26%. Moreover, the

energy conversion efficiency of the PV module in PVVG and PVPDG can be guaranteed as long as it is facing the cold outside environment with more available solar radiation compared with VPVG and VPVDG.

Table 5.7 Average temperature and U-value of different glazing

Glazing	Internal surface Temperature (℃)	External Surface Temperature (℃)	PV module Temperature (℃)	U-value ($W/(m^2 \cdot K)$)
VPVG	18.459	-16.768	18.322	0.87801
VPVDG	19.111	-17.015	19.006	0.66993
PVVG	18.46	-16.769	-16.632	0.87755
PVVDG	19.174	-17.033	-16.931	0.64976

5.3 Impact of critical design factors

In addition to the thermophysical properties of different composite glazing and components, the influence of critical design factors on the thermal performance is subject to detailed analyses across the previous four glazing configurations. The overall heat transfer coefficient (i.e., the U-value) is evaluated as the thermal performance indicator in this session. The concerned factors and corresponding components are listed in Table 5.8, while heat transfer models are based on the boundary conditions in Table 5.1. The following models are

established assuming that both the surfaces in vacuum gap are coated ($\varepsilon = 0.03$), except for the cases investigating the impact from the emissivity of low-e coatings.

Table 5.8 Potential factors affecting the U-value

Component	**Specification**
Glass	Thermal conductivity W/(m·K)
Vacuum pillar	Thermal conductivity W/(m·K)
	Separation (mm)
	Diameter (mm)
	Height (mm)
Low-e coating	Emissivity
Air cavity	Width (mm)

5.3.1 Influence of the glass sheet's thermal property

The glass sheet is a major component for composite windows, in which a lower thermal conductivity can contribute to better thermal performance. Fig. 7 compares the impact of glass thermal conductivity on the thermal performance of four glazing configurations. As shown in Figure 5.7, the U-value of all glazing configurations increases linearly with the thermal conductivity of the glass sheet. This tendency is more apparent for VPVG and PVVG with a

much larger slope than the other two cases. Among all these types, VPVDG and PVVDG show lower sensitivity to the glass thermal conductivity. In terms of the variation ratio, the U-value is decreased by around 60.09%, 59.51%, 66.00% and 66.02% for VPVDG, PVVDG, VPVG and PVVG respectively. Given the change in regular patterns, the thermal conductivity of glass sheet is suggested to be as low as possible for better thermal insulation.

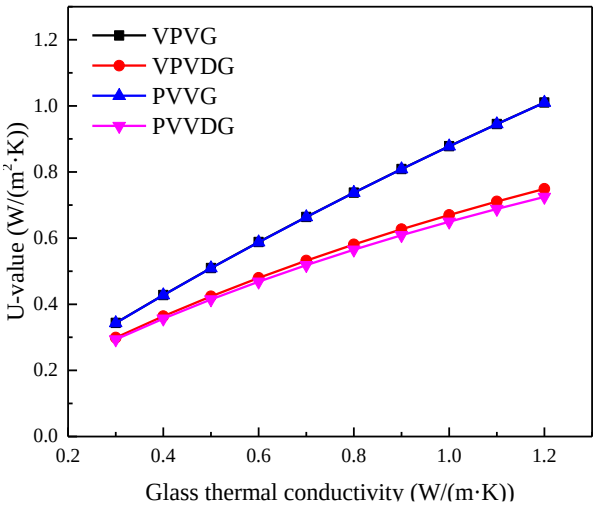

Figure 5.7 The effect of glass sheet on the U-value

5.3.2 Influence of vacuum pillar

Vacuum pillar array is the indispensable part of vacuum glazing to separate and support two glass sheets within a vacuum environment, where conductive and convective heat exchanges can be minimized. In order to maintain a vacuum of 0.1Pa (R. E. Collins & Simko, 1998), the array requires proper materials and designs to endure the great extrusion force from glass sheets. The separation, the diameter and height of a single pillar, as well as the material

thermal conductivity of the pillar array are examined to quantify their impact on the overall U-value of the composite glazing as per Fig. 8.

In Figure 5.8(a), the pillar thermal conductivity affects the U-value greatly within the range from 1 to 10 W/(m·K), whereas the effect becomes weak after exceeding this range. The U-value of VPVG and VPVDG increases by merely 0.07 W/(m^2·K) and 0.06 W/(m^2·K) when pillar thermal conductivity increases from 11 to 40 W/(m·K). It can be concluded that the U-value would be significantly reduced if the stainless-steel pillar can be replaced by a proper material with low thermal conductivity and high compression resistance. As the improvement of the overall glazing U-value can be up to about 42% when decreasing the conductivity from 10 to 1 W/(m·K).

The relationship between the pillar array density and glazing thermal performance is presented in Figure 5.8(b). The U-value generally drops with the separation of pillars with a minor fluctuation when the separation is around 40 mm, which echoes with the key findings on VG in existing references (Philip W. Griffiths, Eames, Hyde, Fang, & Norton, 2006; Manz, Brunner, & Wullschleger, 2006) where the variation gradually levels off. Therefore, the separation is suggested to be as large as possible as long as the array can endure the compression from glass sheet. A tremendous improvement of thermal performance can be achieved by enlarging the separation of pillar array from 20 mm to 60 mm. For instance, the

U-value of VPVG can be reduced by 80.08% from 1.27 to 0.25 W/(m^2·K). Among four glazing configurations, PVVDG with a pillar separation of 60 mm can achieve the lowest U-value of 0.23 W/(m^2·K), which approximates the reported U-value of 0.22 W/(m^2·K) for a triple vacuum glazing (Cuce & Cuce, 2016).

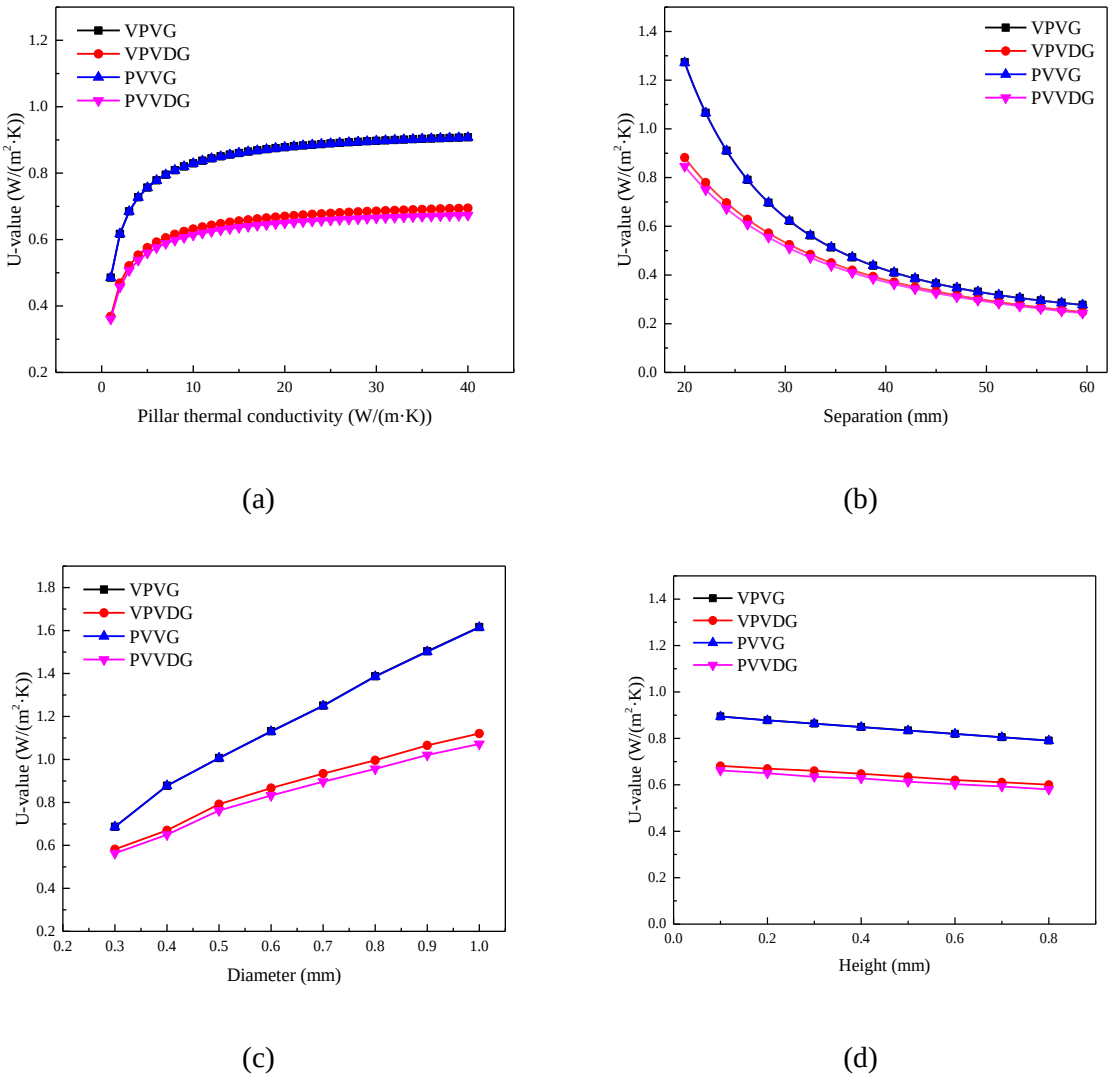

Figure 5.8 The effect of vacuum pillars on the U-value

On the contrary, the U-value obviously rises with the diameter of pillars as shown in Fig. 8(c), as larger diameters increase the contact area of the heat exchange between pillars and

glass sheets (i.e., enlarged cold/heat bridge effect). The result is similar to that of VG reported by Fang et al. (Fang et al., 2014). Therefore, a smaller diameter is preferred for the sake of thermal insulation. The reduction of U-values is 57.52%, 48.07%, 57.51% and 47.48% for VPVG, VPVDG, PVVG and PVVDG respectively when decreasing the pillar diameter from 1 mm to 0.3 mm.

At last, the variation with pillar height (i.e., the width of vacuum gap) is illustrated in Fig. 8(d), which indicates a minor impact on the thermal performance. The overall heat transfer coefficient decreases by 0.11 W/(m^2·K) (12.35%) when the height varies from 0.1 mm to 0.8 mm for the case of PVVDG. Other cases also show slight variations between 11.59-11.90%, which is similar to the effect of pillar thermal conductivity within the range of 11-40 W/(m·K).

5.3.3 Influence of low-e coatings

Low-e coatings reduce the radiative heat transfer through decreasing the emissivity of a standard clear glass (0.84) to the lowest available emissivity (0.013) in the library of Window 7.6 (“Berkeley Lab WINDOW,” n.d.). Therefore, this chapter quantifies the impact of low-e coatings with the emissivity ranging from 0.013 to 0.313 on the composite PV vacuum glazing. Different scenarios are designed as: 1) The inner surface close to the indoor ambiance in vacuum gap is uncoated while the other inner surface in the vacuum gap is coated; 2) Both

inner surfaces in vacuum gap are coated; and 3) Inner surfaces of the air cavity instead of the vacuum gap are coated for PVVDG.

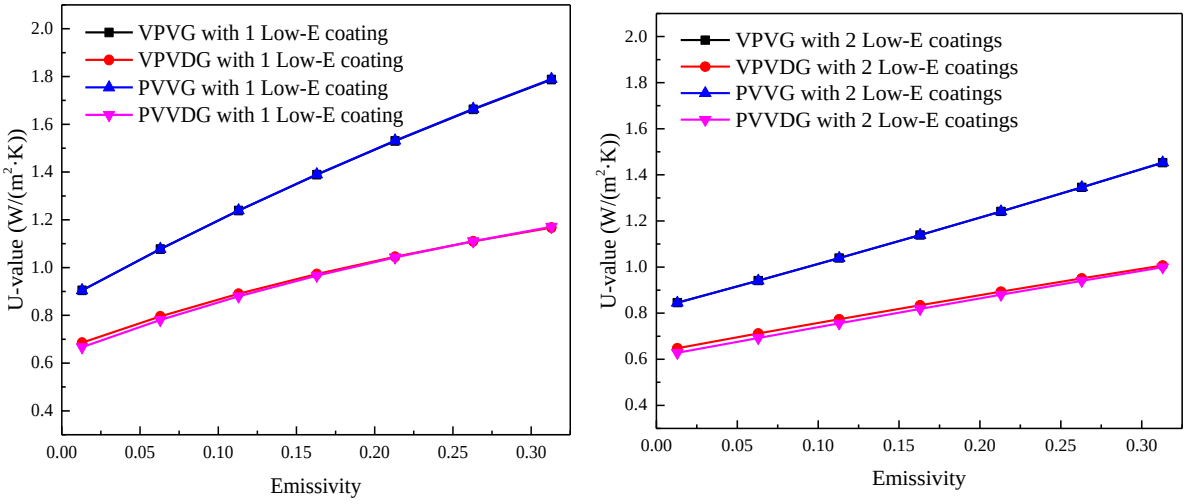

(a) (b)

Figure 5.9 The effect of the low-e coating on the U-value for Scenario 1 and 2

Figure 5.9(a) shows the influence from the low-e coating in the first scenario. VPVG and PVVG tends to be more sensitive to the increase of the emissivity with a variation up to 0.86 W/(m^2·K). In contrast, the U-value of VPVDG and PVVDG only varied by 0.5 W/(m^2·K) due to the additional air cavity. The U-value of different glazing configuration has been varied between 41.24% and 49.45% across the range of emissivity. Similar tendencies can be seen in the second scenario as per Figure 5.9(b), where the U-value increases with the growing emissivity. On condition that the lowest possible emissivity is 0.013 [17], the minimum U-value is merely 0.63 W/(m^2·K) for PVVDG. However, it can be also found that the improvement is not obvious for these cases when adding another layer of low-e coating. The

maximum variation of U-value is only 0.34 W/(m^2·K) across the range of emissivity for all four cases, while the rate of change drops with reducing emissivity. The above findings echo with similar research on the effect of a second low-e coating for PVDG and VG respectively (Fang et al., 2007; J. Han et al., 2010).

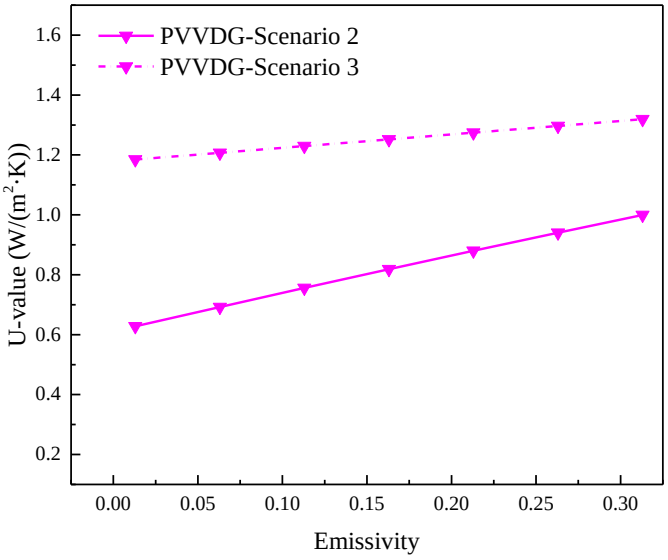

Figure 5.10 The effect of the low-e coating on the U-value for Scenario 2 and 3

As for Scenario 3, the U-value of PVVDG decreases slowly with the emissivity of low-e coatings in the air cavity and is clearly different from other scenarios as per Figure 5.10. The overall heat transfer coefficient stays above 1.18 W/(m^2·K) in Scenario 3, which is higher than the maximum of 1.0 W/(m^2·K) in scenario 2. Coating the inner surfaces in the air cavity is less effective on the overall thermal performance of composite glazing. It can be attributed to the fact that radiation dominates the heat transfer processes in the narrow vacuum gap where the coating can block more thermal energy.

5.3.4 Influence of air cavity

The air cavity contributes to about 46% reduction of the U-value for PVDG compared with that for PVLD in Section 3.2. When the air cavity is added to vacuum glazing, the improvement of U-values for VPVG and PVVG can be anticipated to be less conspicuous. Figure 5.11 shows the effect of air cavity width on the U-value of VPVDG and PVVDG. These two glazing configurations are negatively correlated to the air cavity width, with a reduction of 20.23% for VPVDG and 22.18% for PVVDG across the variation range. The result complies with the variation of heat transfer coefficient when the air cavity width is less than 15 mm as reported in (ASHRAE, 2001). Nonetheless, a wider air cavity is suggested to improve the thermal performance as much as possible.

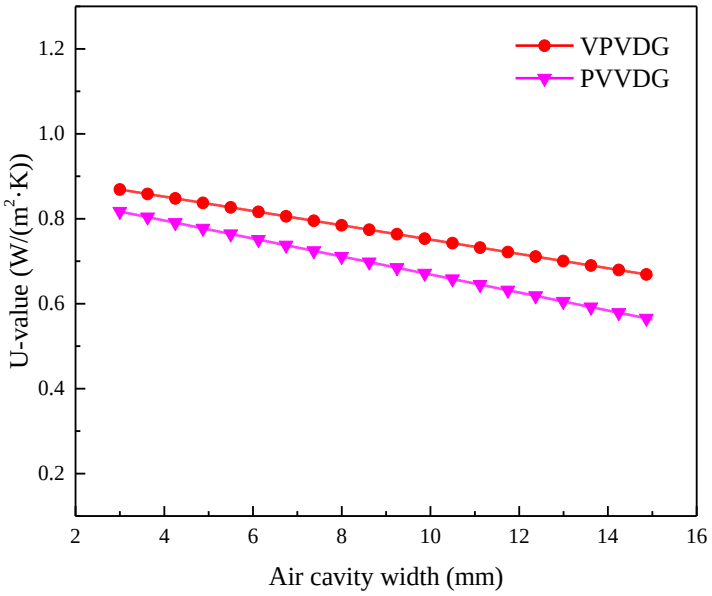

Figure 5.11 The effect of the air cavity width on the U-value

5.3.5 Discussion of impact analyses

This section has investigated the influence from glass sheets, pillars, low-e coatings and the air cavity on the overall heat transfer coefficient of four glazing configurations. The factors can be divided into two categories according to their impact. The first category consists of the thermal conductivity of glass sheets, diameter and height of vacuum pillars, low-e coating and the width of air cavity, to which the U-value responds linearly. Except for the width of air cavity and height of vacuum pillars, the U-value shows positive correlation with the first category of factors. In other words, the overall heat transfer coefficient can be decreased by lowering the thermal conductivity of glass sheet, diameter of vacuum pillars and emissivity of low-e coatings, while increasing the width of vacuum gap and air cavity.

The second category includes the thermal conductivity and separation of vacuum pillars, which contribute to the nonlinear response of the U-value. If allowed by the structure safety, enlarging the separation and lowering the thermal conductivity of pillars to below 10 W/(m·K) can significantly improve the thermal performance.

The optimal thermal performance for all glazing configurations can be determined by considering the negative and positive impact from all design factors. Table 5.9 further summarizes the maximum variation of the overall heat transfer coefficient (i.e., the sensitivity index) as affected by these design factors. A positive percentage means that the U-value

increases with the growing design factor while the negative one indicates that the U-value declines with the growing design factor. It can be concluded that high-impact factors include the glass thermal conductivity, separation and diameter of vacuum pillars, and emissivity of low-e coating. In addition, the pillar thermal conductivity is also a significant factor when it is below 10 W/(m·K). The rate of change of the U-value depends on the distribution range of design factors in the third category.

Table 5.9 Summary of the maximum U-value improvement with critical design factors

Factors	**Unit**	**Range**	**Improvement proportion of U-value**			
			VPVG	**VPVDG**	**PVVG**	**PVVDG**
Glass thermal conductivity	W/(m·K)	0.2-1.2	66.00%	60.09%	66.02%	59.51%
Pillar thermal conductivity	W/(m·K)	1-10	41.48%	41.62%	41.46%	41.22%
Pillar thermal conductivity	W/(m·K)	11-40	7.74%	8.15%	7.74%	8.04%
Separation	mm	20-60	-80.08%	-73.67%	-80.10%	-73.01%
Diameter	mm	0.3-1	57.52%	48.07%	57.51%	47.48%
Height	mm	0.1-0.8	-11.59%	-11.90%	-11.59%	-12.35%
Emissivity (single coating)	-	0.013-0.313	49.38%	41.24%	49.45%	43.06%
Emissivity (double coatings)	-	0.013-0.313	41.78%	35.67%	41.86%	37.18%
Air cavity width	mm	3-15	-	-20.23%	-	-22.18%

5.4 Summary

This chapter presents a robust modelling approach with COMSOL Multiphysics to investigate the thermal properties of different composite glazing integrated by the vacuum layer, photovoltaic module, and air cavity. The complex theoretical heat transfer process is explored, and a numerical model is built based on reasonable assumptions for the standard winter condition. The modelling approach is then cross-validated with published heat transfer simulations and experimental data on the temperature distribution and U-value for vacuum glazing, photovoltaic laminated glazing and double glazing as well as vacuum photovoltaic glazing. The validated model is then used to compare the thermal performance of the vacuum photovoltaic glazing, photovoltaic vacuum glazing as well as proposed vacuum photovoltaic double glazing and photovoltaic vacuum double glazing. Impact analyses of key design factors are also conducted to guide the optimal design of compositive photovoltaic vacuum glazing for improving thermal performances. Some important conclusions are listed below:

(1) The three-dimensional thermal modeling by COMSOL Multiphysics is reliable in determining the temperature distribution as well as the overall heat transfer coefficient. A small average relative error of 2.4% is achieved for VG, PVLG, PVDG and PVVG.

(2) Compared with configurations without the air cavity (i.e., VPVG and PVVG), the U-value can be reduced by 19.6% for the case of VPVDG and 21.5% for PVVDG. PVVDG can

achieve superior thermal and potential power performances as it has the lowest U-value and PV module temperature.

(3) The glass thermal conductivity, separation and diameter of vacuum pillars and emissivity of Low-E coatings are identified as dominant influencing factors on the glazing thermal performance. In contrast, the pillar thermal conductivity beyond 10 W/(m·K) and width of vacuum gap only have relatively weak impacts.

(4) The overall heat transfer coefficient can be decreased by lowering the thermal conductivity of glass sheets and pillars, diameter and density of vacuum pillars and emissivity of Low-E coatings, while increasing the width of the vacuum gap and air cavity. The lowest U-value can be achieved as 0.23 W/(m^2·K) in PVVDG with a pillar separation of 60 mm, and the thermal performance can be further improved with a global optimization.

(5) One layer of Low-E coating can play a significant role in reducing the radiative heat transfer and the corresponding U-value, whereas the second layer brings a limited improvement and is therefore not cost-effective.

(6) This research provides a guide for the selection of different composite PV vacuum glazing configurations for optimized thermal performances. It can also be used as references for further design improvements of the proposed glazing configuration and promote its integration with whole building simulations. Such novel glazing systems can also facilitate the

expansion of renewable applications and corresponding sustainable building designs and retrofitting.

CHAPTER 6 DEVELOPMENT OF MATHEMATICAL THERMAL MODELS OF PHOTOVOLTAIC VACUUM GLAZING

This chapter seeks to provide an approach to evaluate the U-value and solar heat gain coefficient of photovoltaic glazing with different structures and identify the optimal one for various climate zones in terms of the thermal and power performance. A comprehensive heat transfer analysis is presented, and a mathematical heat transfer model is established utilizing MATLAB and validated against published references. The U-value and solar heat gain coefficient are obtained, the window heat gain and power generation are then predicted considering the detailed impact of the Low-E coating.

6.1 Physical properties of photovoltaic glazing

The photovoltaic glazing units studied in this chapter include photovoltaic vacuum glazing (PVVG), hollow photovoltaic glazing (HPVG) and hollow composite photovoltaic vacuum glazing (HPVVG). All involved glazing units (1.2 m $\times$ 0.6 m) use CdTe thin-film solar cells coated on the front glass. HPVG laminates the front glass and the double glazing with a 9 mm air gap, and HPVVG introduces VG behind the air gap of HPVG. PVVG sandwiches the front glass coated with solar cells and encapsulates VG using PVB or EVA.

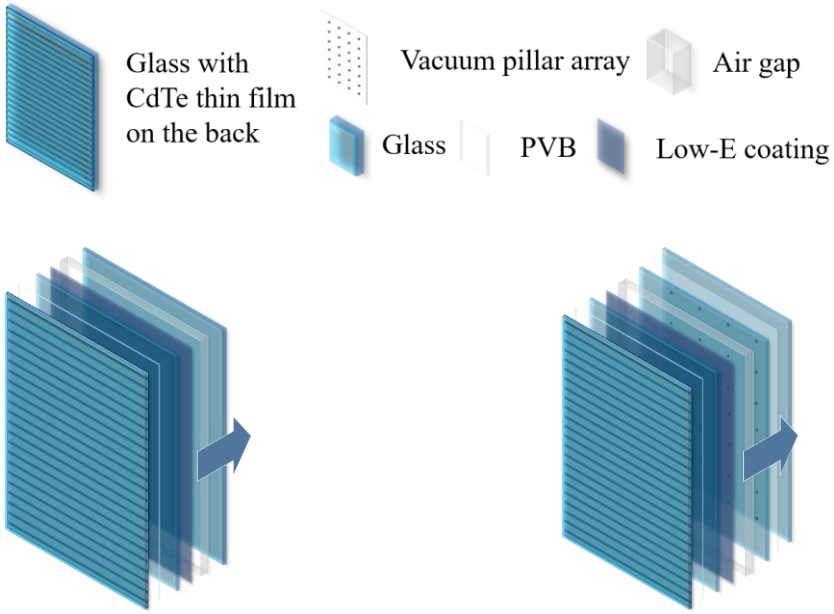

Low-E coating locates before the air gap and faces indoor

(a) HPVG

Low-E coating locates before the air gap and faces indoor

(b) HPVVG

Low-E coating locates after the vacuum gap and faces outdoor

(c) PVVG-A

Low-E coating locates before the vacuum gap and faces indoor

(d) PVVG-B

Figure 6.1 Schematic diagram of different photovoltaic glazing structures

Table 6.1 The structure of different types of photovoltaic vacuum glazing

Layer	HPVG	HVPVG	PVVG-A	PVVG-B
-	Outdoor	Outdoor	Outdoor	Outdoor
1	3.2 mm Float Glass	3.2 mm Float Glass	3.2 mm Float Glass	3.2 mm Float Glass
2	3 μm CdTe Thin Film Solar Cells	3 μm CdTe Thin Film Solar Cells	3 μm CdTe Thin Film Solar Cells	3 μm CdTe Thin Film Solar Cells
3	0.76 mm PVB	0.76 mm PVB	0.76 mm PVB	0.76 mm PVB
4	4 mm Clear Tempered Glass	4 mm Clear Tempered Glass	4 mm Clear Tempered Glass	4 mm Clear Tempered Glass
5	Low-E coating	Low-E coating	Vacuum layer	Low-E coating
6	9 mm Air Gap	9 mm Air Gap	Low-E coating	Vacuum layer
7	5 mm Clear Tempered Glass	4 mm Clear Tempered Glass	4 mm Clear Tempered Glass	4 mm Clear Tempered Glass
8	-	Vacuum layer	-	-
9	-	4 mm Clear Tempered Glass	-	-
-	Indoor	Indoor	Indoor	Indoor

Figure 6.1 shows the schematic diagram of mentioned photovoltaic glazing structures, in which the arrows indicate whether the Low-E coating is facing indoor or outdoor. The dark lines on the back of the front glass represent the CdTe thin film, which covers 60% of the total glazing area. PVVG-A refers to a PVVG with a Low-E coating on the inner surface of the last (innermost) layer of glass, indicating that the Low-E coating is located after the vacuum gap.

PVVG-B means the Low-E coating is located on the middle glass layer before the vacuum gap facing the indoor environment. Glass thickness and structural components are presented in Table 6.1. The emissivity of uncoated and coated glass surfaces is 0.84 and 0.06, respectively. Vacuum pillars are made of stainless steel and their thermal conductivity is 17 W/(m·K). They are separated by 50 mm × 60 mm intervals with a diameter and height of 0.5mm and 0.3mm. The total thickness is 25.7 mm for HPVVG, 22.5 mm for HPVG, and 12.4 mm for PVVG-A and PVVG-B. The thermal conductivity of each single-layer glass is obtained by the thermal conductivity tester, while the transmittance and reflectance are measured by the spectrophotometer.

Cadmium telluride (CdTe) thin-film solar cells are characterized by their high photoelectric conversion efficiency, low power temperature coefficient, good low light performance and high stability. According to the information provided by the manufacturer, Advanced Solar Power (Hangzhou) INC., window modules with full-area coverage cells can reach an efficiency of 13% and a power temperature coefficient of around 0.21%/°C. CdTe is a direct gap material with good light absorption in the full spectrum, so that it generates power better than crystalline silicon, an indirect band gap material, under low light conditions such as the early morning and evening. Furthermore, CdTe thin film solar cells have no intrinsic photoluminescence effect and can guarantee more than 80% power outputs for 25 years. The

electrical performance parameters measured by the manufacturer, including the module efficiency, fill factor, maximum power generation, are summarized in Table 6.2 with HPVVG as an instance. The tests are conducted using the instantaneous solar simulator under approximate standard test conditions: HPVVG receives 1000 W/m^2 solar irradiance when the cell temperature is 25 ℃.

Table 6.2 Electrical properties of HPVVG

Electrical properties	**Value**
Maximum power output (W)	49.6
Voltage at the maximum power point (V)	90.5
Current at the maximum power point (A)	0.55
Open circuit voltage (V)	119.9
Short circuit current (A)	0.65
Module efficiency	7.3%
Fill factor	63.7%

6.2 Theoretical thermal model

This section covers three general forms of the heat transfer with exhaustive illustration the process in both the air and vacuum gap. Unlike the air gap, the vacuum gap is more complex and involves various design constraints. Therefore, the air gap and vacuum gap are analyzed separately.

6.2.1 General forms of heat transfer

Conduction, convection, and radiation are the three general heat transfer forms, the last of which occurs between object surfaces without the need for a medium. The heat flow rate due to these three heat transfer forms is calculated as follows:

$$q_{cond} = \frac{(T_i - T_{i+1})k}{d} \tag{6.1}$$

$$q_{conv} = h_{conv}\left(T_{flu} - T_{sur}\right) \tag{6.2}$$

$$q_{rad} = \varepsilon_{eff}\sigma\left(T_i^4 - T_j^4\right) \tag{6.3}$$

$$\varepsilon_{eff} = \frac{1}{\frac{1}{\varepsilon_i} + \frac{1}{\varepsilon_j} - 1} \tag{6.4}$$

where, q_{cond} is the conductive heat flow rate (W/m^2), T_i and T_{i+1} are the temperatures (K) of two surfaces perpendicular to the direction of heat transfer, k and d are the thermal conductivity (W/(m·K)) and the thickness (m) in the direction of heat transfer; q_{conc} is the convective heat flux (W/m^2), h_{conv} is the convective heat transfer coefficient (W/(m^2·K)), T_{flu} is the temperature (K) of the fluid, and T_{sur} is the temperature (K) of exposed surface; σ is the Stefan–Boltzmann Constant that equals to 5.67×10^{-8} W/m^2 K^4, T_i and T_j are the

temperatures (K) of surface i and surface j, and ε_i and ε_j are the surface emissivity of surface i and surface j, respectively.

Among these equations, the convective heat transfer coefficient needs to be determined on a case-by-case basis. Heat is transferred by natural convection when the fluid flow rate is less than 0.3 m/s. Otherwise, heat should be calculated in accordance with forced and mixed convection. An accurate determination of this convective heat transfer on both indoor and outdoor boundary surfaces is extremely difficult and can only be done by careful measurements and computer simulations (ASHRAE, 2017). Normally the overall heat transfer coefficient of the interior surface of a vertical window, with natural convection, can be determined by Equation (6.5) if the emissivity of the surface is known (Y. Lu, 2008). Thus, 8.0 W/(m^2·K) is recommended as the overall heat transfer coefficient for an uncoated glass surface. As for the glass surface exposed to surroundings, Equation (6.6) can be an approximate expression of the overall heat transfer coefficient (Y. Lu, 2008). Both Equation (6.5) and (6.6) are often used in thermal calculations for glass surfaces. In engineering projects, the exterior surface heat transfer coefficient is estimated to be 23 W/(m^2·K).

$$h_{int} = h_{rad} + h_{conv} = 4.4\varepsilon/0.837 + 3.6 \tag{6.5}$$

$$h_{ext} = 10 + 4.1v \tag{6.6}$$

where, h_{int} and h_{ext} are the combined heat transfer coefficients (W/(m^2·K)) of the interior and exterior surfaces, respectively; v is the wind speed (m/s) around the glass surface.

6.2.2 Heat transfer in the air gap

The above Equation (6.2) describes the heat convection at the glass surface, while the convective heat flow in the vertical air gap can be described as the following Equation (6.7) (EN, 2011a; ISO, 2003):

$$q_{conv} = Nu \frac{k_{air}(T_i - T_{i+1})}{d_{air}} \tag{6.7}$$

where, Nu is the Nusselt number, k_{air} and d_{air} are the thermal conductivity (W/(m·K)) of the air filling the gap and the thickness (m) of the air gap, respectively.

The following equations are presented for determining the Nusselt number of the vertical air gap, when windows inclined at 90° (ISO, 2003). The equation for Rayleigh number is as well given below, in which the dynamic viscosity can be obtained by the interpolation approach using the data given in the standard (EN, 2011a).

$$Nu = (Nu_1, Nu_2)_{max} \tag{6.8}$$

$$Nu_1 = \begin{cases} 0.067383Ra^{\frac{1}{3}}, & 5 \times 10^4 < Ra < 10^6 \\ 0.028154Ra^{0.4134}, & 10^4 < Ra \leq 5 \times 10^4 \\ 1 + 1.7596678 \times 10^{-10} Ra^{2.2984755}, & Ra \leq 10^4 \end{cases} \tag{6.9}$$

$$Nu_2 = 0.242 \left(\frac{Ra}{A}\right)^{0.272} \tag{6.10}$$

where, Ra is the Rayleigh number, the dimensionless number associated with buoyancy-driven convection (also called free convection or natural convection), A is the area (m^2).

$$Ra = \frac{g\beta\rho^2 L^3 C_p \Delta T}{\mu k_{air}} \tag{6.11}$$

where, g is the acceleration due to gravity (m/s^2), β, ρ, and C_p are the thermal expansion coefficient, density (kg/m^3), and specific heat (kJ/kg·K) of the filling gas, L is the height (m) of the air gap, μ is the dynamic viscosity ($N \cdot s/m^2$), ΔT is the temperature drop (℃) across the air gap.

Apart from the radiative heat transfer between the surfaces in the air gap, the dominance between heat conduction and heat convection depends on the filling gas and gap width. It is concluded that 12 mm should be chosen as the width for a gap filled with air or argon while 6 mm is recommended as the optimal width for a gap filled with Krypton (Lawrence Berkeley National Laboratory, 2019). Filling Krypton makes the window more compact but more expensive. Studies also found that the optimal thickness for minimizing the heat flow is also related to the climate (Arici & Karabay, 2010; Aydin, 2000). Generally, conduction dominates in narrower gaps while convection dominates in wider gaps (Lawrence Berkeley National Laboratory, 2019). Numerical investigations for optimizing the air layer behind semi-transparent PV cells indicate that conduction dominates when the gap is smaller than 10 mm

and Nu equals to 1 when gap width is small enough (J. Han, Lu, & Yang, 2009). In this case, it can be assumed that merely the conductive heat transfer of the air gap needs to be considered.

6.2.3 Heat transfer in vacuum gap

The reason why a vacuum gap can greatly improve the thermal insulation performance is that conduction and convection heat transfer by gas is eliminated from the gap in absence of a medium. The air pressure inside a vacuum gap should be lower than 0.1 Pa, while there is still residual gas in the vacuum gap. The vacuum pillars, usually cylindrical, have too small areas so that the radiation heat transfer between these surfaces and glass can be neglected. Under above conditions, the heat transfer occurring inside the vacuum gap is mainly the radiation between the glass surfaces as well as the heat conduction through the residual gas and vacuum pillar array. The radiant heat flow between the glass surfaces can be obtained by Equation (6.3). The conductive heat flow of the residual gas can be calculated with Equation (6.12) (R. E. Collins & Simko, 1998):

$$q_{cond} = C_{air}(T_i - T_j) \approx 0.8P(T_i - T_j) \tag{6.12}$$

where C_{air} (W/(m^2·K)) is the thermal conductance of the residual gas and P (Pa) is the pressure in the vacuum gap.

For calculating the equivalent thermal conductance of the vacuum pillar array (R. Collins & Fischer-Cripps, 1991), both the thermal conductivity and height of the vacuum pillar need

to be considered as per Equation (6.13)) and Equation (6.14) as a rigorous and approximate solution, respectively (R. E. Collins & Simko, 1998).

$$C_{pillar} = \frac{2k_g r}{S^2\left(1 + \frac{2H}{\pi k_p r}\right)} \tag{6.13}$$

$$C_{pillar} \approx \frac{2k_g r}{S^2} \tag{6.14}$$

where, C_{pillar} is the thermal conductance of the vacuum pillar array (W/(m^2·K)), r and H are the radius (m) and height (m) of a single vacuum pillar, k_g and k_p are the thermal conductivity (W/(m·K)) of the glass and vacuum pillar, S is the space between two vacuum pillars (m).

Equation (6.14) does not consider the thermal conductivity and height of the pillar; the latter is also the width of the vacuum gap. The thermal conductance of the pillar array is approximately determined as a constant knowing the thermal conductivity of the glass, the radius and spacing of the vacuum pillar. Such approximation is deemed sufficient when the thermal conductivity of the vacuum pillar is much higher than that of the glass (Charlie Curcija, Simon Vidanovic, Robert Hart, Jacob Jonsson, 2018). It is noteworthy that the vacuum pillar material is stainless steel with a thermal conductivity of about 17 W/(m·K) far greater than that of glass (around 1 W/(m·K)). In the published literature, aerosol-based vacuum pillars with thermal conductivity as low as 0.032 W/(m·K) have been used to further reduce the U-value of the vacuum PV window (Jarimi et al., 2020). In view of this, this chapter will determine a

reasonable range of the vacuum pillar conductivity and height for applying the approximation equation.

Take a vacuum pillar of the cylindrical shape as an instance, its typical diameter and height are 0.5-1.0 mm and 0.05 mm with a separation of about 50mm (Charlie Curcija, Simon Vidanovic, Robert Hart, Jacob Jonsson, 2018). Holding other parameters fixed, the thermal conductance of the vacuum pillar array keeps constant once the thermal conductivity of the vacuum pillar exceeds a certain value. As shown in Figure 6.2, the precise solution of C_{pillar} can be equivalent to the approximate one only if k_p exceeds 5 W/(m·K) in this specific case. In this condition, Equation (6.13) should be used to determine the thermal conductance of the vacuum pillar array when the thermal conductivity of the material is below 5 W/(m·K) (e.g. aerosol-based vacuum pillar).

Figure 6.3 shows that the percentage error between the solutions from Equation (6.13) and (6.14) increases with the growing height (H) of vacuum pillars while decreases with the larger radius of vacuum pillars. This error becomes significant with a radius less than 0.2 mm, especially when the height is greater than 0.1 mm. The approximate solution can be acceptable if the radius of the stainless-steel vacuum pillar is greater than 0.15 mm, and its height is no more than 0.5 mm. It can be seen that the ratio of height to radius cannot exceed certain range

for the error control. The upper limit of this ratio is 2.8 when S=50mm, k_g=1 W/(m·K), k_p=20 W/(m·K).

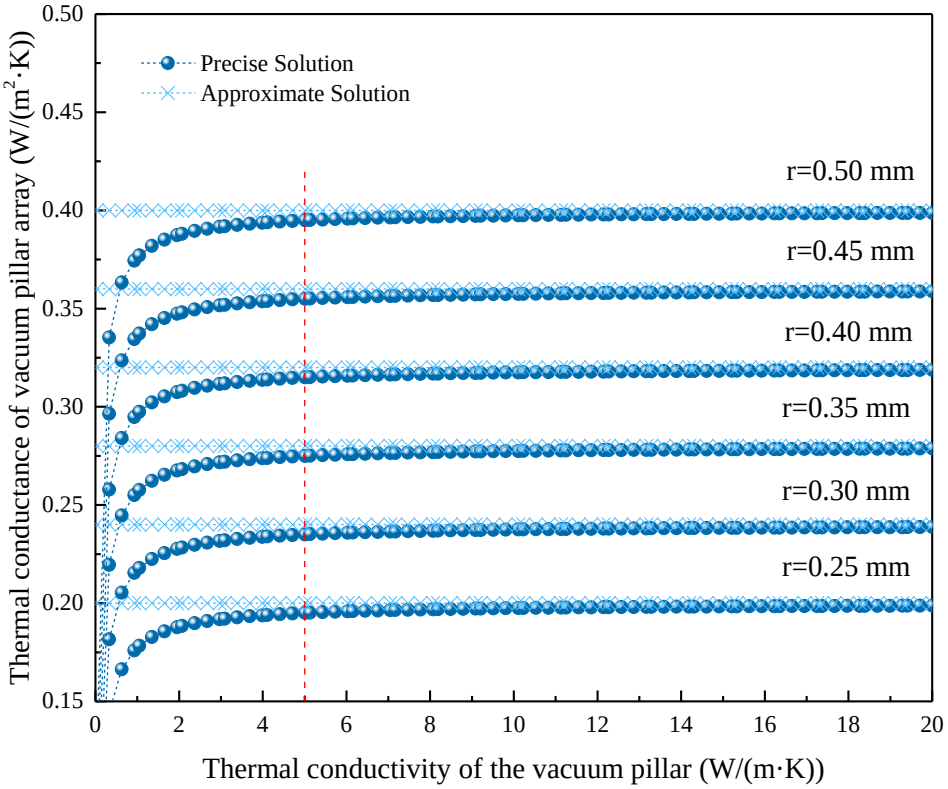

Figure 6.2 The variation of array thermal conductance with pillar radius and thermal conductivity (H=0.05 mm, S=50 mm, k_g=1 W/(m·K))

The design constraints on VG have to be elaborated when discussing the effects of varying the radius and height of vacuum pillars. First of all, the maximum tensile stress on the vacuum pillar cannot exceed 4 MPa (R. Collins & Fischer-Cripps, 1991), while that on the 4 mm glass sheet cannot exceed 35 MPa (B. Chen et al., 2019a). Both the vacuum pillar and glass layer should withstand the stress so that the vacuum pillar array can separate the glass layers and maintain the inside pressure below 0.1 Pa. Secondly, to prevent cone fracture, the relationship

between the vacuum pillar spacing and radius needs to comply with Equation (6.15) (R. Collins & Fischer-Cripps, 1991). Lastly, the thermal conductance of the vacuum pillar array should be less than 0.3 W/(m^2·K) (R. Collins & Fischer-Cripps, 1991). Combining the above limitations, a reasonable range of the vacuum pillar radius and separation can be determined referring to (R. E. Collins & Simko, 1998; Henshall et al., 2016).

$$S \leq 155r^{0.75} \tag{6.15}$$

where S and r are in millimeter.

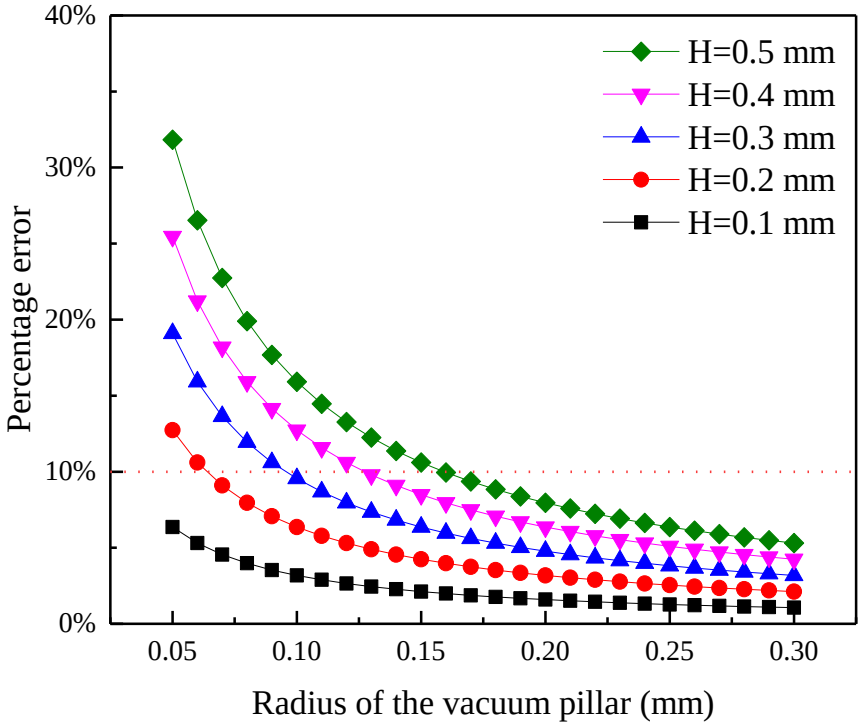

Figure 6.3 Percentage error between approximate solution and precise solution of pillar array thermal conductance of with varied pillar radius and height (S=50 mm, k_g=1 W/(m·K), k_p=20 W/(m·K))

6.3 Thermal Evaluation Metrics

There are two commonly used metrics to evaluate the heat transfer performance of windows. One is the overall heat transfer coefficient, also known as the U-value or U-factor, which describes the heat transported from outdoor to indoor environment through the window when there is no solar irradiance. The U-value can also be used to assess the thermal insulation performance, and a smaller U-value means better thermal insulation with less heat gains or losses. The solar heat gain coefficient is the other metric indicating the solar energy passing through the fenestration system and becoming the heat gain. Apart from the directly transmitted part, some of the solar energy is absorbed by the window and then released to the indoor environment by radiative and convective heat transfer. Cooling dominated areas require a low heat gain from the sun, while heating dominated areas demand high solar heat gain coefficients. In addition, this section also analyzes the heat gain and power generation of PV glazing.

6.3.1 Overall heat transfer coefficient

The U-value is determined using the guarded hot box calorimeter under the winter condition without sun light, as recognized by standards around the world (ASTM, n.d.; EN, 2011b; ISO, 2003; *JGJ/T 151-2008: Calculation specification for thermal performance of windows, doors, and glass curtain-walls (Chinese)*, 2008). The temperature and overall surface heat transfer coefficient need to be controlled on both sides of the window in the standardized

test. The warm (indoor) side's air temperature is controlled as 21℃, while that of the cold (outdoor) side is -18℃. The heat transfer coefficients of the interior and exterior surfaces of the window are 8.3 W/(m^2·K) and 29 W/(m^2·K), respectively (ASTM, n.d.). Such strict control is not easy to achieve under the limited experimental conditions, where accurate and feasible calculation methods become more desirable. There are two main approaches to calculating the U-value. For windows with a simple structure, the U-value mainly depends on the heat transfer coefficient of the interior and exterior surfaces as well as the thermal resistance of the window (Equation (6.16)) (Sun, Wu, & Wilson, 2018). The other approach defines the U-value as the heat flow in watts per hour through each square meter of the window at a difference of 1°C between indoor and outdoor air temperatures (Equation (6.17)) (ASHRAE, 2017).

$$U = \frac{1}{\frac{1}{h_{int}} + R + \frac{1}{h_{ext}}} \tag{6.16}$$

$$U = \frac{Q_{int}}{A(T_{in} - T_{out})} = \frac{q_{conv} + q_{rad}}{T_{in} - T_{out}} \tag{6.17}$$

where, R is the thermal resistance of the glazing (K/W); Q_{int} is the heat flow from the window to the room (W), which is the sum of convective and radiant heat flows of the interior surface; T_{in} and T_{out} are the indoor and outdoor air temperature (℃), respectively.

Taking the most complex structure (HPVVG) as an example, the heat transfer process in the absence of solar radiation can be described by the following set of equations:

$$h_{ext}(T_1 - T_{ext}) = \frac{(T_2 - T_1)k_{pv}}{d_{pv}} \tag{6.18}$$

$$\frac{(T_2 - T_1)k_{pv}}{d_{pv}} = \frac{(T_3 - T_2)k_g}{d_g} \tag{6.19}$$

$$\frac{(T_3 - T_2)k_g}{d_g} = \frac{(T_4 - T_3)k_{air}}{d_{air}} + \sigma\varepsilon_{eff,1}(T_4^4 - T_3^4) \tag{6.20}$$

$$\frac{(T_4 - T_3)k_{air}}{d_{air}} + \sigma\varepsilon_{eff,1}(T_4^4 - T_3^4) = \frac{(T_5 - T_4)k_g}{d_g} \tag{6.21}$$

$$\frac{(T_5 - T_4)k_g}{d_g} = \left(C_{air} + C_p\right)(T_6 - T_5) + \sigma\varepsilon_{eff,2}(T_6^4 - T_5^4) \tag{6.22}$$

$$\left(C_{air} + C_p\right)(T_6 - T_5) + \sigma\varepsilon_{eff,2}(T_6^4 - T_5^4) = \frac{(T_7 - T_6)k_g}{d_g} \tag{6.23}$$

$$\frac{(T_7 - T_6)k_g}{d_g} = h_{int}(T_{int} - T_7) \tag{6.24}$$

Above equations characterize the heat transfer process in the steady state from the outside to inside layer. The heat (cold) is first transferred to the outside layer by convection and radiation as the product of the integrated surface heat transfer coefficient and temperature difference. Within the complex structure, heat is transferred between the glass layers in the form of heat conduction. Because the thickness of the air gap is less than 12 mm, only heat conduction and radiation need to be considered in this part. As for the vacuum gap, the calculation includes radiation between the glass surfaces as well as heat conduction through the residual gas and pillar array.

6.3.2 Solar heat gain coefficient

The solar heat gain coefficient is an indicator of the indoor heat gain caused by the sunlight, and it is commonly referred to as the g-value in Europe (ASHRAE, 2017). From its definition, the solar heat gain includes directly penetrated solar heat and the reradiated, conducted, or convected portion of the absorbed solar radiation into the room. Therefore, Equation (6.25) is used to calculate the solar heat gain coefficient under the solar radiation intensity of 500 W/m^2 (ISO, 2003; JGJ/T 151-2008: Calculation specification for thermal performance of windows, doors, and glass curtain-walls (Chinese), 2008). Moreover, the indoor air temperature is 25 ℃, while the outdoor air temperature and sky radiation temperature are both 30 ℃. The convective heat transfer coefficient on the interior surface of the glass is 2.5 W/(m^2·K) while that on the exterior surface is 8.5 W/(m^2·K) (ISO, 2003; JGJ/T 151-2008: Calculation specification for thermal performance of windows, doors, and glass curtain-walls (Chinese), 2008).

$$SHGC = \frac{Q_{int} + G_\tau}{A(T_{in} - T_{out})} = \frac{A(q_{conv} + q_{rad}) + G_\tau}{A(T_{in} - T_{out})} \tag{6.25}$$

where, G_τ means the part of solar irradiation (W/m^2) directly transmitted through the window into the room.

Unlike the U-value, the entire process of sunlight transmission, absorption, and reflection within the window needs to be considered when calculating the solar heat gain coefficient. The optical characteristics of each glass layer are measured by a spectrophotometer in the 300nm -

2500nm band for all studied composite glazing types. The measurement results are fed into Optics 6 to further derive the transmittance and reflectance of each layer. Then, the absorptance of each glass layer can be calculated by the following Equation (6.26).

$$\alpha = 1 - \tau - \rho_r \tag{6.26}$$

where, α, τ and ρ_r are the absorptance, transmittance and reflectance, respectively.

Using HVPVG as an instance, external heat enters the outer surface of the front glass layer (CdTe thin-film solar cells coated on its back side) by convection and radiation. The heat is then transferred to the next layer by thermal conduction together with the portion absorbed by the first layer. In the meantime, some of the sunlight is absorbed by solar cells and converted to electricity. Equation (6.28) is the traditional linear expression of the PV conversion efficiency (Skoplaki & Palyvos, 2009).

$$\alpha_1 G + h_{ext,conv}(T_{out} - T_1) + \varepsilon_1 \sigma (T_{out}^4 - T_1^4) = \frac{(T_1 - T_2)k_{pv}}{d_{pv}} + \frac{A_{pv}}{A_g}\eta_{pv}\tau_1 G \tag{6.27}$$

$$\eta_{pv} = \eta_{stc}\left(1 - \beta_c\left(T_{pv} - T_{stc}\right)\right) \tag{6.28}$$

where, A_{pv} is the area (m^2) of solar cells, A_g is the area (m^2) of the glazing, η_{stc} is the module efficiency when solar cells receive an irradiance of 1000 W/m^2 at temperature T_{stc} of 25 ℃ under standard test conditions, β_c is the temperature coefficient, η_{pv} is the solar cell efficiency at temperature T_{pv} (℃), which is assumed to equal T_2 (℃).

For the second glass sheet, the absorbed sunlight together with the heat transferred from the first layer through thermal conduction, exchanges heat with the air gap and the surface of the third layer:

$$\alpha_2\tau_1 G + (T_1 - T_2)k_{pv}/d_{pv} = \frac{(T_2 - T_3)k_g}{d_g} \tag{6.29}$$

$$\frac{(T_2 - T_3)k_g}{d_g} = Nu\frac{k_{air}(T_3 - T_4)}{d_{air}} + \varepsilon_{eff,1}\sigma(T_3^4 - T_4^4) \tag{6.30}$$

For the third glass sheet, the heat transferred from the air gap and absorbed sunlight absorbed are transferred to the vacuum gap by heat conduction, while conduction through the residual gas and pillar array as well radiation between glass walls occur within the vacuum gap.

$$\alpha_3\tau_1\tau_2 G + Nu\frac{k_{air}(T_3 - T_4)}{d_{air}} + \varepsilon_{eff,1}\sigma(T_3^4 - T_4^4) = \frac{k_g(T_4 - T_5)}{d_g} \tag{6.31}$$

$$\frac{k_g(T_4 - T_5)}{d_g} = \varepsilon_{eff,2}\sigma(T_5^4 - T_6^4) + \left(C_{air} + C_{pillar}\right)(T_5 - T_6) \tag{6.32}$$

For the back glass, it absorbs the sunlight penetrating two gaps of the glazing and the heat from the vacuum gap, and then continues to transfer heat in a conductive manner. The heat finally reaches the room in radiative and convective manners:

$$\alpha_4\tau_1\tau_2\tau_3 G + \varepsilon_{eff,2}\sigma(T_5^4 - T_6^4) + \left(C_p + C_{pillar}\right)(T_5 - T_6) = \frac{k_g(T_6 - T_7)}{d_g} \tag{6.33}$$

$$\tau_1\tau_2\tau_3\tau_4 G + \frac{k_g(T_6 - T_7)}{d_g} = h_{int,conv}(T_7 - T_{in}) + \varepsilon_2\sigma(T_7^4 - T_{in}^4) \tag{6.34}$$

For other types of PVVGs, the corresponding heat transfer models can be obtained by simplifying the above process as their structures are simpler than the composite HPVVG unit.

6.4 Model validation against existing references

Validation of the proposed heat transfer model is conducted against several references including different types of glazing such as the PV insulated glass unit (Zhang & Lu, 2019), PV laminated glazing (Liao & Xu, 2015), VG (Z. Han et al., 2012), and vacuum glazed PV (Radwan et al., 2020). The physical parameters and boundary conditions for these window structures are drawn from the literature, where the U-value or SHGC is obtained by various means as summarized in Table 6.3. The U-value of VG with two uncoated glass layers is obtained as 2.257 W/(m^2·K) from a simulative study using the finite element model (Z. Han et al., 2012), which is consistent with calculation results in this chapter. Furthermore, Liao and Shen proposes a calculation model to investigate the U-value and SHGC of a sandwich structure of an amorphous silicon photovoltaic window (Liao & Xu, 2015). The window does not contain an air layer, and the total thickness of the solar cell with EVA is 1.5 mm. The presented U-value and SHGC for a Semi-transparent PV insulated glass unit are calculated using Optics and WINDOW developed by the Lawrence Berkeley National Laboratory (Lawrence Berkeley National Laboratory, n.d.). The mentioned unit consists of a PV laminated glass layer, 12 mm thick air gap and clear glass layer (Zhang & Lu, 2019). In addition, Ali

Radwan, et al. determines the U-value of semi-transparent PV with VG (contains four layers of glass) as 1.3 (W/(m^2·K)) using the 3D finite element model (Radwan et al., 2020). The emissivity of each coated surface in the vacuum gap all equals 0.18. Therefore, the simulated results are in good agreement with those presented in listed papers, proving the accuracy of the proposed mathematical heat transfer model by the current study.

Table 6.3 Comparison of the simulated U-value (W/(m^2·K)) and SHGC of different glazing with exiting literatures

Glazing category	**Methods**	**Reference/This work**	
		U-value	**SHGC**
VG (Z. Han et al., 2012)	Simulation	2.19/2.331	-/-
PV glazing (Liao & Xu, 2015)	Calculation	5.18/5.214	0.41/0.43
PV insulated glass unit (Zhang & Lu, 2019)	Simulation	2.635/2.658	0.220/0.213
PV with VG (Radwan et al., 2020)	Simulation	1.2/1.274	-/-

6.5 Thermal performance of different glazing

The predicted U-value and SHGC of different PVVG with the validated heat transfer model are summarized in Table 6.4, where HPVG has the largest U-value while PVVG-A and PVVG-B have the smallest ones. There is no difference in the U-value between PVVG-A and PVVG-B, indicating little impact from changing the location of Low-E coating in a closed cavity. The U-value decreases by 28% if HPVG is integrated with VG, judging by the comparison between HPVVG and HPVG. However, the U-value of HPVVG is still high if compared with PVVG-A or PVVG-B, as the Low-E coating is used in the air gap rather than the vacuum gap. This phenomenon will be further discussed in the following session.

Regarding the SHGC of compared PVVG, it can be found that HPVG brings in more heat gains by solar irradiance, followed by HPVVG and PVVG-A, with the lowest value observed in PVVG-B. The integration of VG can reduce 15% of the solar heat gain when comparing HPVG and HPVVG. However, the combination of the air gap and vacuum gap does not lead to a lower SHGC. Furthermore, SHGC increases when the Low-E coating in the vacuum gap faces the outdoor environment unlike the U-value's case. As a result, PVVG-A may be more suitable for the cold region while PVVG-B suits the hot climate, because a higher SHGC could bring in more solar heat. This finding echoes with the conclusion drawn in the research of the impact from changing position of the single Low-E coating in double glazing (T. P. Wang &

Wang, 2014). For better explanation, Figure 6.4 is present to demonstrate that Low-E coating' facing direction should be consistent with the heat flow direction.

Table 6.4 Predicted U-value and SHGC for different PV glazing

Glazing category	**HPVVG**	**HPVG**	**PVVG-A**	**PVVG-B**
U-value (W/(m^2·K))	1.40	1.93	0.48	0.48
SHGC	0.190	0.223	0.191	0.170

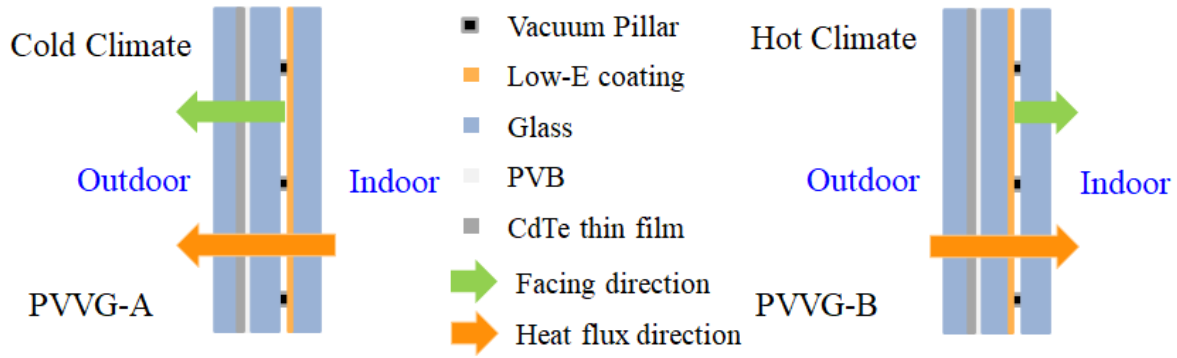

Figure 6.4 The Low-E coating's facing direction (in PVVGs) and hear flux direction

Low-E coating is supposed to effectively reduce the heat transfer through radiation. The most complex structure, HPVVG, has two internal gaps and thus four inner surfaces available for coating. To decide the preferred coating surface, four cases HPVVG-1, HPVVG-2, HPVVG-3, and HPVVG-4 are named according to the order of four surfaces from outdoor to indoor, as indicated by Figure 6.5. The first two coated surfaces are located in the air gap, while the last two are in the vacuum gap. Comparing the U-value of these four glazing types in Table

6.5, the overall heat transfer is remarkably cut down if coating a surface in the vacuum gap instead of the air gap. Such results can be derived from the fact that the main heat transfer mode in the vacuum gap is radiation, which allows the Low-E coating to perform effectively by changing the glazing surface property. The U-values of HPVVG-3 and HPVVG-4 are lower than those of PVVG-A and PVVG-B, owing to the integration with the air gap. Comparing the SHGC across the four structures, it is revealed that Low-E coating on a surface facing indoor can contribute to a smaller heat gain from sunlight no matter in the air or vacuum gap. Combining the variation of both the U-value and SHGC, it can then be summarized that the Low-E coated surface should be within the vacuum gap, facing indoor (HPVVG-3) for cooling dominated areas while facing outdoor (HPVVG-4) for heating dominated areas.

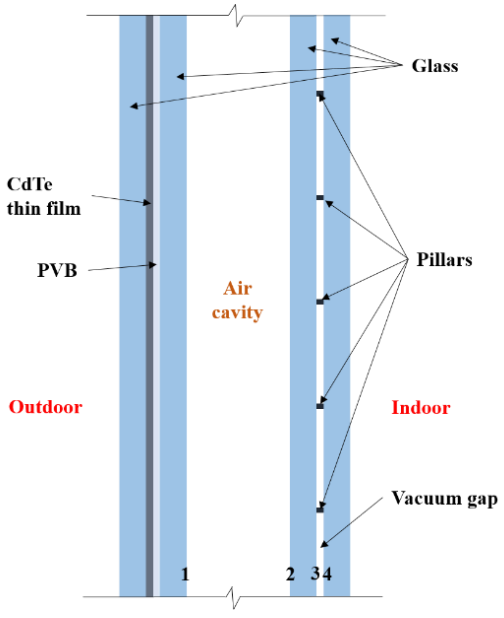

Figure 6.5 The structure of HPVVG

Table 6.5 Predicted U-value and SHGC for different HPVVGs

Glazing category	HPVVG-1	HPVVG-2	HPVVG-3	HPVVG-4
U-value (W/(m^2·K))	1.40	1.40	0.45	0.45
SHGC	0.190	0.200	0.157	0.173

Table 6.6 Temperature distribution of different glazing (°C)

Layer	HPVVG-1	HPVG	PVVG-A	PVVG-B	HPVVG-2	HPVVG-3	HPVVG-4
1	43.19	42.57	42.99	43.73	42.70	43.88	43.28
2	43.17	42.52	42.97	43.76	42.65	43.92	43.27
3	43.07	42.36	42.93	43.72	42.57	43.94	43.24
4	34.76	30.30	28.14	26.76	36.39	44.83	42.45
5	34.66	30.10	28.04	26.71	36.31	44.86	42.42
6	29.00				29.68	26.83	27.93
7	28.88				29.54	26.77	27.84

Table 6.6 illustrates the temperature distribution of different structures under the same boundary conditions, with layers sorted by direction from outdoor to indoor. The first layer refers to the exterior surface of each structure, while the last layer is the interior surface. The solar cell is located on the second layer and represents the layer temperature. HPVG has the lowest solar cell temperature among all the cases, as solar cells have difficulty in heat

dissipation when integrated with VG of excellent insulation performances. However, the solar cell temperature difference between these structures is not substantial. HPVVG-1 and HPVVG-2 have higher interior surface temperatures than HPVVG-3 and HPVVG-4, confirming that Low-E coating can block more heat if used in the vacuum gap rather than the air gap. Both PVVG-A and HPVVG-4 share the same coating configuration and higher interior surface temperatures than PVVG-B and HPVVG-3, proving that Low-E coating facing outdoor is indeed suitable for cold regions.

6.6 Summary

The current study presents a comprehensive heat transfer model to determine the thermal metrics such as the U-value and SHGC of different photovoltaic glazing panels, including hollow photovoltaic glazing, photovoltaic vacuum glazing, and hollow photovoltaic vacuum glazing. Based on the combination of basic heat transfer patterns, the heat transfer in the air and vacuum gap is revealed with detailed illustrations. The heat transfer model for evaluating the U-value and SHGC is established based on detailed analyses and validations against existing literatures for accurately modeling the vacuum glazing, hollow photovoltaic glazing, and photovoltaic vacuum glazing. The validated model is then used to predict the U-value, and SHGC for different glazing, and major findings are summarized as below:

(1) Combining vacuum glazing and hollow PV glazing, the U-value of hollow PV glazing can be significantly reduced by 28% while the solar heat gain can be cut down by 15%. Such reduction can be further enhanced if the Low-E coating is applied in the vacuum gap. PV vacuum glazing has a lower U-value and SHGC comparable to hollow PV vacuum glazing.

(2) In the air gap or vacuum gap, the location of the Low-E coating does not affect the U-value, but it does change the SHGC and temperature distribution. Low-E coating' facing direction should be consistent with the heat flow direction. When facing outdoor, it is suitable for cold regions. Low-E coatings can more effectively reduce the overall heat transfer in a vacuum gap rather than an air gap. Therefore, the hollow photovoltaic vacuum glazing has a lower U-value and SHGC if the Low-E coating is applied on the internal surfaces of vacuum gap, as the heat loss in winter and heat gain in summer can be reduced.

CHAPTER 7 EXPERIMENTAL INVESTIGATION AND MODEL VALIDATION OF PHOTOVOLTAIC VACUUM GLAZING

Hollow photovoltaic glazing, photovoltaic vacuum glazing and hollow photovoltaic vacuum glazing are evaluated through experiments and numerical simulations, with double glazing as the baseline. A test rig is built for both indoor and outdoor experiments to study the thermal and electrical performance of different photovoltaic glazing. Physical parameters including thermal conductivity, optical and electrical properties are measured. A simplified heat transfer model is proposed based on detailed thermal analysis and reasonable assumptions. The model is validated against the experimental data, proving the adequate ability to accurately predict the performance of photovoltaic glazing with various structures. In this context, the climate suitability is analyzed for targeted glazing in terms of heating load, cooling load and power output.

7.1 Physical Characteristics

The section below provides different perspectives on the physical properties of different PV glazing, including dimensions, structural parameters, thermal conductivity, optical

properties, and electrical performance. All types of PV glazing are fabricated and supplied by Advanced Solar Power (Hangzhou).

7.1.1 Basic parameters

Four types of PV glazing are involved in the current work, which are hollow PV glazing (HPVG), PV vacuum glazing (PVVG) and hollow PV vacuum glazing (HPVVG). Figure 7.1 shows the structural diagrams of these four types of glazing. The difference between PVVG-A and PVVG-B lies in the location of Low-E coating, which is applied on the front of the last glass after the vacuum gap facing outdoor in PVVG-A, while on the back of the middle glass before the vacuum gap facing indoor in PVVG-B. And the Low-E coating locates before the air gap in both HPVVG and HPVG. The HPVVG is a composite structure with both a gas layer and a vacuum layer. The gas layer is filled with a 9 mm wide air layer in both HPVG and HPVVG.

The Cadmium-Telluride (CdTe) thin film solar cells are grid-shaped and coated on the back of the front glass in all glazing. And the solar cells cover 60% area of the glazing. The thickness of the front glass is 3.2 mm while it is merely 3 μm for the thin film. Moreover, the thickness of the other glass is 4 mm, except for the last layer of glass in hollow PV glazing which is 5 mm. All the glazing types are fabricated 1.2 m high and 0.6 m wide. In the vacuum gap, pillars are separated by 50 mm $\times$ 60 mm. A single pillar has a diameter of 0.5 mm and a

height of 0.4 mm, which is made of stainless steel with thermal conductivity of 17 W/(m·K). Ethylene-vinyl acetate (EVA) and polyvinyl butyral (PVB) are often used for laminating, and their thermal conductivities are 0.34 W/(m·K) and 0.76 W/(m·K), respectively (B. Chen et al., 2019b). PVB is utilized in current study. The Low-E coating is applied facing indoor with an emissivity of 0.06 and locates in the air gap within HPVG and HPVVG. However, the Low-E coating faces outdoor in the vacuum gap within PVVG. Table 7.1 gives the detailed structural information of different PV glazing.

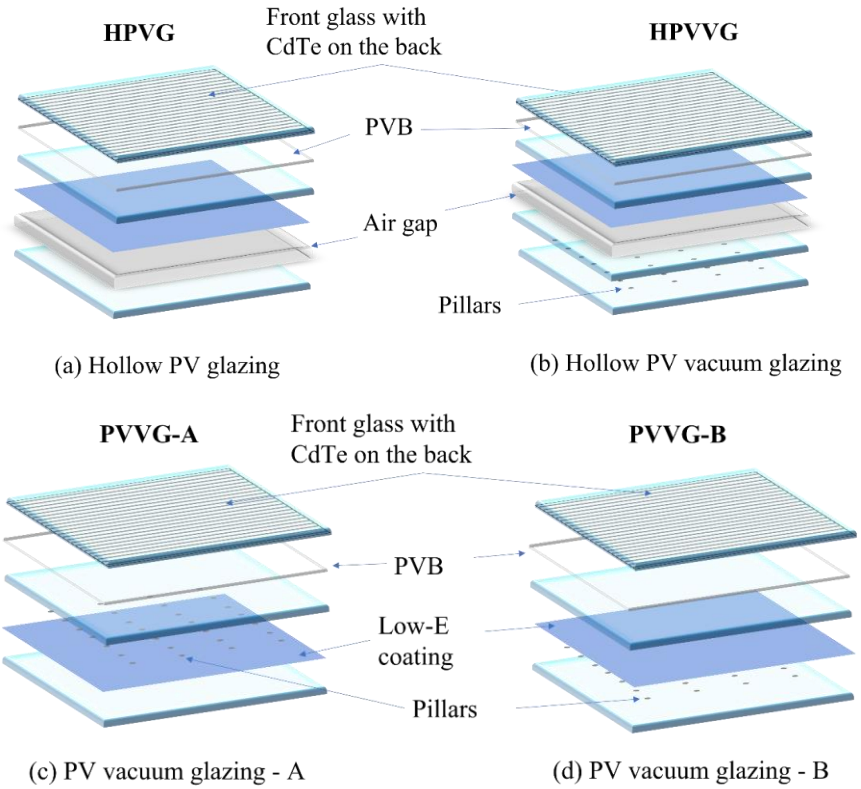

Figure 7.1 Structural diagrams of different PV glazing

Table 7.1 The structure of different PV glazing

Glazing	Structure
HPVG	Outdoor/3.2 mm FG/PVB/4 mm TG with Low-E coating on the back/9 mm A/5 mm TG /Indoor
HPVVG	Outdoor/3.2 mm FG/PVB/4 mm TG with Low-E coating on the back/9 mm A/4 mm TG /0.4 mm V/4 mm TG/Indoor
PVVG-A	Outdoor/3.2 mm FG/PVB/4 mm TG/0.4 mm V/4 mm TG with Low-E coating on the front/Indoor
PVVG-B	Outdoor/3.2 mm FG/PVB/4 mm TG with Low-E coating on the back/0.4 mm V/4 mm TG /Indoor

Note: FG means the float glass with CdTe thin film solar cells on the back, TG means the tempered glass, A means the air gap, V means the vacuum gap.

The thermal conductivity of each layer shown in both Figure 7.1 and Table 7.1 is measured using the TC 3000E from XIATECH. All of the tempered glass of 4 mm and 5 mm thick, Low-E coated tempered glass and the float glass with CdTe thin film solar cells on the back have a thermal conductivity around 1 W/(m·K) with very limited differences. Table 7.2 gives the measured value of each layer.

Table 7.2 The thermal conductivity of glass layers

Layer	Thermal conductivity
4 mm tempered glass	0.96 W/(m·K)
5 mm tempered glass	0.96 W/(m·K)
Tempered glass with Low-E coating	0.97 W/(m·K)
Float glass with CdTe thin film solar cells on the back	1 W/(m·K)

7.1.2 Optical properties

The structure of PV vacuum glazing is complex, and the optical properties of each layer can affect the final solar heat gain coefficient. Thus, the transmittance and reflectance of different PV glazing are measured using the UH4150 UV/VIS/NIR spectrophotometer from 300 nm to 2500 nm. For testing purposes, each layer of involved PV glazing shown in Figure 7.1 is tested using small-size samples (0.3×0.3 m^2). The front glass sample (0.1×0.1) is as well fabricated with CdTe thin film solar cells on its back (Figure 7.2(a)). Figure 7.2(b) shows the curves of transmittance, front and back reflectance, and absorptance of the tested front glass. Measured parameters, such as thickness, thermal conductivity, and optical characteristics, are then imported into Optics6, which further analyzes the optical properties of different layers in PV glazing. Table 7.3 summarizes the obtained optical parameters. Figure

7.3 shows the photo of PVVG-A placed behind the glass curtain wall, and the CdTe thin film does not affect the view and appears to be only less bright.

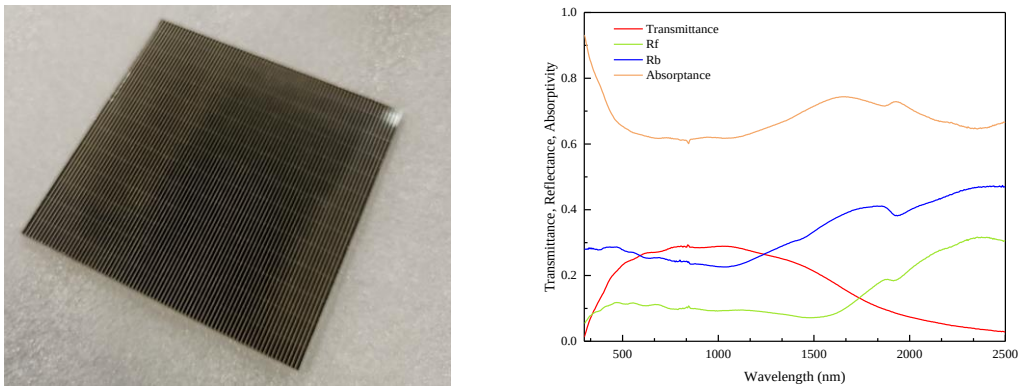

(1) Front glass ($0.1 \times 0.1\ m^2$)　　(2) Optical properties

Figure 7.2 Front glass with CdTe on the back and its Optical properties

Figure 7.3 Prototypes of PVVG-A and HPVVG

Table 7.3 Optical parameters of each layer in different glazing

Layer	4 mm tempered glass	5 mm tempered glass	Low-E coated glass	Front glass
T_sol	0.901	0.894	0.660	0.243
Rf_sol	0.072	0.078	0.214	0.109
Rb_sol	0.072	0.078	0.171	0.273
T_pho	0.911	0.910	0.873	0.249
Rf_pho	0.075	0.081	0.045	0.113
Rb_pho	0.075	0.081	0.050	0.268

Note: T_sol means solar transmittance while T_pho means visible light transmittance. Rf and Rb are the reflectances of the front and back surfaces, respectively.

7.1.3 Electrical properties

The electrical properties of PV modules are usually measured under standard testing conditions, i.e., 1000 W/m^2, 25 °C, and AM 1.5. In order to determine the electrical performance of PV glazing, the manufacturer places the glazing to stand for a period until the glazing reaches ambient temperature, the instantaneous solar simulator is then turned on. The power generated by the module is measured at solar irradiance of 1000W/m^2 when the

temperature of solar cells gets 25 °C. Taking the PVVG as an example, the following I-V and P-V curves can be obtained as shown in Figure 7.4.

Table 7.4 also gives the measured data provided by the manufacturer, including short-circuit current, open-circuit voltage, maximum power generation and photovoltaic conversion efficiency, etc. Moreover, the temperature coefficient is 0.214 %/°C for the CdTe thin film solar cells. And the output power is guaranteed to reach 90% of rated output power within 10 years and 80% within 25 years.

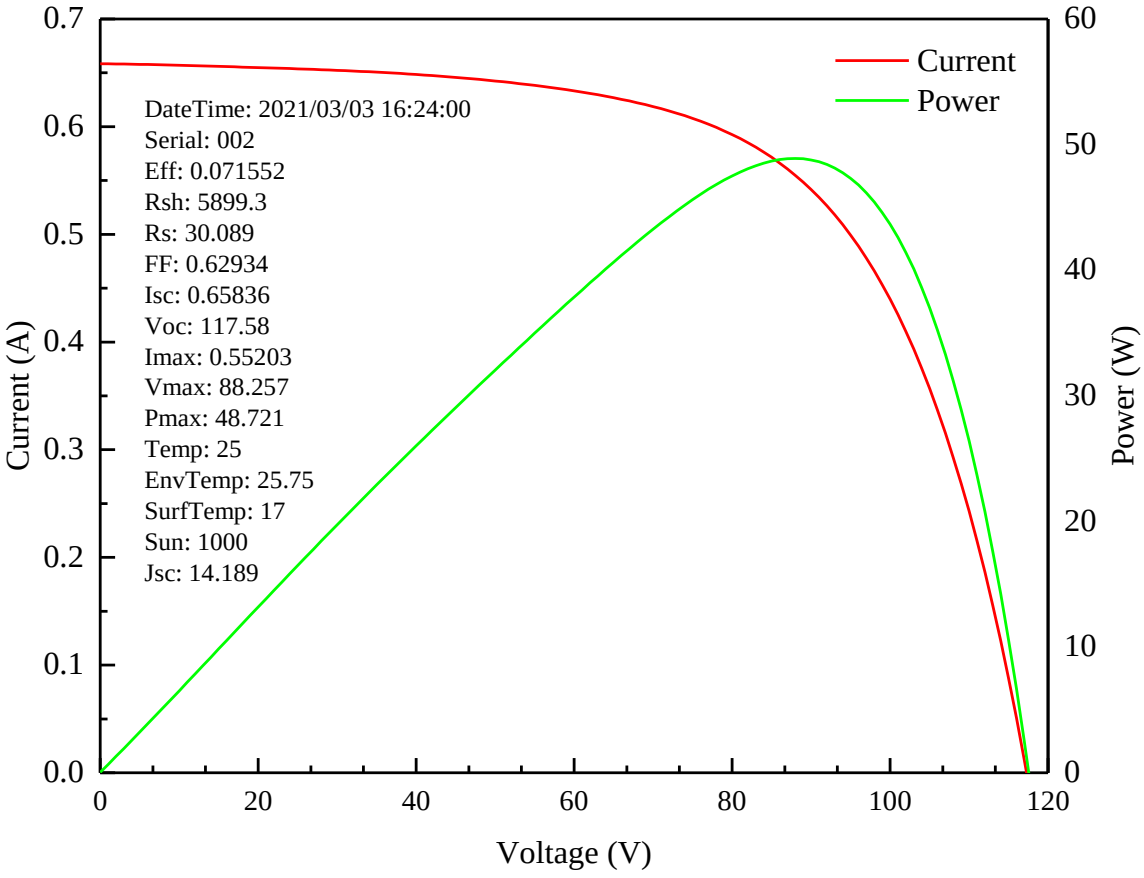

Figure 7.4 The I-V and P-V curves of PVVG-A under STC

Table 7.4 Electrical properties of PVVG-A

Electrical properties	**Value**
Maximum power output (W)	48.7
Voltage at the maximum power point (V)	88.3
Current at the maximum power point (A)	0.55
Open circuit voltage (V)	117.6
Short circuit current (A)	0.66
Module efficiency	7.16%
Fill factor	62.9%

7.2 Experimental methodology

This section introduces the setup of the test rig and equipment. Different settings of indoor test and outdoor test are also described.

7.2.1 Test rig

A wooden cabinet is designed for building the test rig. As shown in Figure 7.5, a window-type air conditioner is installed on the left, under which a shelf is assembled for placing a heater controller, an I-V checker MP170, a computer and data loggers. A heater is placed inside the cabinet and connected to the heat controller with PID settings for stable temperature control.

The core of the heater controller is PXF4 from Fuji Electric. I-V checker MP170 is used to measure the real-time data of current, voltage and maximum power output of PV glazing. Two pyranometers are prepared to measure the solar irradiance received by the vertical façade and entering the cabinet through the glazing. Thus, one pyranometer is placed on the top of the cabinet while the other is placed inside the cabinet. Temperature sensors are suspended in the cabinet to monitor the air temperature. Data logger GL840 and GL800 are responsible for collecting data on temperature, heat flux and solar irradiance. The configuration of the temperature and heat flow sensors will be described in the following paragraphs. Except for the skeletonized area (around 1.2 m × 0.6 m) left for test samples, the cabinet is covered by 20 mm thick insulation cotton with aluminum foil. Four snaps are installed to prevent the test samples from tipping over.

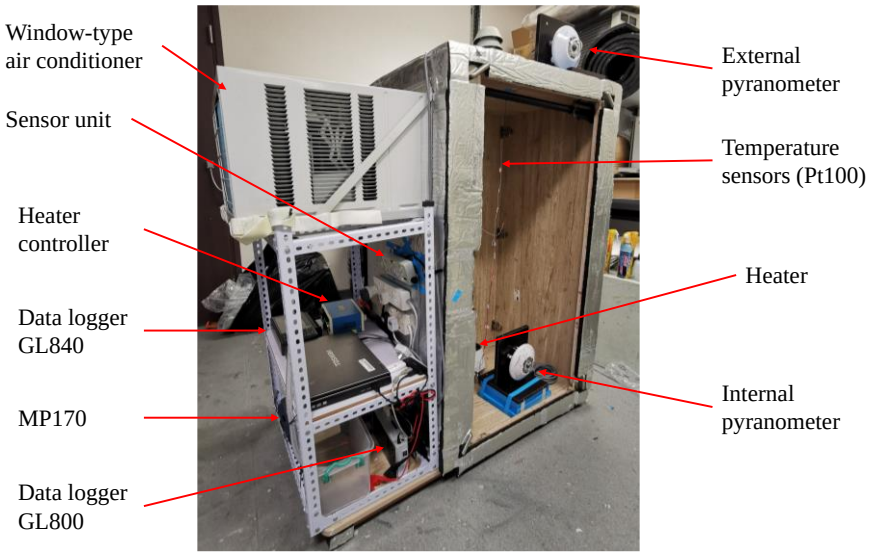

Figure 7.5 Overview of the test rig

7.2.2 Indoor test

In addition to measuring physical parameters, including thickness, thermal conductivity, and optical properties, indoor experiments include utilizing the test rig to monitor the thermal performance of different PV glazing at a temperature difference of 15 ℃. This temperature difference is decided by referring to the standardized boundary conditions for determining U-value for windows (EN, 2011a). The indoor test is conducted without light, and the room temperature is controlled by the air conditioner in the room at about 20 ℃, while the temperature inside the cabinet is controlled by the heater at around 35 ℃. Thus, neither the window-type air conditioner nor the pyranometers are not in use. Merely the temperature and heat flux data are collected. 12 temperature sensors and 4 heat flux sensors are prepared, half of which are attached on the interior surface and the other half are attached to the exterior surface. In order to reduce the measurement error and make the measured data more accurately reflect the surface temperature and heat flux, these sensors are evenly distributed on the surface.

Figure 7.6 shows the equipment for measuring thermal conductivity (TC 3000E), optical properties (UH4150) and the distribution of temperature and heat flux sensors. Although each heat flux sensor will cover a 0.1×0.1 m^2 area, the heat flow entering the cabinet through the glazing will not be affected as the indoor test needs no light. However, since sunlight is an important boundary condition for outdoor tests, only one heat flux sensor will be used on both

the exterior and interior surface in the outdoor test so that the impact from the shadow can be reduced. To reduce the effect of the radiation from surroundings and to improve the accuracy, mentioned sensors are covered by aluminum foil tape and coated with heat-conducting silicone grease before being applied to the glass surface. The temperature sensors are calibrated using an ice and water mixture prior to use.

(a) TC 3000E

(b) UH4150

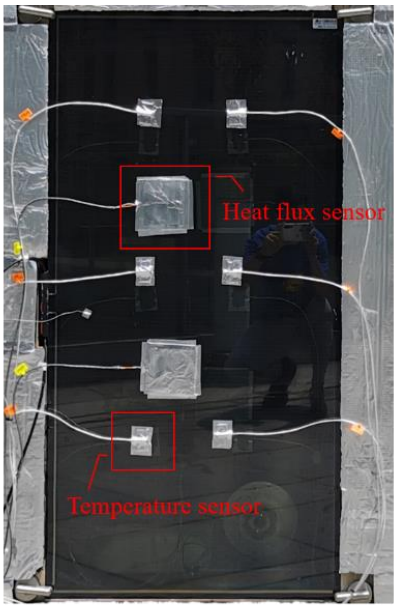

(c) Sensor distribution

Figure 7.6 Indoor test: (a) TC 3000E, (b) UH4150, and (c) sensor distribution

7.2.3 Outdoor test

Different from the settings of indoor test, the outdoor test should collect data of ambient temperature and wind speed in addition to surface temperature and heat flux. Thus, a mini weather station is placed near the cabinet as shown in Figure 7.7. A pyranometer is installed

on the top of the cabinet to collect the data of solar irradiance on the vertical façade, which is set facing south. A T-type thermocouple is positioned next to this pyranometer to measure the ambient temperature. Another T-type thermocouple is adhered to the exterior surface of the glazing with aluminum foil tape. These two thermocouples and one pyranometer are directly connected to the sensor unit, which is taped to the outer surface of the cabinet under the window-type air conditioner (as shown in Figure 7.5). Using RS-485, the data can be transferred from the sensor unit to the MP-170 I-V checker (main unit). This allows the measurement of incident solar irradiance, ambient temperature and the approximate back-side temperature of the PV module while measuring the I-V curve on the main unit at the same time. As the CdTe thin film solar cells are coated on the back of the front glass, which is laminated with another layer of glass, making it difficult to measure the back-side temperature of the solar cells. Thus, in current case, the T-type thermocouple measures the exterior surface temperature to replace this temperature. Figure 7.8 shows the configuration of the I-V checker and sensor unit. According to the manual for MP-170, running the main unit and sensor unit simultaneously enables easy conversion of Standard Test Conditions (STC) to JIS C8914 standard. Table 7.5 summarizes the instruments and sensors used in the indoor and outdoor tests.

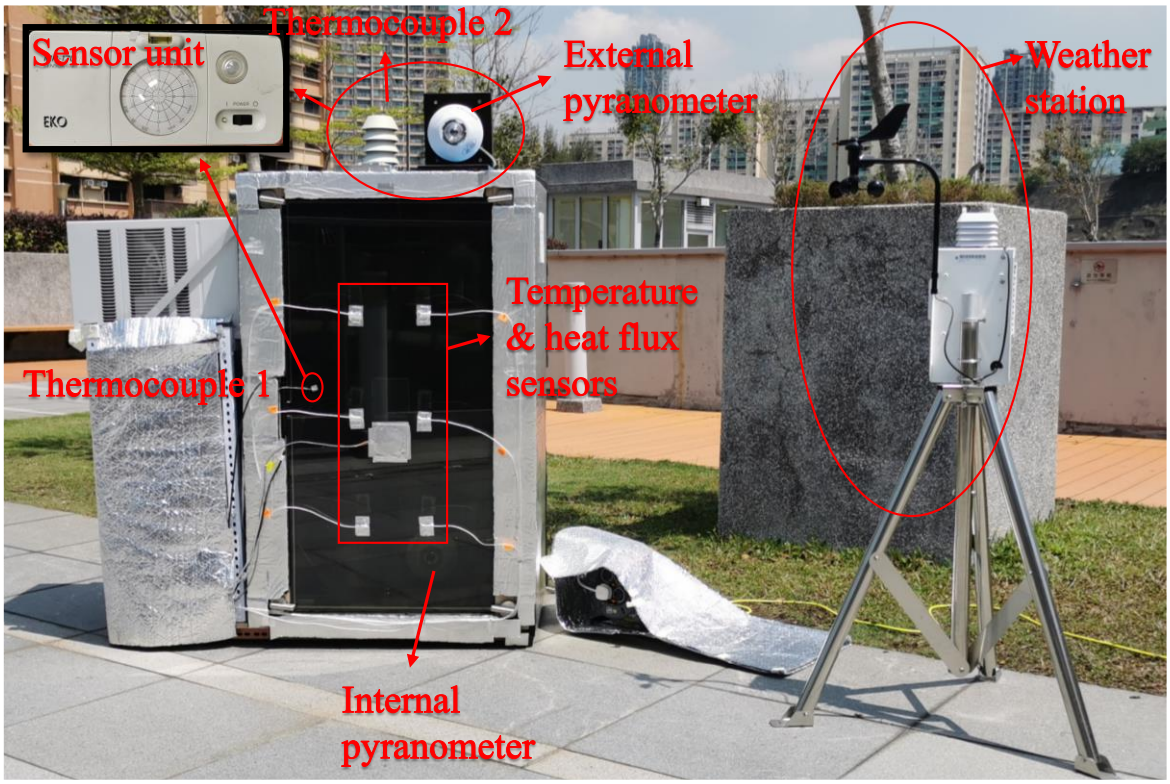

Figure 7.7 Outdoor test

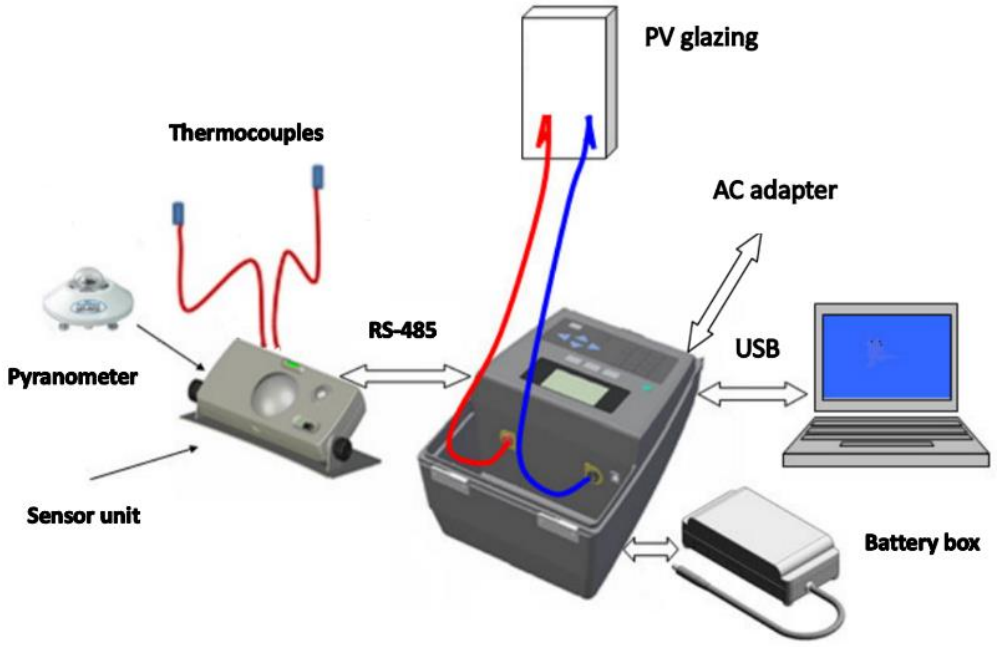

Figure 7.8 System Configuration of MP-170 I-V checker

Table 7.5 The experimental instruments and their specifications

Equipment	**Manufacturer and model**	**Technical data**	**Uncertainty**
Heat flux sensor	EKO HF-10S	Sensitivity: approx. 12 μV/W/m²; Thermal resistance: approx. 0.0016 °C/(W/m^2)	-
Temperature sensor	Pt100	-50° to 200 °C	±0.2 °C
Pyranometer	EKO MS-802	Sensitivity: approx. 7 μV/W/m²	Directional response at 1000W/m²: ± 10 W/m²
Heater	Midea HFY20Y	Power: 1000-1999 W	-
Micro control X	Fuji Electric PXF4	Proportional band: 0.1 to 999.9% Integration time: 0 to 3200 s Differential time: 0.0 to 999.9 s	-
Datalogger	Graphtec GL800 & GL840	Pt100: -200 to 850 °C Voltage: ± 0.1 % of F.S.	Temperature: ± 0.8 ºC Voltage: ± (0.05% of F.S. + 10μV)

Weather station	Spectrum WatchDog 2550	Wind speed: 0, 3-241 km/h Air temperature: -32° to 100 °C	Wind speed: ±3 km/h; Air temperature: ±0.6 °C
Thermal conductivity meter	XIATECH TC 3000E	Accurate: 3 % for most samples with flat surface in the range of (0.001~10W/(mK))	-
Window-type air conditioner	Rasonic RC-HZ70Y	Cooling Capacity: 7,400 (3,482-7,648) BTU/h (3/4HP) Heating Capacity: 7,400 (3,448-7,614) BTU/h (3/4HP)	-

7.3 Experimental results and its validation with the heat transfer model

This section presents the experimental data and the validation against the simulative results by the mathematical heat transfer model built in Chapter 6. In the indoor experiment, four PV glazing were replaced one after another and installed vertically in the reserved cutout position of the cabinet. The air temperature in the cabinet was maintained around 35 ℃ by the heater with PID control while the temperature outside the cabinet was controlled as about 20 ℃ using the indoor air conditioner. For the case of HPVVG, it took 3 hours for the air temperature in cabinet became stable starting from 24.1 ℃ as shown in Figure 7.9. Ultimately

this temperature fluctuated between 33.5 to 33.8 ℃. Moreover, the ambient temperature showed a continuous fluctuation from the lowest 17.9 ℃ to the highest 19.7 ℃. In the actual simulation calculation process, the boundary conditions were obtained from the data when the fluctuation was relatively stationary.

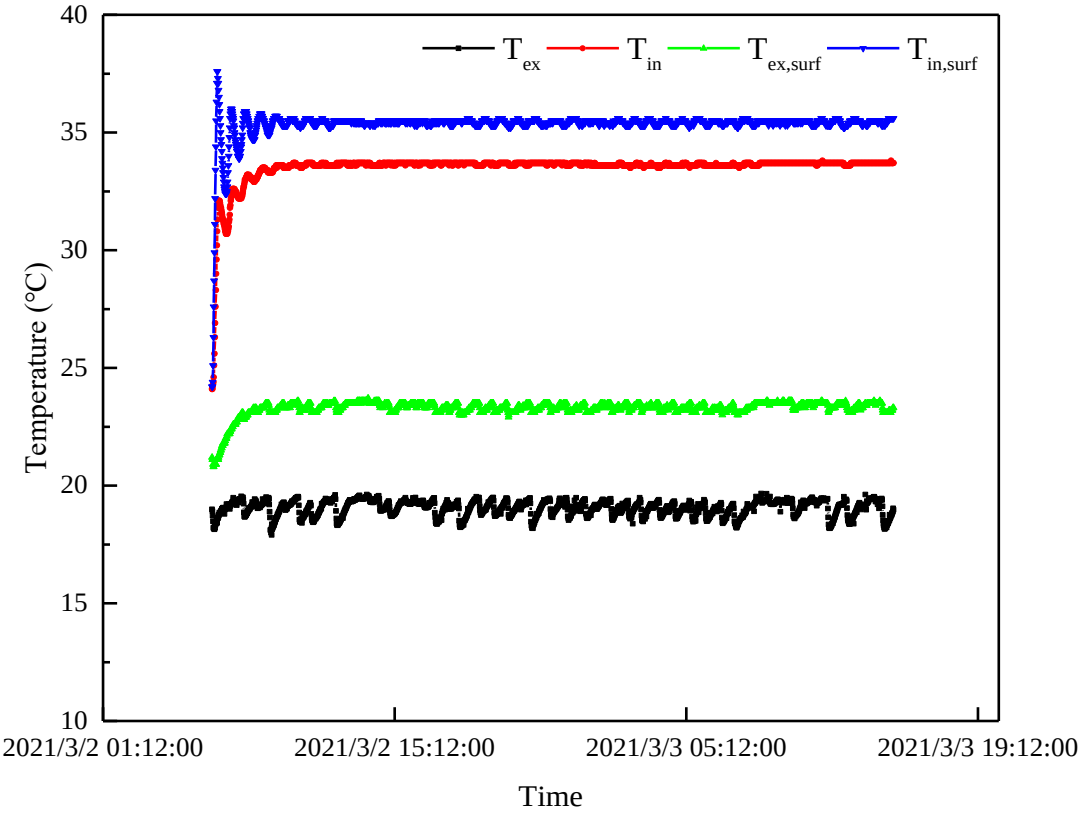

Figure 7.9 Ambient and surface temperature of HPVVG during indoor test

The experimental and simulated results for different PV glazing are summarized in Table 7.6. The heat transfer coefficients for the exterior and interior surfaces are obtained through the value measured by heat flux sensors over temperature difference. Judging from the results shown in Table 7.6, the simulation by proposed heat transfer model is in good agreement with the indoor experiments. 2.62% is the average error between experimental and simulated

temperatures of exterior and interior surfaces. Table 7.7 shows the results obtained by 3D finite element models as presented in Chapter 5, which simulates the surface temperature utilizing COMSOL Multiphysics. The results in Table 7.6 derived by the simplified heat transfer model present considerable computational accuracy, compared with those by 3D finite element models in Table 7.7. Researchers have also conducted contrast between analytic models and 3D finite models (Simko et al. 1995; Wilson, Simko, and Collins 1998), which deliver consistent results for vacuum glazing. Therefore, one-dimensional simplified models are sufficient to simulate PV glazing with vacuum structures, while complex numerical simulations consume more computational resources and time.

Table 7.6 Comparison between indoor experimental and simulated results

Glazing type	**Experimental results**						**Simulated results**	
	T_{ex}	T_{in}	h_{ex}	h_{in}	$T_{ex,surf}$	$T_{in,surf}$	$T_{ex,surf}$	$T_{in,surf}$
HPVG	19.0	33.6	4.26	25.34	24.2	34.7	25.9	35.9
HPVVG	19.0	33.7	4.04	13.03	23.3	35.4	24.1	35.2
PVVGA	18.8	34.8	2.70	4.84	21.3	36.6	22.1	36.6
PVVGB	19.0	34.5	2.70	4.34	21.4	36.4	22.2	36.5

Note: the unit of *T* is converted into °C.

Table 7.7 Comparison between indoor experimental results and simulated ones by COMSOL Multiphysics

Glazing type	Experimental results		Simulated results by COMSOL Multiphysics	
	$T_{ex,surf}$	$T_{in,surf}$	$T_{ex,surf}$	$T_{in,surf}$
HPVG	24.2	34.7	26.5	34.6
HPVVG	23.3	35.4	25.0	35.2
PVVG-A	21.3	36.6	20.0	34.0
PVVG-B	21.4	36.4	20.1	33.6

Note: the unit of *T* is converted into ℃.

Outdoor tests were conducted between late April and early May 2021 excluding rainy days. Unlike indoor experiments that do not require light, the PV glazing in outdoor experiments receives real-time dynamic solar irradiance. The window-type air conditioner was turned on to control the temperature in the cabinet at around 21 ℃. The maximum temperature difference between exterior and interior surfaces was monitored and recorded in Table 7.8. On these days when the weather is similar, PV vacuum glazing could achieve a maximum temperature difference at about 20 ℃, which is sufficient to prove its excellent thermal performance. And PVVG-A has the highest temperature difference while HPVG owns the lowest one. However, this temperature difference is caused by complex weather factors,

including outside temperature, wind speed and solar radiation intensity. The corresponding power output of involved PV glazing as well depends on the solar irradiance. Thus, the following Section 5.2 will continue to compare the overall performance of all the glazing under the same climatic conditions.

Table 7.8 The maximum temperature difference between exterior and interior surfaces

Glazing type	$(T_{ex,surf} - T_{in,surf})_{max}$	**Date**
HPVG	16.2	May 8, 2021
HPVVG	20.4	Apr 23, 2021
PVVG-A	23.1	May 5, 2021
PVVG-B	19.2	May 10, 2021

Take PVVG-A as the instance, the comparison between experimental data and simulative results is presented in Figure 7.10. Due to fluctuations in measured values exceeding the range described in the manual for heat flux sensor, the surface heat transfer coefficients are determined by Equations (6.5) and (6.6). The indoor temperature in the cabinet was controlled by the window-type air condition, which shows an obvious fluctuation. This unstable temperature is the result of the window-type air condition's cooling power being greater than the load in the cabinet. The trends of the temperature of the interior and exterior surfaces mainly follow the indoor and ambient temperatures. Moreover, the temperature error on the interior

and exterior surfaces is within the acceptable range, with a mean value of 6.68%. Therefore, the heat transfer model has sufficient capability to simulate the hourly heat gain or loss caused by the PV glazing.

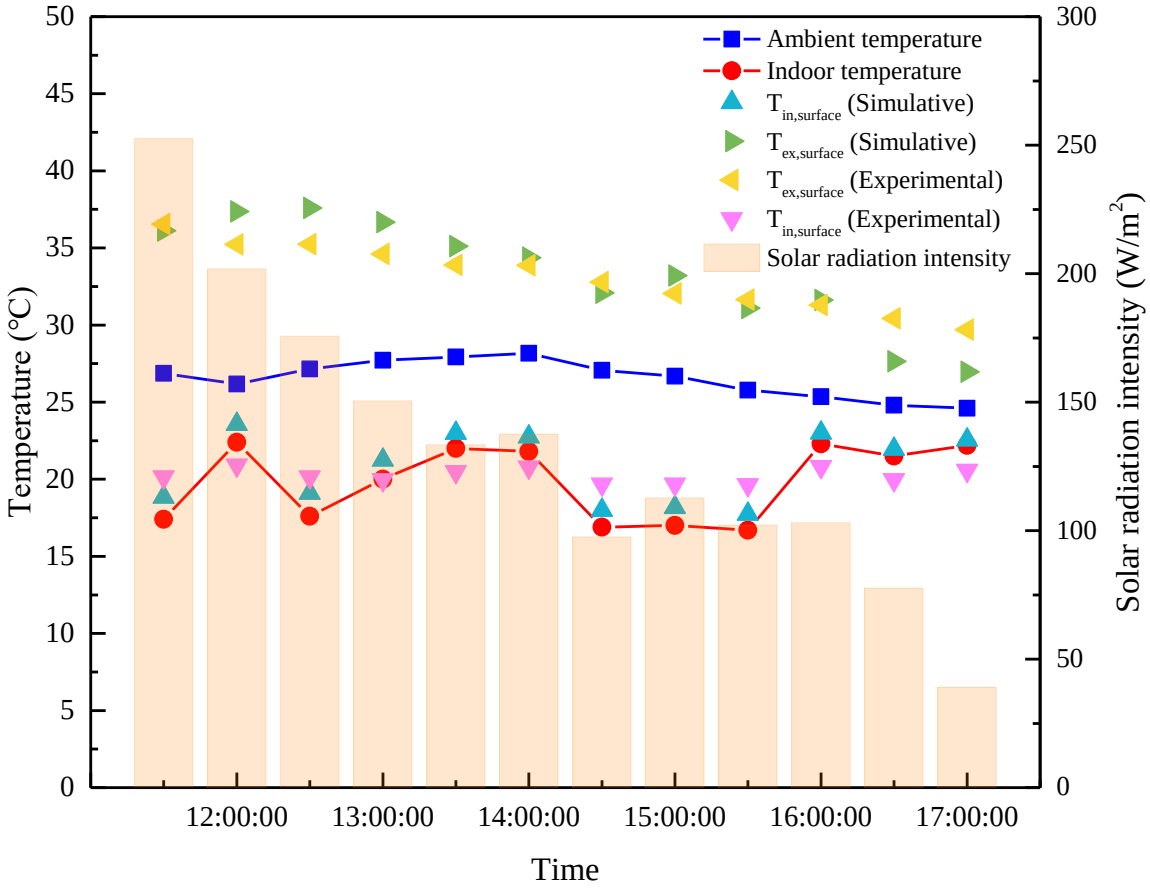

Figure 7.10 Experimental and simulative results of PVVG-A in the outdoor test

Figure 7.11 shows the electricity output and transmitted solar irradiation of PVVG-A monitored by MP-170 and data logger. As the total area of PVVG-A is merely 0.72 m^2 and the actual power generation efficiency is about 5%, the max amount of generated electricity shown in the figure is less than 8 W/m^2. The power generation efficiency will be higher, if further sacrifice the amount of incoming light to improve the cell coverage area, as currently solar cells

cover 60% of the total glazing. As for the rate of transmitted solar irradiation over solar radiation intensity, the average value is 0.13, slightly higher than the vacuum photovoltaic insulated glass unit (W. Zhang, Lu, and Chen 2017). This low solar transmittance indicates the ability to block a significant portion of solar radiation.

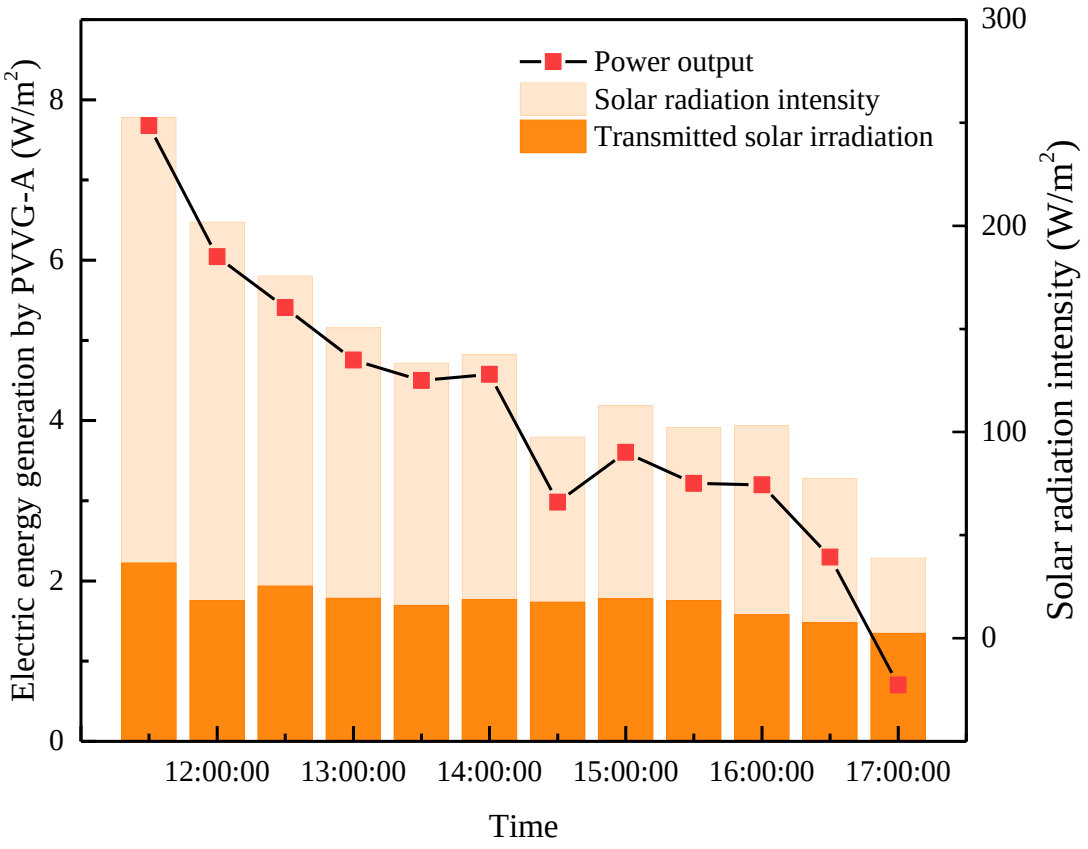

Figure 7.11 Electric energy generation and transmitted solar irradiation of PVVG-A (W/m^2)

7.4 Summary

The present chapter is undertaken to investigate the overall performance of different PV glazing, especially the hollow photovoltaic vacuum glazing, through experiments and simulations. Indoor and outdoor tests are conducted to obtain the physical, thermal, optical,

and electrical properties of different PV glazing. The maximum temperature difference between interior and exterior surface of the glazing could be about 20 ℃ for the PV vacuum glazing and hollow PV vacuum glazing during outdoor tests, which illustrates their ability to block most of the heat from outdoor environment.

Using the measured parameters, the simulative results by the proposed heat transfer model match well with the experimental data in both indoor and outdoor tests. Validated by the experimental data, the heat transfer model can accurately predict the surface temperature under zero and real-time sunlight. The experimental studies lay the foundation for the numerical simulation of thermal and electrical performance for various PV glazing in different climate zones.

CHAPTER 8 ANNUAL OVERALL PERFORMANCE EVALUATION AND COMPARISON OF DIFFERENT GLAZING

The mathematical heat transfer model, proposed in Chapter 6, is validated against published articles for both BIPV and VG in Section 6.4, and validated by the experimental data in Chapter 7. The theoretical model with proved accuracy is then used to predict the annual overall performance of different glazing in terms of heating load, cooling load, and power generation. The comprehensive comparison is conducted between double glazing, vacuum glazing, and PV glazing with diverse structures in various climate regions. Thus, the climate suitability can as well be analyzed for different glazing facing four orientations.

8.1 Annual overall performance

The total instantaneous heat flow from the glazing to the room can be summarized by Equation (8.1), considering the heat transfer resulting from the temperature difference, solar radiation and air leakage (ASHRAE, 2017). However, it is difficult to distinguish the heat flow due to the temperature difference and solar radiation in the presence of the sunlight. The temperature of the exterior window surface is the result of combining the outdoor air temperature, solar radiation intensity, sky temperature, and emissivity of surrounding surfaces.

Simplified calculations often equalize the temperature of the sky, surrounding surfaces, and ambient air. In accordance with the definitions of the U-value and SHGC, the heat gain and loss with and without solar radiation are calculated. The U-value is determined in the absence of sunlight mainly as a result of the temperature difference, which can also be caused by the solar irradiance during the daytime, especially by the rising temperature of solar cells under sunlight.

$$Q_{total} = UA_g(T_{out} - T_{in}) + (SHGC)A_gG + (AL)A_g\rho C_p(T_{out} - T_{in}) \qquad (8.1)$$

Moreover, the U-value and SHGC are dynamic in Equation (8.1) because the weather data varies all the time. It has been investigated that the time lag for hollow double glazing is merely around 0.25 hour in both summer and winter, quite small compared with the brick wall (8 hours) or concrete wall (6.6 hours) (T. P. Wang & Wang, 2016). Time lag is the time taken for a temperature wave to pass through the building envelope (Huang, Yu, & Yang, 2018). Thus, it is much easier for a window to get the thermal balance as indicated by the short time lag. Moreover, a comparison has been made between a simplified analytic model and a 3D finite element model for modelling the thermal performance of vacuum glazing, and results showed a good agreement (Simko, Collins, Beck, & Arasteh, 1995). Another study related to vacuum glazing also states that the complex numerical modelling is not necessary as the results yielded

from the simplified analytic model is consistent with that of finite element model (Wilson, Simko, & Collins, 1998). In this case, it is possible to suppose that windows reach thermal equilibrium at each hour, and the heat transfer models presented in Chapter 6 can be used to predict the heat gain and loss with the typical meteorological data. Assuming a consistent air infiltration and considering only the heat gain through the structure, Equation (8.2) can be used to compare the heat gain and loss through PV glazing with different structures. If the value is positive, the room gains heat through the glazing, and vice versa, the room loses heat. Heat gain increases the indoor air conditioning load (cooling load) in the summer but helps to relieve heating energy consumption (heating load) in the winter. The opposite is true for heat loss.

$$Q \approx A_g \sum U(T_{out} - T_{in})_m + A_g \sum (SHGC) G_n \tag{8.2}$$

where AL ($m^3/(s \cdot m^2)$) is the air leakage, n and m is the time of day when there is solar radiation and no solar radiation, respectively.

To make the comparison between HPVG, PVVG and HPVVG, the generated electricity should as well be taken into consideration. The electricity generation and heating load (or cooling load) reduction produced by the above glazing contribute to reducing the total annual electricity consumption of buildings. Herein, the heating load (or cooling load) caused by the glazing is converted into the corresponding electricity consumption of air conditioning with

assumed COP values of 3 in both the cooling and heating seasons, respectively (Hu et al., 2017), which is also the COP of the adopted window-type air conditioner. Thus, the annual overall performance of different PV glazing can be evaluated by Equation (8.3).

$$E_{op} = \begin{cases} E - Q/COP, & cooling\ seaon \\ E + Q/COP, & heating\ season \end{cases} \tag{8.3}$$

where, E_{op} is the saved electricity (kWh/m^2) considering both power output and heat/cooling consumption, which indicates the annual overall performance of different glazing per unit area.

Table 8.1 Heating and cooling season for different climate regions in China (J. Liu et al., 2020)

City	**Climate**	**Heating season**	**Cooling season**
Harbin	Severe cold	Oct. 20 to Apr. 20	Jun. 15 to Aug. 15
Beijing	Cold	Nov. 15 to Mar. 15	Jun. 1 to Sep. 30
Wuhan	Hot summer & cold winter	-	May 15 to Oct. 15
Guangzhou	Hot summer & warm winter	-	Apr. 15 to Oct. 31

Table 8.1 sorts the heating and cooling season for different climate zones in China except for the mild climate. Hourly weather data for representative cities will be used as boundary conditions to be input into the heat transfer model to evaluate the combined performance of different glazing. Involved glazing units are assumed to be vertically installed on the façade

facing four orientations, and the air conditioning setpoints are 24 ℃ in summer and 21 ℃ in winter (X. Chen, Yang, & Peng, 2019). The indoor temperature is assumed to be a constant 22 ℃ during the rest of the year.

8.2 Comprehensive comparison between different glazing

Proved with adequate accuracy to predict the surface temperature of PV glazing, the heating and cooling load caused by different glazing in various climate regions can be calculated using the built heat transfer model. Table 8.2 gives the U-value and SHGC of double glazing and vacuum glazing, which are the benchmarks for selecting the optimal glazing in studied climate zones. DG and VG are made of 4 mm thick tempered glass with a Low-E coating (emissivity=0.06) on the inner surface (facing towards indoor) in the air and vacuum gap, respectively. DG has a 9 mm air gap as HPVG, HPVVG-1 and HPVVG-3, while VG has the same vacuum pillar array design as PVVG-A, PVVG-B, HPVVG-1, and HPVVG-3. As mentioned in Chapter 6, the Low-E coating faces outdoor in PVVG-A while faces indoor in PVVG-B. Moreover, the Low-E coating faces indoor in both HPVVG-1 and HPVVG-3 but locates in the air gap in the former while locates in the vacuum gap in the latter.

Table 8.2 U-value and SHGC of studied glazing

Glazing category	DG	VG	HPVG	PVVG-A	PVVG-B	HPVVG-1	HPVVG-3
U-value (W/(m^2·K))	1.948	0.475	1.93	0.48	0.48	1.40	0.45
SHGC	0.702	0.621	0.223	0.191	0.170	0.190	0.157

8.2.1 Glazing orienting south

The bar charts in Figure 8.1 show the annual overall performance of different glazing orienting south in various climate zones, in terms of heating load, cooling load, power generation and energy saving. These values are caused by different glazing per unit area. The negative values of heating loads mean the energy saving owing to the heat gain in the heating season, which is a combined results of high transparency and thermal insulation performance. This also explains why the VG saves the most energy for heating, as it does not have solar cells to block the penetration of sunlight and its U-value is as low as 0.48. Although the thermal insulation of DG may be poor because of relative high U-value, but its high SHGC brings in more heat gain from solar to indoor in heating season. So DG saves the second amount of heating energy. On the other hand, resulting from the same reason, the cooling load caused by DG and VG is much more than other glazing.

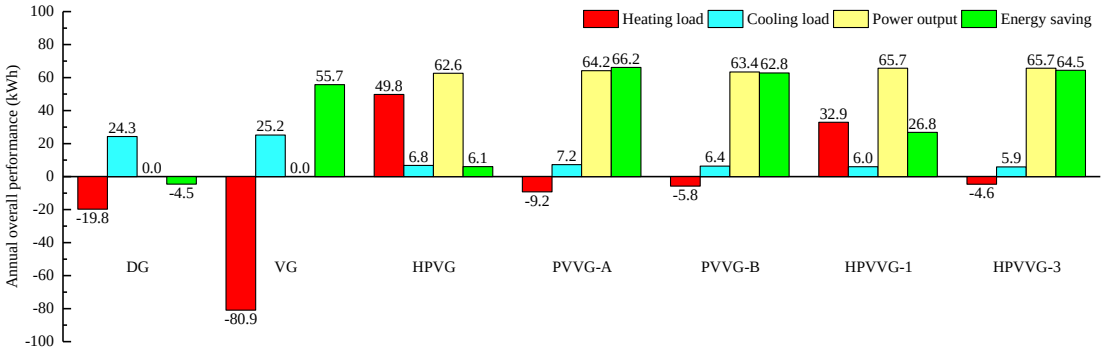

(a) Harbin (severe cold region)

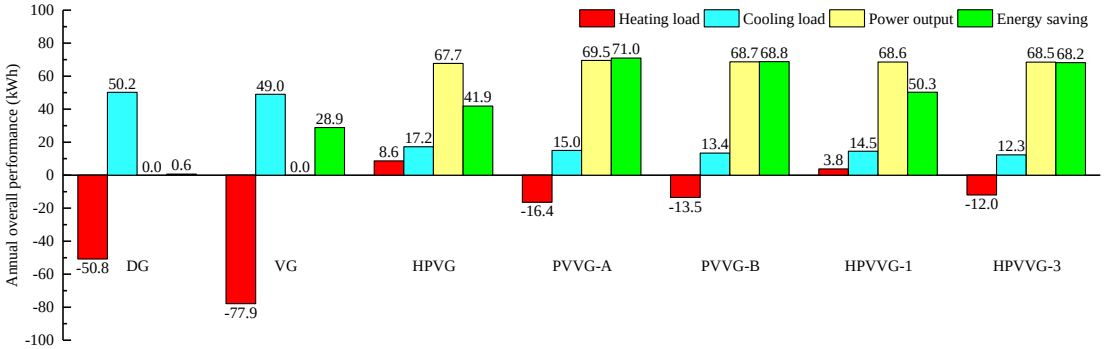

(b) Beijing (cold region)

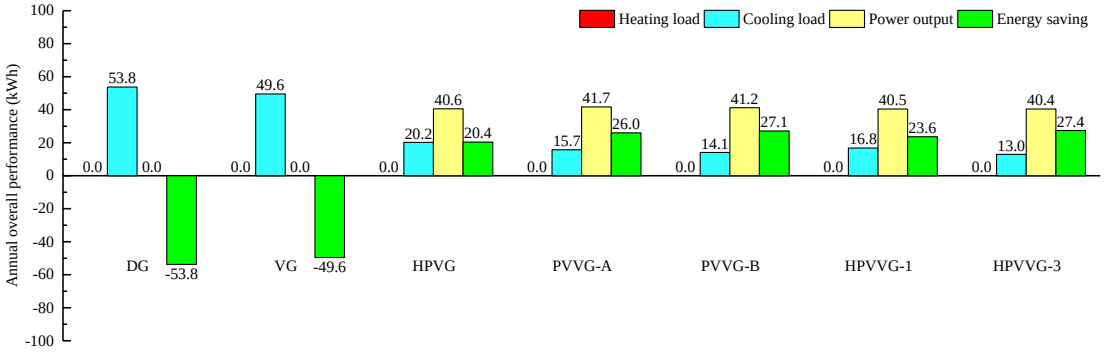

(c) Wuhan (hot summer and cold winter region)

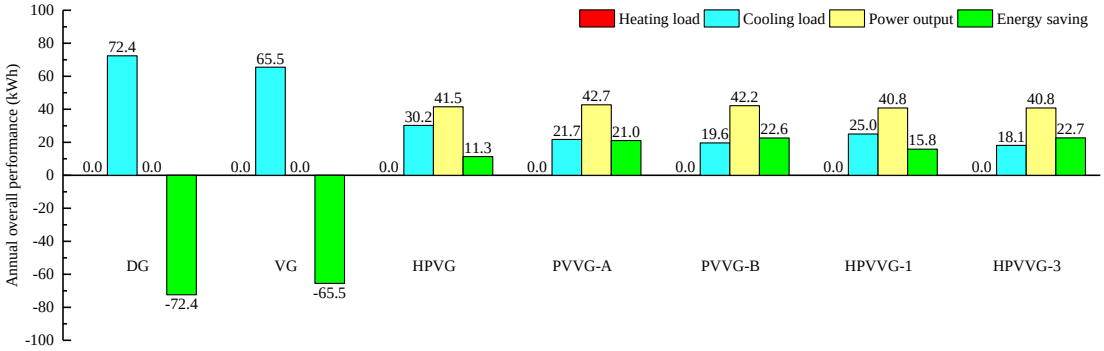

(d) Guangzhou (hot summer and warm winter region)

Figure 8.1 Annual overall performance of different glazing (orienting south) in various climate regions

Among the glazing orienting south in all climate regions, the top three glazing are PVVG-A, PVVG-B, and HPVVG-3. HPVVG-3 saves the most energy in Wuhan and Guangzhou while PVVG-A performs as the optimal one in Harbin and Beijing, although the advantages are not greatly significant compared to PVVG-B. HPVVG-3 contributes to the lowest consumption of cooling energy while PVVG-A helps save the most heating energy, leading to a result that PVVG-A offers better performance than HPVVG-3 in Harbin and Beijing. PVVG-B outperforms PVVG-A in hot climates like Wuhan and Guangzhou, which coincides with the conclusion in Section 6.5 based on the analysis of both U-value and SHGC. Furthermore, PVVG-A yields a little more power than PVVG-B does because the lower temperature of solar cells, as predicted in Table 6.6.

HPVVG-1 behaves better than HPVG in all studied climates, though the percentage of energy savings decrease in the regions that cooling demands dominate, i.e., Wuhan and Guangzhou. As HPVVG-3 shows the performance to overtake HPVVG-1 in all regions in terms of reducing heating and cooling energy consumption, it can be concluded that the Low-E coating should be applied in the vacuum gap other than the air layer to achieve better thermal

performance. The same result can be found in the other three orientations comparing HPVVG-3 with HPVVG-1 from the annual overall performance.

Compared with VG, HPVG and HPVVG-1 do not demonstrate much dominance in Harbin, especially HPVG. As there is the shade from the solar cells in HPVG and HPVVG-1, which allows less heat gain into the room to reduce the heating load.

8.2.2 Glazing orienting north

Compared with the situation of glazing facing south, glazing orienting north causes more heating energy consumption. For instance, DG could save heating energy because it brings about solar heat gain in both Harbin and Beijing when facing south but it in turn results in consuming more heat energy when facing north. This also happens to VG. And the power generation by PV glazing is obviously cut down because less solar irradiance is received. For the most notable examples, the electric energy production by HPVG and HPVVG is difficult to offset the heating and cooling load (Figure 8.2). As the reduction of cooling needs does not make up for the omission of the above two, glazing orienting north contributes to the lowest energy conservation in all orientations. And in this context, HPVVG-3 becomes the best glazing in all climate regions considering the annual overall performance. The main reason why HPVVG-3 is superior to PVVG-A is that the gap in heating energy use has narrowed. The same reasoning applies to the interpretation of PVVG-B over PVVG-A in Beijing.

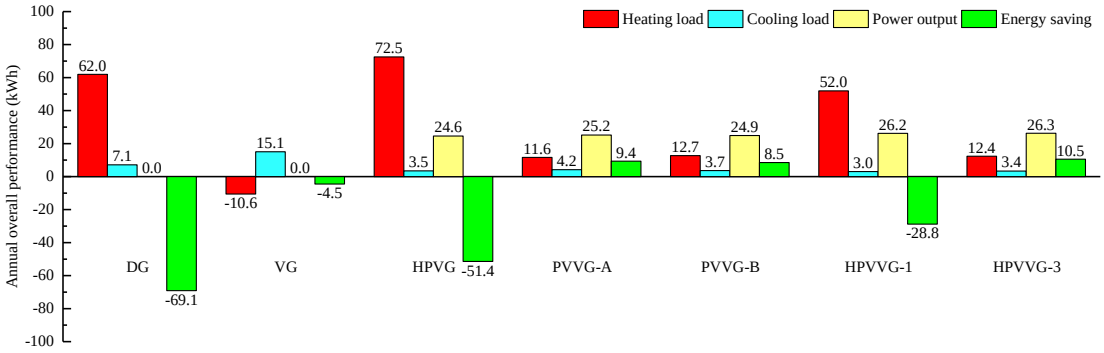

(a) Harbin (severe cold region)

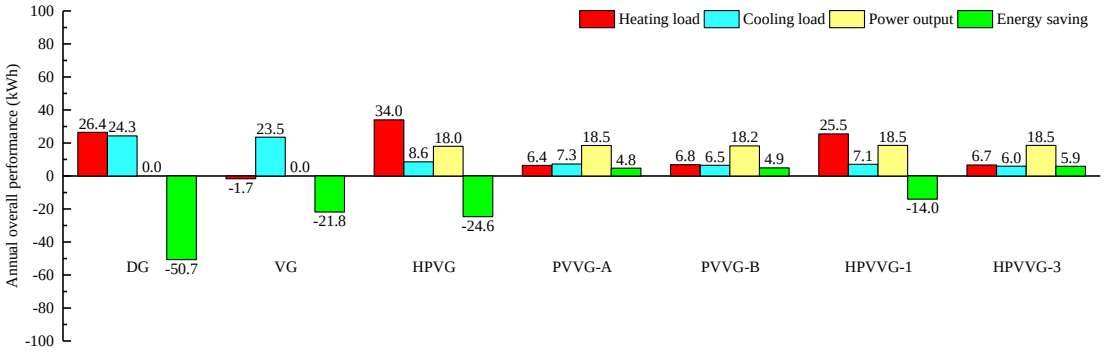

(b) Beijing (cold region)

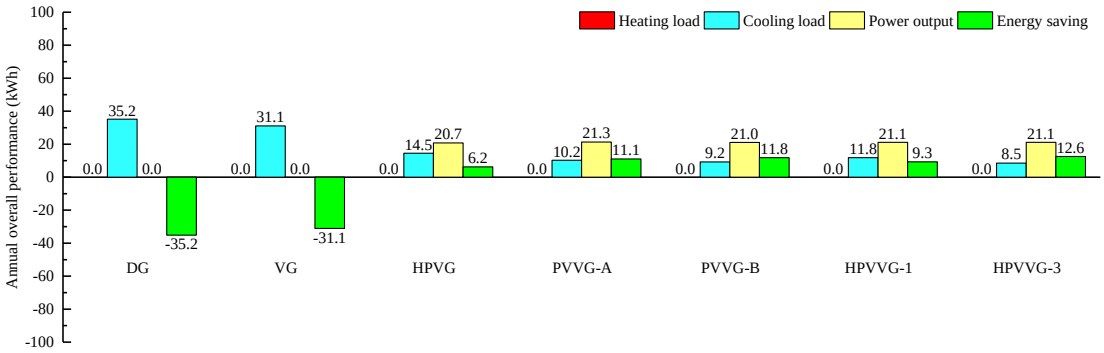

(c) Wuhan (hot summer and cold winter region)

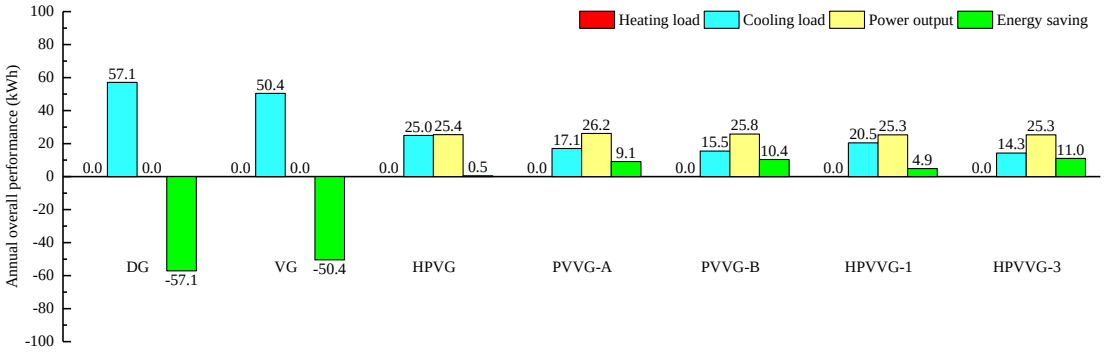

(d) Guangzhou (hot summer and warm winter region)

Figure 8.2 Annual overall performance of different glazing (orienting north) in various climate regions

Because of less electric energy production and poor thermal insulation, HPVG and HPVVG-1 shows disappointing annual overall performance. Once again, it is confirmed that the further integration with vacuum glazing enhances the thermal performance of HPVG, but the Low-E coating should be used in the vacuum gap instead of the air gap.

8.2.3 Glazing orienting east

The results for the glazing orienting east are much the same as those for the north orientation, and even the performance comparison between PVVG-A and PVVG-B shows the consistent outcome. The main difference is that the east orientation allows the glazing to receive more solar irradiance and therefore generate significantly more power than north-facing glazing. When the glazing is installed on east façade, HPVVG-3 shows the utmost superiority among 7 types of glazing (Figure 8.3), followed by PVVG-A and PVVG-B. In the cold areas, the situation in which the annual overall performance of PVVG-B exceeds PVVG-A occurs only in the east and north orientations. Other than that, the other results are in line with the rule that PVVG-A is more suitable for cold areas and PVVG-B is more suitable for hot areas in all orientations.

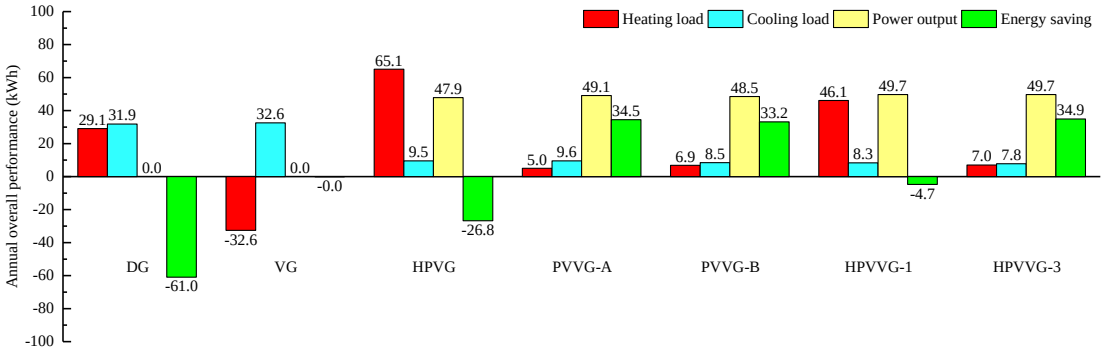

(a) Harbin (severe cold region)

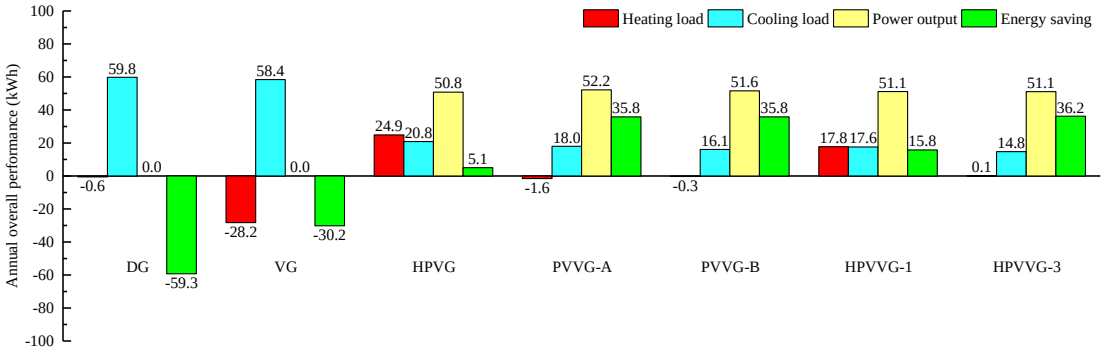

(b) Beijing (cold region)

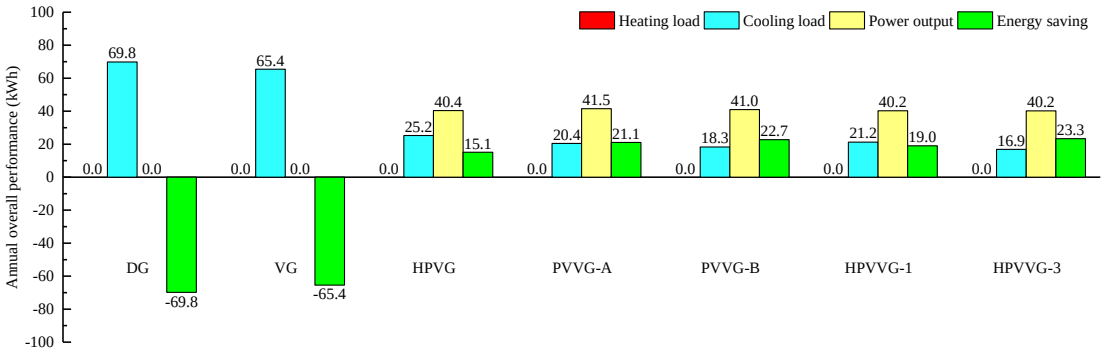

(c) Wuhan (hot summer and cold winter region)

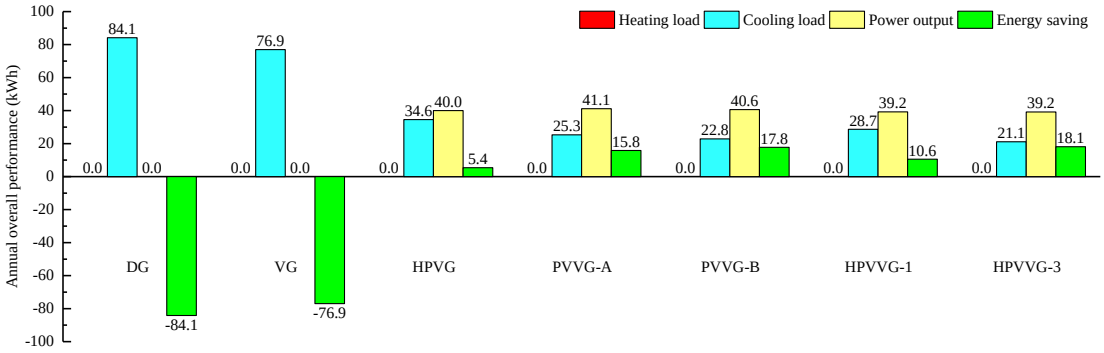

(d) Guangzhou (hot summer and warm winter region)

Figure 8.3 Annual overall performance of different glazing (orienting east) in various climate regions

HPVG and HPVVG-1 cannot achieve energy savings in the severe cold city due to their disappointing thermal performance – high U-value and low SHGC makes them consume more energy for heating although they have reduced cooling load compared with DG and VG. The situation in Beijing is somewhat similar to that described above, although HPVG and HPVVG-1 already generate enough power to offset the heating and cooling needs.

8.2.4 Glazing orienting west

As for the glazing orienting west, the best performers are PVVG-A in Harbin and Beijing and HPVVG-3 in Wuhan and Guangzhou, which is consistent with the conclusion of the south orientation. Except for this, the tendency in all other aspects is identical to that of the east orientation, including heating load, cooling load, and power output in four types of climates. The same conclusions will not be repeated further. Figure 8.4 shows the detail information about the annual overall performance of different glazing orienting west in various climate regions.

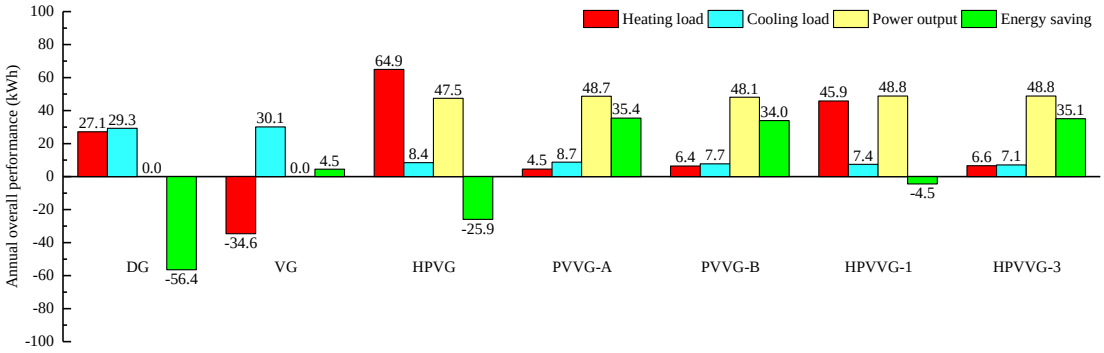

(a) Harbin (severe cold region)

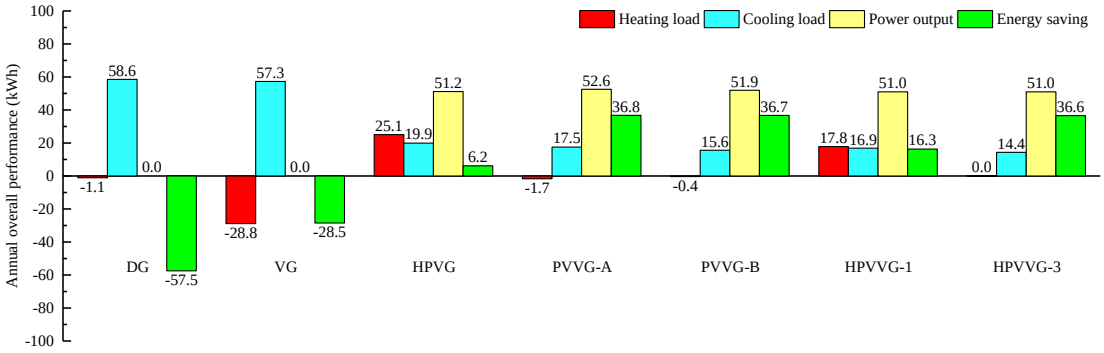

(b) Beijing (cold region)

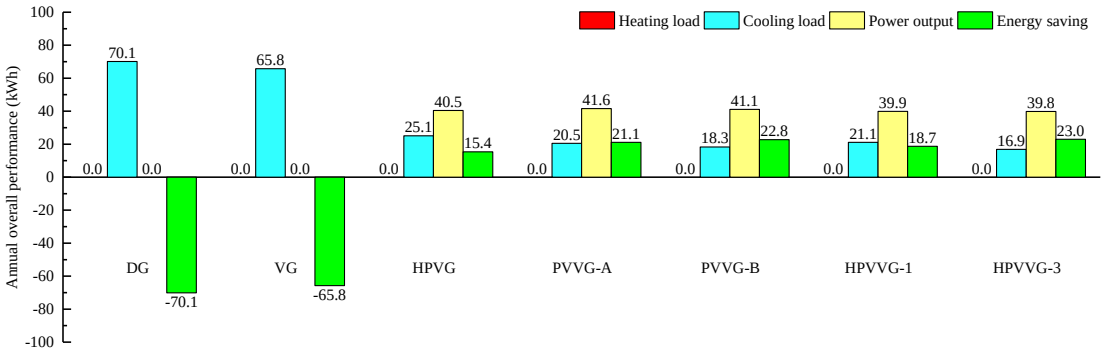

(c) Wuhan (hot summer and cold winter region)

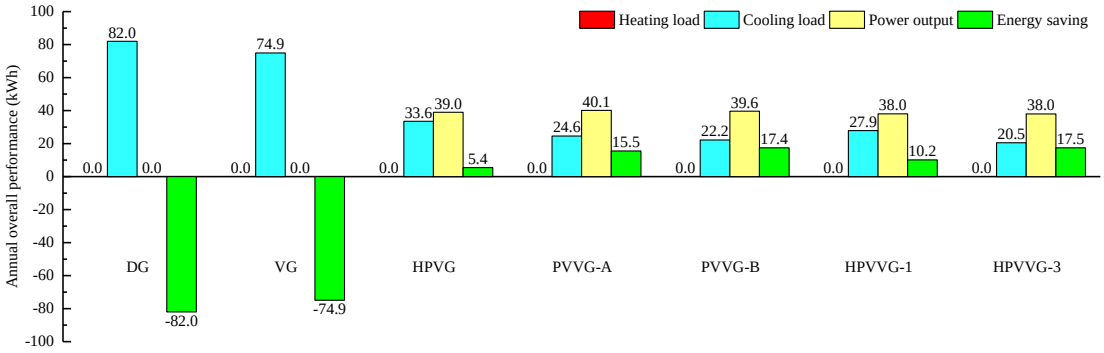

(d) Guangzhou (hot summer and warm winter region)

Figure 8.4 Annual overall performance of different glazing (orienting west) in various climate regions

Table 8.3 and Table 8.4 give the specific data to facilitate further quantitative analysis. If DG is used as a benchmark, the average energy savings by the optimal glazing (HPVVG-3 or PVVG-A) are 84.5 kWh/m^2 in Harbin, 79.2 kWh/m^2 in Beijing, 78.8 kWh/m^2 in Wuhan and 91.2 kWh/m^2 in Guangzhou. These values become 22.9 kWh/m^2 in Harbin, 50.4 kWh/m^2 in Beijing, 74.5 kWh/m^2 in Wuhan and 84.2 kWh/m^2 in Guangzhou when the reference object is changed to VG. This difference results from the fact that VG saves much more heating energy than DG does in cold and severe cold region. Among all the results shown in Table 8.4, HPVVG-3 orienting east in Guangzhou contributes to the most energy conservation regardless of whether it is compared with DG or VG. The interesting finding is that south orientation is not the choice which saves the most energy, and it turns out to be the east orientation instead when considering the annual overall performance. The possible reason lies in the fact that glazing orienting east consumes more cooling energy than the glazing facing south, as suggested by the simulative results. A similar conclusion can also be found in reference (Yang et al., 2015). As the authors stated, the annual cooling consumption was greater when the glazing faced east and south. Moreover, the DG and VG cause more heating load when facing

east (Figure 8.3) but save more heating energy when facing south as they receive more solar heat gain (Figure 8.1). An agreement can be identified in the research on the energy saving of a building office in Tianjin (Wei Zhang, 2005). Taking these two points into consideration, the baselines, DG and VG, consume more energy for heating and cooling when facing east, which makes the HPVVG-3 and PVVG-A become more energy-efficient although south orientation enhances the electric energy production.

Table 8.3 The energy savings (E_{op} (kWh/m^2)) by different glazing per unit area

City		DG	VG	HPVG	PVVG-A	PVVG-B	HPVVG-1	HPVVG-3
Harbin	East	-61.0	0.0	-26.8	34.5	33.2	-4.7	34.9
	West	-56.4	4.5	-25.9	35.4	34.0	-4.5	35.1
	South	-4.5	55.7	6.1	66.2	62.8	26.8	64.5
	North	-69.1	-4.5	-51.4	9.4	8.5	-28.8	10.5
Beijing	East	-59.3	-30.2	5.1	35.8	35.8	15.8	36.2
	West	-57.5	-28.5	6.2	36.7	36.7	16.3	36.6
	South	0.6	28.9	41.9	71.0	68.8	50.3	68.2
	North	-50.7	-21.8	-24.6	4.8	4.9	-14.0	5.9
Wuhan	East	-69.8	-65.4	15.1	21.1	22.7	19.0	23.3
	West	-70.1	-65.8	15.4	21.1	22.8	18.7	23.0
	South	-53.8	-49.6	20.4	26.0	27.1	23.6	27.4
	North	-35.2	-31.1	6.2	11.1	11.8	9.3	12.6
Guangzhou	East	-84.1	-76.9	5.4	15.8	17.8	10.6	18.1
	West	-82.0	-74.9	5.4	15.5	17.4	10.2	17.5
	South	-72.4	-65.5	11.3	21.0	22.6	15.8	22.7
	North	-57.1	-50.4	0.5	9.1	10.4	4.9	11.0

The north is, not surprisingly, the least energy-efficient orientation almost in all the regions. If the contribution from power generation is not considered, HPVVG-3 can save

averagely 75.3% heating and cooling energy consumption in all the scenarios in contrast to DG. This percentage changes to be 59.2% when comparing HPVVG-3 with HPVG.

Table 8.4 The energy savings (kWh/m^2) by the optimal glazing compared with DG and VG

City		$(E_{op})_{max} - E_{op,DG}$	$(E_{op})_{max} - E_{op,VG}$	Optimal glazing
Harbin	East	95.9	35.0	HPVVG-3
	West	91.9	31.0	PVVG-A
	South	70.7	10.5	PVVG-A
	North	79.6	15.0	HPVVG-3
Beijing	East	95.5	66.4	HPVVG-3
	West	94.3	65.3	PVVG-A
	South	70.3	42.1	PVVG-A
	North	56.6	27.7	HPVVG-3
Wuhan	East	93.1	88.8	HPVVG-3
	West	93.0	88.7	HPVVG-3
	South	81.2	77.0	HPVVG-3
	North	47.7	43.7	HPVVG-3
Guangzhou	East	102.2	95.0	HPVVG-3
	West	99.4	92.4	HPVVG-3
	South	95.1	88.2	HPVVG-3
	North	68.1	61.4	HPVVG-3

8.3 Summary

The current chapter compares the annual overall performance of different glazing in various orientations and climates, considering the heating energy, cooling energy and electric energy generation. Studied glazing includes double glazing, vacuum glazing, hollow PV glazing, PV vacuum glazing with Low-E coating on different surfaces, and hollow PV vacuum glazing with Low-E coating in the air gap or vacuum gap. Conclusions can be drawn as follows:

(1) PVVG-A, PVVG-B and HPVVG-3 perform better than DG, VG, and other types of PV glazing in all orientations and climates. PVVG-A is recommended for the west and south orientations in cold and severe cold areas while HPVVG-3 shows as the most exceptional one for the east and north orientations in cold and severe cold areas, and all the orientations in hot climates.

(2) In all the studied cases, HPVVG-3 presents better annual overall performance than HPVVG-1 does, indicating that Low-E coating used in the vacuum gap contribute to more energy savings than in the air gap.

(3) PVVG-A is more suitable for cold areas while PVVG-B suits more for hot areas in all orientations, with two exceptions - in the cold areas, the annual overall performance of PVVG-B precedes PVVG-A in the east and north orientations. Generally, the Low-E coating is suggested facing outdoor in hot climate and facing indoor in cold region, i.e. kept consistent with the heat flux direction, if only one layer of Low-E coating is applied in the vacuum gap.

(4) Compared with the double glazing, HPVVG-3 can help reduce averagely 75.3% energy consumption for heating and cooling in all the studied orientations and climatic zones, among which east orientation shows the most energy saving potential in all regions.

CHAPTER 9 CONCLUSIONS AND RECOMMANDATIONS FOR FURTURE WORK

This thesis started with a preliminary investigation of the energy saving potential of photovoltaic vacuum glazing by developing simulation models and exploring the optimization of utilizing photovoltaic vacuum glazing within passive building design through sensitivity analysis and genetic algorithm. Then, a novel idea was proposed to further integrate an air layer with the photovoltaic vacuum glazing, proposing the novel hollow photovoltaic vacuum glazing. The following work was done to investigate the glazing design factors and impacts from orientations and climate variations, through the approaches of 3D finite element models, mathematical heat transfer models and experiments. A comprehensive comparison between double glazing, vacuum glazing, hollow PV glazing, PV vacuum glazing and hollow PV vacuum glazing was conducted for selecting the proper glazing in specific application scenario. This chapter summarizes the main findings, academic contributions, limitations and future research directions.

9.1 Summary of Key Findings

The key findings from this research project are summarized as follows:

(1) The vacuum photovoltaic insulated glass unit (VPV IGU) can reduce up to 81.63%

and 75.03% of heat gain from building envelopes in summer in Hong Kong and in Harbin respectively, compared to the baseline building envelopes of normal windows. Meanwhile, heat loss in winter can be decreased by 31.94% and 32.03% respectively in the two climatic areas. When comparing buildings with VPV IGU to buildings without the PV glazing and daylight control, approximately 32% reduction of the energy demand can be achieved in both Hong Kong and Harbin. Furthermore, PV power supplies can further increase the saving of total energy use to 37.79% and 39.82% respectively in the two areas.

(2) Window dimensions and physical properties are proved to be significant factors for the PV envelope design in Hong Kong. However, the wall thermal insulation (i.e., WTR) and airtightness (i.e., IACH) substitute for the visible lighting transmittance (VT) and light-to-solar gain ratio (LSG) as key design factors in Harbin.

(3) The difference of net energy saving with both optimization approaches was within 5%, indicating that high-efficiency simplified optimization based on key design factors is suitable and reliable for initial design pursuing a swift decision-making process. Up to 52.11% and 62.98% energy conservation can be achieved with reference to the benchmarking building design. The integrated design optimization validated that VPV IGU is more suitable for application in cold areas, where a low U-value between 0.211

and 0.345 is recommended.

(4) Compared with the configurations without air cavity (i.e., vacuum PV glazing and PV vacuum glazing), the U-value can be reduced by 19.6% for the case of vacuum PV double glazing and 21.5% for PV vacuum double glazing. PV vacuum double glazing can achieve superior thermal and potential power performances as it has the lowest U-value and PV module temperature.

(5) The overall heat transfer coefficient can be decreased by lowering the thermal conductivity of glass sheets and pillars, diameter and density of vacuum pillars and emissivity of Low-E coatings, while increasing the width of the vacuum gap and air cavity. The lowest U-value can be achieved as 0.23 W/(m^2·K) in the PVVDG with a pillar separation of 60 mm, and the thermal performance can be further improved with a global optimization. One layer of Low-E coating can play a significant role in reducing the radiative heat transfer and the corresponding U-value, whereas the second layer brings a limited improvement and is therefore not cost-effective.

(6) Combining vacuum glazing and hollow PV glazing, the U-value of hollow PV glazing can be significantly reduced by 28% while the solar heat gain can be cut down by 15%. Such reduction can be further enhanced if the Low-E coating is applied in the vacuum gap. PV vacuum glazing has a lower U-value and SHGC comparable to hollow PV

vacuum glazing.

(7) In the air gap or vacuum gap, the location of the Low-E coating does not affect the U-value, but it does change the SHGC and temperature distribution. Low-E coating' facing direction should be consistent with the heat flow direction. Low-E coatings can more effectively reduce the overall heat transfer in a vacuum gap rather than an air gap. Therefore, the hollow photovoltaic vacuum glazing has a lower U-value and SHGC if the Low-E coating is applied on the internal surfaces of vacuum gap, as the heat loss in winter and heat gain in summer can be reduced.

(8) The maximum temperature difference between interior and exterior surfaces of the glazing could be about 20 ℃ for the PV vacuum glazing and hollow PV vacuum glazing during outdoor tests, which illustrates their ability to block most of the heat transferred from outdoor environment. Compared with the double glazing, the HPVVG-3 can help reduce averagely 75.3% energy consumption for heating and cooling in all the studied orientations and climatic zones, among which east orientation shows the most energy saving potential in all the regions.

(9) The PVVG-A, PVVG-B and HPVVG-3 perform better than the DG, VG, and other types of PV glazing in all orientations and climates. The PVVG-A is recommended for the west and south orientations in cold and severe cold areas while HPVVG-3

shows as the most exceptional one for the east and north orientations in cold and severe cold areas, and all the orientations in hot climates.

9.2 Academic contributions

This study incorporated PV envelope systems with passive architectural designs, where a consecutive input distribution space covering important independent and dependent design factors was comprehensively investigated. Both qualitative and quantitative sensitivity analyses were conducted, and their factor-prioritizing results achieved an ideal consistency. The sensitivity of PV envelope designs to external environmental conditions were validated by applying the design optimization process to diverse climates, where the vacuum PV glazing was found to be more suitable for heating-dominated conditions. The possibility of approaching net-zero energy high-rise buildings was explored by deriving the maximum energy saving potential with coupled passive design and PV envelope systems.

This research proposed a novel structure that further integrating an air layer with PV vacuum glazing. The air cavity is combined with PV vacuum glazing to further decrease the overall heat transfer coefficient and its specific impact on the glazing thermal performance is quantified. A three-dimensional heat transfer model is established to characterize the temperature and heat flux of four configurations of PV vacuum glazing, which are derived from combinations of the PV location (facing indoor/outdoor environment) and the existence

(with/without) of the air cavity between PV and vacuum glazing. A comprehensive sensitivity analysis is conducted for the thermal performance of PV vacuum glazing based on key design parameters, including the thermal property of components, dimension and distribution of vacuum pillars, configuration of Low-E coatings and width of air cavity. A guideline is provided for the initial design of PV vacuum glazing to enhance the thermal performances of Low-Energy buildings.

A mathematical heat transfer model was established based on comprehensive analysis on the complex heat transfer and reasonable assumptions, and validated by existing publications and experimental data, which can be applied to the thermal modeling of PV glazing with diverse structures. This theoretical model can be used to accurately determine the overall heat transfer coefficient and solar heat gain coefficient for different glazing, and predict the corresponding heating load, cooling load and electric energy generation. The study can provide references for selecting proper photovoltaic glazing as the building envelope for energy conservation in different orientations and climate regions.

9.3 Limitations and suggestions for future research

It is important to note that there are still limitations to the existing work within the thesis, which may be compensated by the following recommended research:

(1) The optimization study in this thesis focuses on the introduction of PV vacuum glazing

into passive building, leading to optimal building design but not the optimal glazing design. Although factors affecting the thermal performance of PV vacuum glazing have been investigated, the optimal glazing design should also consider the daylighting performance, which cannot be analyzed by thermal modelling only. Thus, the optimal design of PV vacuum glazing and hollow PV vacuum glazing still requires further study.

(2) The width of the air cavity within vacuum PV double glazing and PV vacuum double glazing is recommended to be enlarged for achieving lower U-value. However, convective heat transfer will become dominant and not negligible when the width goes beyond 15 mm, which requires further discussions in future work. Detailed global sensitivity analyses and optimizations should also be conducted to obtain a feasible final design solution with the consideration of mechanical constraints.

(3) Due to the limited experimental conditions, the data collection process was not able to cover both the reference and comparison groups, leading to a reliance on simulation results. Where feasible, experiments with a reference group can provide a more visual indication of the performance of the target glazing. Moreover, the experiments can be extended to compare multiple orientations as well as to collect cooling load data, making the experiments more informative.

(4) The integration of vacuum glazing with PV glazing will make the initial investment

increase for BIPV applications, not to mention the further combination with another air layer. Additional concerning factor is the degradation of the vacuum glazing. Further research should be undertaken to assess the lifecycle of the composite photovoltaic vacuum glazing and compare it with conventional photovoltaic glazing.

References

Akan, M. Ö. A., Selam, A. A., & Firat, S. Ü. O. (2016). *Renewable energy sources: Comparison of their use and respective policies on a global scale*. *Handbook of Research on Green Economic Development Initiatives and Strategies*. https://doi.org/10.4018/978-1-5225-0440-5.ch0011

Alvarez, G., Flores, J. J., Aguilar, J. O., Gó Mez-Daza, O., Estrada, C. A., Nair, M. T. S., & Nair, P. K. (2004). Spectrally selective laminated glazing consisting of solar control and heat mirror coated glass: preparation, characterization and modelling of heat transfer. https://doi.org/10.1016/j.solener.2004.06.021

Anatol C, Francesco F, N. K. (2011). *Building Integrated Photovoltaics – Thermal Aspects – Low Energy House for Testing BIPV Systems*.

Arici, M., & Karabay, H. (2010). Determination of optimum thickness of double-glazed windows for the climatic regions of Turkey. *Energy and Buildings*, *42*(10), 1773–1778. https://doi.org/10.1016/j.enbuild.2010.05.013

Ascione, F., Bianco, N., De Stasio, C., Mauro, G. M., & Vanoli, G. P. (2016). Multi-stage and multi-objective optimization for energy retrofitting a developed hospital reference building: A new approach to assess cost-optimality. *Applied Energy*, *174*, 37–68. https://doi.org/10.1016/j.apenergy.2016.04.078

Ascione, F., De Masi, R. F., de Rossi, F., Ruggiero, S., & Vanoli, G. P. (2016). Optimization of building envelope design for nZEBs in Mediterranean climate: Performance analysis of residential case study. *Applied Energy*, *183*, 938–957. https://doi.org/10.1016/j.apenergy.2016.09.027

ASHRAE. (2001). *Fundamentals*.

ASHRAE. (2017). *Handbook of Fundamentals* (SI Edition).

ASTM. (n.d.). *C1199: Standard Test Method for Measuring the Steady-State Thermal Transmittance of Fenestration Systems Using Hot Box Methods*.

Aydin, O. (2000). Determination of optimum air-layer thickness in double-pane windows. *Energy and Buildings*, *32*(3), 303–308. https://doi.org/10.1016/S0378-7788(00)00057-8

Barman, S., Chowdhury, A., Mathur, S., & Mathur, J. (2018). Assessment of the efficiency of window integrated CdTe based semi-transparent photovoltaic module. *Sustainable Cities and Society*, *37*, 250–262. https://doi.org/10.1016/j.scs.2017.09.036

Berkeley Lab WINDOW. (n.d.). Retrieved April 19, 2021, from https://windows.lbl.gov/software/window

BP. (2019). *BP Statistical Review of World Energy 2019, 68th edition*. Retrieved from https://www.bp.com/en/global/corporate/energy-economics/statistical-review-of-world-energy.html

Buildings – A source of enormous untapped efficiency potential. (n.d.). Retrieved June 7, 2021, from https://www.iea.org/topics/buildings

Campolongo, F., & Saltelli, A. (1997). Sensitivity analysis of an environmental model: an application of different analysis methods. *Reliability Engineering & System Safety*, *57*(1), 49–69. https://doi.org/10.1016/S0951-8320(97)00021-5

Cao, X., Dai, X., & Liu, J. (2016). Building energy-consumption status worldwide and the state-of-the-art technologies for zero-energy buildings during the past decade. *Energy and Buildings*, *128*, 198–213. https://doi.org/10.1016/j.enbuild.2016.06.089

Carlucci, S., Cattarin, G., Causone, F., & Pagliano, L. (2015). Multi-objective optimization of a nearly zero-energy building based on thermal and visual discomfort minimization using a non-dominated sorting genetic algorithm (NSGA-II). *Energy and Buildings*, *104*, 378–394. https://doi.org/10.1016/J.ENBUILD.2015.06.064

Charlie Curcija, Simon Vidanovic, Robert Hart, Jacob Jonsson, R. M. (2018). *WINDOW Technical Documentation*.

Chastas, P., Theodosiou, T., & Bikas, D. (2016, August 15). Embodied energy in residential buildings-towards the nearly zero energy building: A literature review. *Building and Environment*. Elsevier Ltd. https://doi.org/10.1016/j.buildenv.2016.05.040

Chen, B., Lv, H., Liao, J., Dong, S., Cheng, C., Lv, Q., … Riffat, S. (2019a). Thermal insulation

performance of an advanced photovoltaic vacuum glazing: A numerical investigation and simulation. *Journal of Renewable and Sustainable Energy*, *11*(1). https://doi.org/10.1063/1.5055363

Chen, B., Lv, H., Liao, J., Dong, S., Cheng, C., Lv, Q., … Riffat, S. (2019b). Thermal insulation performance of an advanced photovoltaic vacuum glazing: A numerical investigation and simulation. *Journal of Renewable and Sustainable Energy*, *11*(1), 015101. https://doi.org/10.1063/1.5055363

Chen, X., & Yang, H. (2017). A multi-stage optimization of passively designed high-rise residential buildings in multiple building operation scenarios. *Applied Energy*, *206*(September), 541–557. https://doi.org/10.1016/j.apenergy.2017.08.204

Chen, X., & Yang, H. (2018). Integrated energy performance optimization of a passively designed high-rise residential building in different climatic zones of China. *Applied Energy*, *215*(November 2017), 145–158. https://doi.org/10.1016/j.apenergy.2018.01.099

Chen, X., Yang, H., & Peng, J. (2019). Energy optimization of high-rise commercial buildings integrated with photovoltaic facades in urban context. *Energy*, *172*, 1–17. https://doi.org/10.1016/j.energy.2019.01.112

Chen, X., Yang, H., & Sun, K. (2016). A holistic passive design approach to optimize indoor environmental quality of a typical residential building in Hong Kong. *Energy*, *113*, 267–

281. https://doi.org/10.1016/j.energy.2016.07.058

Chen, X., Yang, H., & Sun, K. (2017). Developing a meta-model for sensitivity analyses and prediction of building performance for passively designed high-rise residential buildings. *Applied Energy*, *194*, 422–439. https://doi.org/10.1016/j.apenergy.2016.08.180

Chen, X., Yang, H., & Zhang, W. (2018). Simulation-based approach to optimize passively designed buildings: A case study on a typical architectural form in hot and humid climates. *Renewable and Sustainable Energy Reviews*. https://doi.org/10.1016/j.rser.2017.06.018

Chow, T. tai, Li, C., & Lin, Z. (2010). Innovative solar windows for cooling-demand climate. *Solar Energy Materials and Solar Cells*, *94*(2), 212–220. https://doi.org/10.1016/j.solmat.2009.09.004

Collins, R. E., & Simko, T. M. (1998). Current status of the science and technology of vacuum glazing. *Solar Energy*, *62*(3), 189–213. https://doi.org/10.1016/S0038-092X(98)00007-3

Collins, R., & Fischer-Cripps, A. (1991). Design of Support Pillar Arrays in Flat Evacuated Windows. *Australian Journal of Physics*, *44*(5), 545. https://doi.org/10.1071/ph910545

COMSOL Multiphysics. (n.d.). Retrieved from https://www.comsol.asia/

Cuce, E. (2018). Accurate and reliable U -value assessment of argon-filled double glazed windows: A numerical and experimental investigation. *Energy and Buildings*, *171*, 100–106. https://doi.org/10.1016/j.enbuild.2018.04.036

Cuce, E., & Cuce, P. M. (2016). Vacuum glazing for highly insulating windows: Recent developments and future prospects. *Renewable and Sustainable Energy Reviews*, *54*, 1345–1357. https://doi.org/10.1016/j.rser.2015.10.134

Cuce, E., & Riffat, S. B. (2015). Vacuum tube window technology for highly insulating building fabric: An experimental and numerical investigation. *Vacuum*, *111*, 83–91. https://doi.org/10.1016/J.VACUUM.2014.10.002

Custom Tinted Glass, Cut Tempered Glass | One Day Glass. (n.d.). Retrieved June 9, 2021, from https://www.onedayglass.com/custom-orders/custom-glass-processing/glass-tints-or-colors/

Delgarm, N., Sajadi, B., Kowsary, F., & Delgarm, S. (2016). Multi-objective optimization of the building energy performance: A simulation-based approach by means of particle swarm optimization (PSO). *Applied Energy*, *170*, 293–303. https://doi.org/10.1016/j.apenergy.2016.02.141

Dincer, I. (1998). Energy and Environmental Impacts: Present and Future Perspectives. *ENERGY SOURCES*, *20*, 427–453. https://doi.org/10.1080/00908319808970070

Du, Y., Tao, W., Liu, Y., Jiang, J., & Huang, H. (2017). Heat transfer modeling and temperature experiments of crystalline silicon photovoltaic modules. *Solar Energy*, *146*, 257–263. https://doi.org/10.1016/j.solener.2017.02.049

EIA. (2020). *Country Analysis Executive Summary: China*.

EMSD. (2019). *Hong Kong Energy End-use Data 2019*. Hong Kong. https://doi.org/10.18356/de48b538-en

EMSD. (2020). *Hong Kong Energy End-use Data (HKEEUD) 2020*.

EN. (2011a). *673: Glass in building - Determination of thermal transmittance (U value) - Calculation method*.

EN. (2011b). *674: Glass in building – determination of thermal transmittance (U value) – Guarded hot plate method*.

Energy and Pollution: Where Do We Pollute the Most? - Nature's Path. (n.d.). Retrieved June 6, 2021, from https://www.naturespath.com/en-us/blog/energy-pollution-pollute/

Energy use in buildings. (n.d.). Retrieved June 7, 2021, from https://www.velux.com/what-we-do/research-and-knowledge/deic-basic-book/energy/energy-use-in-buildings?consent=preferences,statistics,marketing&ref-original=https%3A%2F%2Fwww.google.com%2F

Fang, Y., Eames, P. C., Norton, B., & Hyde, T. J. (2006). Experimental validation of a numerical model for heat transfer in vacuum glazing. *Solar Energy, 80*(5), 564–577. https://doi.org/10.1016/j.solener.2005.04.002

Fang, Y., Eames, P. C., Norton, B., Hyde, T. J., Zhao, J., Wang, J., & Huang, Y. (2007). Low

emittance coatings and the thermal performance of vacuum glazing. *Solar Energy*, *81*(1), 8–12. https://doi.org/10.1016/j.solener.2006.06.011

Fang, Y., Hyde, T. J., Arya, F., Hewitt, N., Eames, P. C., Norton, B., & Miller, S. (2014, September 1). Indium alloy-sealed vacuum glazing development and context. *Renewable and Sustainable Energy Reviews*. Pergamon. https://doi.org/10.1016/j.rser.2014.05.029

Fang, Y., Hyde, T. J., Arya, F., Hewitt, N., Wang, R., & Dai, Y. (2015). Enhancing the thermal performance of triple vacuum glazing with low-emittance coatings. *Energy and Buildings*, *97*, 186–195. https://doi.org/10.1016/j.enbuild.2015.04.006

Fang, Y., Hyde, T. J., & Hewitt, N. (2013). A Novel Building Component Hybrid Vacuum Glazing—A Modelling And Experimental Validation. *ASHRAE Transactions*, *119*(October), 13–14.

Fung, T. Y. Y., & Yang, H. (2008). Study on thermal performance of semi-transparent building-integrated photovoltaic glazings. *Energy and Buildings*, *40*(3), 341–350. https://doi.org/10.1016/j.enbuild.2007.03.002

Gao, T., Ihara, T., Grynning, S., Jelle, B. P., & Lien, A. G. (2016). Perspective of aerogel glazings in energy efficient buildings. *Building and Environment*, *95*, 405–413. https://doi.org/10.1016/j.buildenv.2015.10.001

Garcia Sanchez, D., Lacarrière, B., Musy, M., & Bourges, B. (2014). Application of sensitivity

analysis in building energy simulations: Combining first- and second-order elementary effects methods. *Energy and Buildings*, *68*(PART C), 741–750. https://doi.org/10.1016/j.enbuild.2012.08.048

German Industry and Commerce Ltd. (n.d.). Building Energy Efficiency: The Key to a Green City. Retrieved April 16, 2021, from https://hongkong.ahk.de/news/news-details/building-energy-efficiency-the-key-to-a-green-city

Ghabra, N., Rodrigues, L., & Oldfield, P. (2017). The impact of the building envelope on the energy efficiency of residential tall buildings in Saudi Arabia. *International Journal of Low-Carbon Technologies*. https://doi.org/10.1093/ijlct/ctx005

Ghosh, A., Norton, B., & Duffy, A. (2016). Measured thermal & daylight performance of an evacuated glazing using an outdoor test cell. *Applied Energy*, *177*, 196–203. https://doi.org/10.1016/j.apenergy.2016.05.118

Ghosh, A., Norton, B., & Duffy, A. (2017). Effect of sky clearness index on transmission of evacuated (vacuum) glazing. *Renewable Energy*, *105*, 160–166. https://doi.org/10.1016/j.renene.2016.12.056

Ghosh, A., Sarmah, N., Sundaram, S., & Mallick, T. K. (2019). Numerical studies of thermal comfort for semi-transparent building integrated photovoltaic (BIPV)-vacuum glazing system. *Solar Energy*, *190*, 608–616. https://doi.org/10.1016/j.solener.2019.08.049

Ghosh, A., Sundaram, S., & Mallick, T. K. (2018). Investigation of thermal and electrical performances of a combined semi-transparent PV-vacuum glazing. *Applied Energy*, *228*(April), 1591–1600. https://doi.org/10.1016/j.apenergy.2018.07.040

Ghosh, A., Sundaram, S., & Mallick, T. K. (2019). Colour properties and glazing factors evaluation of multicrystalline based semi-transparent Photovoltaic-vacuum glazing for BIPV application. *Renewable Energy*, *131*, 730–736. https://doi.org/10.1016/j.renene.2018.07.088

GovHK: Feed-in Tariff. (n.d.). Retrieved June 7, 2021, from https://www.gov.hk/en/residents/environment/renewable/feedintariff.htm

Green, S. S. S., Moran, A. B. B., JOHNSTON, R. W. W., Uhler, P., & Chiu, J. (1982). The Incidence of Salmonella Species and Serotypes in Young Whole Chicken Carcasses in 1979 as Compared with 1967, *61*(2), 288–293. Retrieved from https://www.sciencedirect.com/science/article/pii/S0032579119347650?via%3Dihub

Griffiths, P W, Di Leo, M., Cartwright, ‡ P, Eames, P. C., Yianoulis, § P, Leftheriotis, G., & Norton, B. (1998). *FABRICATION OF EVACUATED GLAZING AT LOW TEMPERATURE* (Vol. 63).

Griffiths, Philip W., Eames, P. C., Hyde, T. J., Fang, Y., & Norton, B. (2006). Experimental Characterization and Detailed Performance Prediction of a Vacuum Glazing System

Fabricated With a Low Temperature Metal Edge Seal, Using a Validated Computer Model. *Journal of Solar Energy Engineering, Transactions of the ASME*, *128*(2), 199–203. https://doi.org/10.1115/1.2188529

Gueymard, C. A., & DuPont, W. C. (2009). Spectral effects on the transmittance, solar heat gain, and performance rating of glazing systems. *Solar Energy*, *83*(6), 940–953. https://doi.org/10.1016/j.solener.2008.12.012

Han, J., Lu, L., & Yang, H. (2009). Thermal behavior of a novel type see-through glazing system with integrated PV cells. *Building and Environment*, *44*(10), 2129–2136. https://doi.org/10.1016/j.buildenv.2009.03.003

Han, J., Lu, L., & Yang, H. (2010). Numerical evaluation of the mixed convective heat transfer in a double-pane window integrated with see-through a-Si PV cells with low-e coatings. *Applied Energy*, *87*(11), 3431–3437. https://doi.org/10.1016/j.apenergy.2010.05.025

Han, Z., Bao, Y., Wu, W., Liu, Z., Liu, X., & Tian, Y. (2012). *Evaluation of thermal performance for vacuum glazing by using three-dimensional finite element model*. *Key Engineering Materials* (Vol. 492). https://doi.org/10.4028/www.scientific.net/KEM.492.328

Han, Zhiming, Bao, Y., Wu, W., Liu, Z., Liu, X., & Tian, Y. Evaluation of thermal performance for vacuum glazing by using three-dimensional finite element model, 492 Key

Engineering Materials § (2012). https://doi.org/10.4028/www.scientific.net/KEM.492.328

Heinstein, P., Ballif, C., & Perret-Aebi, L. E. (2013, June 14). Building integrated photovoltaics (BIPV): Review, potentials, barriers and myths. *Green*. Walter de Gruyter GmbH. https://doi.org/10.1515/green-2013-0020

Henshall, P., Eames, P., Arya, F., Hyde, T., Moss, R., & Shire, S. (2016). Constant temperature induced stresses in evacuated enclosures for high performance flat plate solar thermal collectors. *Solar Energy*, *127*, 250–261. https://doi.org/10.1016/j.solener.2016.01.025

Hu, Z., He, W., Ji, J., Hu, D., Lv, S., Chen, H., & Shen, Z. (2017). Comparative study on the annual performance of three types of building integrated photovoltaic (BIPV) Trombe wall system. *Applied Energy*, *194*, 81–93. https://doi.org/10.1016/j.apenergy.2017.02.018

Huang, J., Yu, J., & Yang, H. (2018). Effects of key factors on the heat insulation performance of a hollow block ventilated wall. *Applied Energy*, *232*, 409–423. https://doi.org/10.1016/j.apenergy.2018.09.215

Huo, T., Ren, H., Zhang, X., Cai, W., Feng, W., Zhou, N., & Wang, X. (2018). China's energy consumption in the building sector: A Statistical Yearbook-Energy Balance Sheet based splitting method. *Journal of Cleaner Production*, *185*, 665–679. https://doi.org/10.1016/J.JCLEPRO.2018.02.283

IEA. (2019a). Global Energy & CO2 Status Report. https://doi.org/10.4324/9781315252056

IEA. (2019b). World Energy Outlook 2019. *World Energy Outlook 2019*, 1. Retrieved from https://www.iea.org/reports/world-energy-outlook-2019%0Ahttps://www.iea.org/reports/world-energy-outlook-2019%0Ahttps://webstore.iea.org/download/summary/2467?fileName=Japanese-Summary-WEO2019.pdf

ISO. (2003). *15099: Thermal performance of windows, doors and shading devices-Detailed calculations*.

Jarimi, H., Lv, Q., Omar, R., Zhang, S., & Riffat, S. (2020). Design, mathematical modelling and experimental investigation of vacuum insulated semi-transparent thin-film photovoltaic (PV) glazing. *Journal of Building Engineering*, *31*, 101430. https://doi.org/10.1016/j.jobe.2020.101430

Jarimi, H., Qu, K., Zhang, S., Lv, Q., Cooper, D., Su, Y., & Riffat, S. (2019). Performance Analysis of an integrated Semi-Transparent Thin Film PV Vacuum Insulated Glazing. *Hittite Journal of Science & Engineering*, *6*(4), 275–286. https://doi.org/10.17350/hjse19030000158

Jelle, B. P. (2016). Building integrated photovoltaics: A concise description of the current state of the art and possible research pathways. *Energies*, *9*(1), 1–30.

https://doi.org/10.3390/en9010021

Jelle, B. P., Breivik, C., Drolsum Røkenes, H., Petter Jelle, B., Breivik, C., & Røkenes, H. D. Building integrated photovoltaic products: A state-of-the-art review and future research opportunities, 100 Solar Energy Materials and Solar Cells § (2012). Elsevier. https://doi.org/10.1016/j.solmat.2011.12.016

JGJ/T 151-2008: Calculation specification for thermal performance of windows, doors, and glass curtain-walls (Chinese). (2008).

Jha, A., & Tripathy, P. P. (2019). Heat transfer modeling and performance evaluation of photovoltaic system in different seasonal and climatic conditions. *Renewable Energy*, *135*, 856–865. https://doi.org/10.1016/j.renene.2018.12.032

Kalogirou, S. A. (2015). Building integration of solar renewable energy systems towards zero or nearly zero energy buildings. *International Journal of Low-Carbon Technologies*, *10*(4), 379–385. https://doi.org/10.1093/ijlct/ctt071

Khoroshiltseva, M., Slanzi, D., & Poli, I. (2016). A Pareto-based multi-objective optimization algorithm to design energy-efficient shading devices. *Applied Energy*, *184*, 1400–1410. https://doi.org/10.1016/j.apenergy.2016.05.015

Kylili, A., & Fokaides, P. A. (2014). Investigation of building integrated photovoltaics potential in achieving the zero energy building target. *Indoor and Built Environment*,

23(1), 92–106. https://doi.org/10.1177/1420326X13509392

Kylili, A., & Fokaides, P. A. (2015). European smart cities: The role of zero energy buildings. *Sustainable Cities and Society*, *15*(2015), 86–95. https://doi.org/10.1016/j.scs.2014.12.003

Lawrence Berkeley National Laboratory. (n.d.). Software tools. Retrieved from https://windows.lbl.gov/software

Lawrence Berkeley National Laboratory. (2019). *WINDOW 7 User Manual*.

Li, D. H. W., Lam, T. N. T., Chan, W. W. H., & Mak, A. H. L. (2009). Energy and cost analysis of semi-transparent photovoltaic in office buildings. *Applied Energy*, *86*(5), 722–729.

Liao, W., & Xu, S. (2015). Energy performance comparison among see-through amorphous-silicon PV (photovoltaic) glazings and traditional glazings under different architectural conditions in China. *Energy*, *83*, 267–275. https://doi.org/10.1016/j.energy.2015.02.023

Liu, J., Zhang, J., Zhang, D., Jiao, S., Xing, J., Tang, H., … Zuo, J. (2020). Sub-ambient radiative cooling with wind cover. *Renewable and Sustainable Energy Reviews*, *130*(June), 109935. https://doi.org/10.1016/j.rser.2020.109935

Liu, P. S., & Chen, G. F. (2014). Applications of Polymer Foams. In *Porous Materials* (pp. 383–410). Elsevier. https://doi.org/10.1016/b978-0-12-407788-1.00008-3

Liu, Z., Liu, Y., He, B. J., Xu, W., Jin, G., & Zhang, X. (2019, March 1). Application and

suitability analysis of the key technologies in nearly zero energy buildings in China. *Renewable and Sustainable Energy Reviews*. Elsevier Ltd. https://doi.org/10.1016/j.rser.2018.11.023

Lu, L., & Law, K. M. (2013). Overall energy performance of semi-transparent single-glazed photovoltaic (PV) window for a typical office in Hong Kong. *Renewable Energy*, *49*, 250–254. https://doi.org/10.1016/j.renene.2012.01.021

Lu, Y. (2008). *Practical Heating and Air Conditioning Design Manual (in Chinese)* (Second).

Luo, Y., Zhang, L., Wang, X., Xie, L., Liu, Z., Wu, J., … He, X. (2017). A comparative study on thermal performance evaluation of a new double skin façade system integrated with photovoltaic blinds. *Applied Energy*, *199*, 281–293. https://doi.org/10.1016/j.apenergy.2017.05.026

Lyons, P., Arasteh, D., & Huizenga, C. (n.d.). *Window Performance for Human Thermal Comfort*.

Manz, H., Brunner, S., & Wullschleger, L. (2006). Triple vacuum glazing: Heat transfer and basic mechanical design constraints. *Solar Energy*, *80*(12), 1632–1642. https://doi.org/10.1016/j.solener.2005.11.003

Marinoski, D. L., Güths, S., Pereira, F. O. R. R., & Lamberts, R. (2007). Improvement of a measurement system for solar heat gain through fenestrations. *Energy and Buildings*,

39(4), 478–487. https://doi.org/10.1016/j.enbuild.2006.08.010

Mechri, H. E., Capozzoli, A., & Corrado, V. (2010). USE of the ANOVA approach for sensitive building energy design. *Applied Energy*, *87*(10), 3073–3083. https://doi.org/10.1016/j.apenergy.2010.04.001

Menberg, K., Heo, Y., & Choudhary, R. (2016). Sensitivity analysis methods for building energy models: Comparing computational costs and extractable information. *Energy and Buildings*, *133*, 433–445. https://doi.org/10.1016/j.enbuild.2016.10.005

Méndez Echenagucia, T., Capozzoli, A., Cascone, Y., & Sassone, M. (2015). The early design stage of a building envelope: Multi-objective search through heating, cooling and lighting energy performance analysis. *Applied Energy*, *154*, 577–591. https://doi.org/10.1016/j.apenergy.2015.04.090

Nabil, A., & Mardaljevic, J. (2006). Useful daylight illuminances: A replacement for daylight factors. *Energy and Buildings*, *38*(7), 905–913. https://doi.org/10.1016/J.ENBUILD.2006.03.013

Omar, E. A., & Al-Ragom, F. (2002). On the effect of glazing and code compliance. *Applied Energy*, *71*(2), 75–86. https://doi.org/10.1016/S0306-2619(01)00047-2

Park, K. E. E., Kang, G. H. H., Kim, H. I. I., Yu, G. J. J., & Kim, J. T. T. (2010). Analysis of thermal and electrical performance of semi-transparent photovoltaic (PV) module. *Energy*,

35(6), 2681–2687. https://doi.org/10.1016/j.energy.2009.07.019

Peng, C., Huang, Y., & Wu, Z. (2011). Building-integrated photovoltaics (BIPV) in architectural design in China. *Energy and Buildings*, *43*(12), 3592–3598. https://doi.org/10.1016/j.enbuild.2011.09.032

Peng, J. (2019, February 1). Simulation studies on advanced window technologies. *Building Simulation*. Tsinghua University Press. https://doi.org/10.1007/s12273-019-0517-5

Peng, J., Curcija, D. C., Lu, L., Selkowitz, S. E., Yang, H., & Zhang, W. (2016a). Numerical investigation of the energy saving potential of a semi-transparent photovoltaic double-skin facade in a cool-summer Mediterranean climate. *Applied Energy*, *165*, 345–356. https://doi.org/10.1016/j.apenergy.2015.12.074

Peng, J., Curcija, D. C., Lu, L., Selkowitz, S. E., Yang, H., & Zhang, W. (2016b). Numerical investigation of the energy saving potential of a semi-transparent photovoltaic double-skin facade in a cool-summer Mediterranean climate. *Applied Energy*, *165*, 345–356. https://doi.org/10.1016/j.apenergy.2015.12.074

Peng, J., Lu, L., & Yang, H. (2013). An experimental study of the thermal performance of a novel photovoltaic double-skin facade in Hong Kong. *Solar Energy*, *97*, 293–304. https://doi.org/10.1016/j.solener.2013.08.031

Peng, J., Lu, L., Yang, H., & Han, J. (2013). Investigation on the annual thermal performance

of a photovoltaic wall mounted on a multi-layer façade. *Applied Energy*, *112*, 646–656. https://doi.org/10.1016/j.apenergy.2012.12.026

Peng, J., Lu, L., Yang, H., & Ma, T. (2015). Comparative study of the thermal and power performances of a semi-transparent photovoltaic façade under different ventilation modes. *Applied Energy*, *138*, 572–583. https://doi.org/10.1016/j.apenergy.2014.10.003

Qiu, C., Yang, H., & Zhang, W. (2018). Investigation on the energy performance of a novel semi-transparent BIPV system integrated with vacuum glazing. *Building Simulation*, 1–11. https://doi.org/10.1007/s12273-018-0464-6

Radwan, A., Katsura, T., Memon, S., Serageldin, A. A., Nakamura, M., & Nagano, K. (2020). Thermal and electrical performances of semi-transparent photovoltaic glazing integrated with translucent vacuum insulation panel and vacuum glazing. *Energy Conversion and Management*, *215*, 112920. https://doi.org/10.1016/j.enconman.2020.112920

Renewable Energy | Types, Forms & Sources | EDF. (n.d.). Retrieved June 7, 2021, from https://www.edfenergy.com/for-home/energywise/renewable-energy-sources

Residential solar prices hit record low in 2020, says EnergySage | Renewable Energy World. (n.d.). Retrieved June 7, 2021, from https://www.renewableenergyworld.com/solar/residential-solar-prices-hit-record-low-in-2020-says-energysage/

Rezaei, S. D., Shannigrahi, S., & Ramakrishna, S. (2017). A review of conventional, advanced, and smart glazing technologies and materials for improving indoor environment. *Solar Energy Materials and Solar Cells*, *159*, 26–51. https://doi.org/10.1016/j.solmat.2016.08.026

Sabri, L., & Benzirar, M. (2014). Effect of Ambient Conditions on Thermal Properties of Photovoltaic Cells: Crystalline and Amorphous Silicon. *International Journal of Innovative Research in Science, Engineering and Technology*, *03*(12), 17815–17821. https://doi.org/10.15680/ijirset.2014.0312010

Saltelli, A., Tarantola, S., Campolongo, F., & Ratto, M. (2004). Sensitivity Analysis in Practice: A Guide to Assessing Scientific Models. In *Sensitivity Analysis in Practice* (pp. 109–149). https://doi.org/10.1002/0470870958.ch5

Sánchez-Palencia, P., Martín-Chivelet, N., & Chenlo, F. (2019). Modeling temperature and thermal transmittance of building integrated photovoltaic modules. *Solar Energy*, *184*, 153–161. https://doi.org/10.1016/j.solener.2019.03.096

Santos Silva, A., Susan, L., Almeida, S., Ghisi, E., Silva, A. S., Almeida, L. S. S., & Ghisi, E. (2016). Decision-making process for improving thermal and energy performance of residential buildings: A case study of constructive systems in Brazil. *Energy and Buildings*, *128*, 270–286. https://doi.org/10.1016/j.enbuild.2016.06.084

Simko, T., Collins, R., Beck, F., & Arasteh, D. (1995). Edge conduction in vacuum glazing. *Proceedings of the Thermal Performance of the Exterior Envelopes of Buildings IV*. Retrieved from http://eande.lbl.gov/sites/all/files/publications/36958.pdf

Skandalos, N., & Karamanis, D. (2015). PV glazing technologies. *Renewable and Sustainable Energy Reviews*, *49*, 306–322. https://doi.org/10.1016/j.rser.2015.04.145

Skoplaki, E., & Palyvos, J. A. (2009). On the temperature dependence of photovoltaic module electrical performance: A review of efficiency/power correlations. *Solar Energy*, *83*(5), 614–624. https://doi.org/10.1016/j.solener.2008.10.008

Statista. (2019). *Energy Consumption Worldwide*. Retrieved from https://www.statista.com/study/46227/energy-consumption-globally/

Sun, Y., Wu, Y., & Wilson, R. (2018, July 15). A review of thermal and optical characterisation of complex window systems and their building performance prediction. *Applied Energy*. Elsevier Ltd. https://doi.org/10.1016/j.apenergy.2018.03.144

Thomas, P. C., & Thomas, L. (2003). ADVANCED GLAZING SYSTEMS IN COMMERCIAL BUILDINGS. *Source: Environment Design Guide , PRO*, *19*, 1–6. https://doi.org/10.2307/26148387

Tian, W., & Wei, T. (2013). A review of sensitivity analysis methods in building energy analysis. *Renewable and Sustainable Energy Reviews*, *20*(June), 411–419.

https://doi.org/10.1016/j.rser.2012.12.014

Use of energy in explained - U.S. Energy Information Administration (EIA). (n.d.). Retrieved June 6, 2021, from https://www.eia.gov/energyexplained/use-of-energy/

Van Hooff, T., Blocken, B., Timmermans, H. J. P. J. P., & Hensen, J. L. M. L. M. Analysis of the predicted effect of passive climate adaptation measures on energy demand for cooling and heating in a residential building. *Energy*, *94*, 811–820. Retrieved from http://dx.doi.org/10.1016/j.energy.2015.11.036

Wang, M., Peng, J., Li, N., Lu, L., Ma, T., & Yang, H. (2016). Assessment of energy performance of semi-transparent PV insulating glass units using a validated simulation model. *Energy*, *112*, 538–548. https://doi.org/10.1016/j.energy.2016.06.120

Wang, M., Peng, J., Li, N., Yang, H., Wang, C., Li, X., & Lu, T. (2017). Comparison of energy performance between PV double skin facades and PV insulating glass units. *Applied Energy*, *194*, 148–160. https://doi.org/10.1016/j.apenergy.2017.03.019

Wang, T. P., & Wang, L. B. (2014). A steady heat transfer model of hollow double glazing under entire wave length heat radiation. *Energy and Buildings*, *81*, 72–83. https://doi.org/10.1016/j.enbuild.2014.06.014

Wang, T. P., & Wang, L. B. (2016). The effects of transparent long-wave radiation through glass on time lag and decrement factor of hollow double glazing. *Energy and Buildings*,

117, 33–43. https://doi.org/10.1016/j.enbuild.2016.02.009

Wilson, C. ., Simko, T. ., & Collins, R. . (1998). HEAT CONDUCTION THROUGH THE SUPPORT PILLARS IN VACUUM GLAZING. *Solar Energy*, *63*(6), 393–406. https://doi.org/10.1016/S0038-092X(98)00079-6

WINDOW | Windows and Daylighting. (n.d.). Retrieved June 9, 2021, from https://windows.lbl.gov/software/window

World Energy Council. (2019). *World Energy Issues Monitor 2019 GLOBAL AND REGIONAL PERSPECTIVES*. Retrieved from www.worldenergy.org

Xu, G., & Wang, W. (2020). China's energy consumption in construction and building sectors: An outlook to 2100. *Energy*, *195*, 117045. https://doi.org/10.1016/J.ENERGY.2020.117045

Zhang, W., & Lu, L. (2017). Energy performance and heat transfer characteristics of photovoltaic double skin facades (PV-DSFs): a review. *Sustainable Energy & Fuels*, *1*(7), 1502–1515. https://doi.org/10.1039/C7SE00175D

Zhang, W., & Lu, L. (2019). Overall energy assessment of semi-transparent photovoltaic insulated glass units for building integration under different climate conditions. *Renewable Energy*, *134*, 818–827. https://doi.org/10.1016/j.renene.2018.11.043

Zhang, W., Lu, L., & Chen, X. (2017). Performance Evaluation of Vacuum Photovoltaic

Insulated Glass Unit. *Energy Procedia*, *105*, 322–326. https://doi.org/10.1016/j.egypro.2017.03.321

Zhang, W., Lu, L., Peng, J., & Song, A. (2016). Comparison of the overall energy performance of semi-transparent photovoltaic windows and common energy-efficient windows in Hong Kong. *Energy and Buildings*, *128*, 511–518. https://doi.org/10.1016/j.enbuild.2016.07.016

Zhou, J., Zhao, X., Yuan, Y., Li, J., Yu, M., & Fan, Y. (2020). Operational performance of a novel heat pump coupled with mini-channel PV/T and thermal panel in low solar radiation. *Energy and Built Environment*, *1*(1), 50–59. https://doi.org/10.1016/j.enbenv.2019.08.001

Zoller, F. (1924). Hollow pane of glass, German Patent: 387656.